Czech University of Life Sciences Prague
Faculty of Environmental Sciences
Department of Water Resources and Environmental Modelling

Avalanche hazard in the Krkonoše mountains and refinement of snow data collection methods

Dissertation thesis

Mgr. Markéta Součková

PhD programme: Environmental Modelling

Branch of Study: Landscape Enginering

Supervisor: prof. Ing. Martin Hanel, Ph.D.

Karlovy Vary, January 2024

DECLARATION

I hereby declare I have written this doctoral thesis independently and quoted all the sources of information used in accordance with methodological instructions on ethical principles for writing an academic thesis. Moreover, I state that the thesis has neither been submitted nor accepted for any other degree.

In Karlovy Vary, January 2024

……

Mgr. Markéta Součková

ACKNOWLEDGEMENT:

This dissertation was performed at the Department of Water Resources and Environmental modelling at CZU. I would like to thank all who were involved in some way. I would especially like to thank my supervisor, Martin Hanel, for his mentorship, positive approach, time and patience during dissertation writing. Furthermore, I would like to acknowledge Theodora Lendzioch (Charles University, Faculty of Science) for introducing me the UAS monitoring, doing field work, proofreading and being a good friend. Jirka Pavlásek for giving me recommendations on how to better connect the chapters, how to make a conclusion of the thesis, and constructive critique (Faculty of Environmental Sciences CZU Prague). Roman Juras (Faculty of Environmental Sciences CZU Prague) for field work, proofreading, ensuring the equipment, and connecting me with some people from the Mountain Rescue Team. Dr. Benjamin Fersch for mentoring me at the Karlsruhe Institute of Technology (KIT) internship, Institute of Meteorology and Climate Research Department of Atmospheric Environmental Research (IMK-IFU). Zdeněk Svatý (Czech Technical University in Prague, Faculty of Transportation Sciences) for giving me UAS flying and Agisoft processing recommendations. Johanna Ruth Blöcher for being a great discussion team worker during the publishing the NHESS article. I would like to thank to Helena Michálková and Petr Bašta for their administrative support in IGA process. Lastly, I would like to thank to my family.

Funding:

The project was supported by Internal grant agency: IGA project of the Faculty of Environmental Sciences, Czech University of Life Sciences Prague, Czechia (2-years project): “Avalanche hazard in the Krkonoše mountains and refinement of snow data collection methods”, project number: 2020B0006.

Key words

Snow, snow avalanche, snow mapping, snow depth, Krkonoše mountains, release zones, avalanche path, RAMMS, Unmanned Aerial Systems, photogrammetry, Structure from Motion, Cosmic Ray Neutron Sensing

Abstract

The impact of climate change on avalanches presents a nuanced picture, with variations depending on local conditions. While lower elevations may experience fewer, wetter, and smaller avalanches due to declining snow cover, higher-altitude regions might witness more frequent and spontaneously triggered snow avalanches. This dissertation theses aims to address several key aspects related to avalanche dynamics and monitoring:

1. Analysis of long-term trends in wet and slab avalanche activity over 59 winter seasons (1962–2021), including examination of frequency, magnitude, and orientation. Additionally, identification of the main meteorological and snow variables of these avalanches from 1979 to 2020 using machine learning techniques, particularly the Random Forest (RF) method.
2. Evaluation of the effectiveness of Unmanned Aerial Systems (UAS) snow depth (SD) monitoring in two distinct environments: the Krkonoše Mountains (Mts) and the Northern Limestone Alps in low altitude mountain ranges.
3. Simulation of selected avalanche path extend in the Krkonoše Mts using the RAMMS model.
4. Introduction to snow monitoring using Cosmic Rays Neutron Sensors (CRNS), providing insights into this advanced technique.
5. Promoting science to the public and schools, emphasizing modern learning methodologies tailored to the 21st century.

The analysis reveals significant changes in avalanche dynamics, with an increase in the number and size of wet avalanches during February and March, while the number of slab avalanches has decreased over the past three decades. This rise in wet avalanches correlates with a 1.8°C increase in winter season air temperature since 1979. Machine learning techniques, particularly RF analysis, offer insights into the driving variables of avalanche activity, enhancing decision-making processes for avalanche hazard mitigation. Recommendations include a holistic approach combining expert knowledge, snow profile measurements, and continuous monitoring of meteorological and snow variables to assess avalanche hazards. Close-range sensing techniques, including UAS and CRNS, provide valuable tools for spatial monitoring of avalanche paths and spatial SD distribution. Ongoing research by the Cosmic Sense unit further investigates the CRNS method. The findings can be utilized by public authorities such as the Krkonoše National Park administration, the Mountain Rescue Service of the Czech Republic, and the Institute of Forest Management.

OUTLINE

LIST OF FIGURES

LIST OF TABLES

1 Preface

"I picked a flower; it wilted. I caught a butterfly, and it died. Only then did I understand that beauty must be touched with the heart."

1.1 Forword

Since childhood, I have been passionate about spending time in nature. It started with my enthusiasm, loving being outdoorsy, hiking, and climbing in mountainous, alpine areas. But also, with getting older, take a break, breath, and listen to nature's silence and, with gratitude and humility, observe the landscape, natural processes, and the whole cycle. When I am in the mountains, I feel closer to myself – standing up even at the small peak means freedom. Therein, in my opinion, lies the ancient attraction of the mountains. Detailed information on the spatio-temporal distribution of seasonal snow in mid-mountain terrain plays a significant role in the hydrological cycle, natural hazard management, flora, fauna, and tourism. So, I was motivated to discover processes by observing and doing experiments. Moreover, I wished to connect people (in this dissertation thesis KRNAP Administrative to cooperate with Avalanche preventist, Scientists and KRNAP visitors altogether. Listen to different perspectives and needs and develop a solution that benefits and suits all of us: stakeholders and humankind. Furthermore, I wished to teach theoretical knowledge in practical skills ways. I made some connections; however, I doubt it lasts once you leave the field or scientific community. Therefore, I am oriented to enlightenment and teaching children how to be connected and live in harmony with nature, how to care about it and kindly speak together, and discuss by learning by doing. The above-mentioned quotation could empower these words.

1.2 Scientific motivation

The motivation behind my research stems from a deep fascination with mountain or alpine environments, particularly the study of natural hazards and snow hydrology. I am driven by the desire to mitigate natural hazards, specifically focusing on rapid geophysical mass movements such as snow avalanches and raise awareness about the snow environment. I thoroughly enjoy working in mountainous terrain and I am committed to providing clear information to the public. My dissertation topic focuses on avalanche hazard in low-altitude mountain range in Czechia. This includes using Unmanned Aerial Systems (UAS) and Cosmic Ray Neutron Sensors (CRNS) to monitor the spatial distribution of snow depth. During my time at KIT-Campus Alpin, Institute of Meteorology and Climate Research (IFU), under the Deutsche Bundesstiftung Umwelt (DBU) Fellowship, I had the opportunity to gain a brief introduction to the CRNS which can be considered to fill the gap between small-scale measurements (such as snow pits and snow cores) and Remote Sensing (RS) data. In the context of Czechia, close-range sensing techniques have the potential to provide high-resolution spatial data on snow, which is currently lacking. I believe in the potential of collaborative groups and open-source data. By utilizing new technologies and approaches effectively and purposefully, we can timely screen and analyse big data formats, leading to a better understanding of underlying mechanisms.

1.3 Thesis structure

This thesis consists of one published paper: “What weather variables are important for wet and slab avalanches under a changing climate in a low-altitude mountain range in Czechia?” and two studies – first focuses on the avalanche path in Krkonoše Mts: Žlab Úpičky. Second focuses on UAS and CRNS monitoring in the Northern Limestone Alps done during Deutsche Bundesstiftung Umwelt (DBU) Internship at KIT IMK-IFU. The thesis consists of five Parts. **Part I** focuses on the Literature review and is divided into two main topics: Chapter 2. Snow avalanche changes and their drivers and Chapter 3. Snow monitoring. **Part II** concentrates on Wet snow and slab avalanches in the Krkonoše mountains, and **Part III** concentrates on Monitoring Spatial Snow Distribution, which are both divided into Study area and data, Methods and Results chapters. **Part IV** encompasses Promoting science: public awareness, Scio school projects, and 21st-century learning. The thesis concludes with **Part V** – Discussion & Conclusion consisting of the two main chapters: Chapter 11. Drivers of wet and slab avalanches according to machine learning and Chapter 12. Advances in higher-resolution snow monitoring methods. In conclusion, the key findings are summarised, and the research aims are answered.

1.4 AIMS of the thesis

This thesis aims to understand the avalanche activity process in the Krkonoše Mts. The first aim is to analyse changes in avalanche type and weather variables. The second aim is to compare SD measurement methods, including manual, UAS, and CRNS based methods. SD spatial data are not available in Czechia, but they are important for avalanche modelling. The RAMMS model was used to simulate avalanche release in the Krkonoše Mountains and compare the results with SD data from UAS. In addition, the thesis investigated the feasibility of using UAS to collect SD data from steep terrain and flat terrain. The CRNS method translating neutron counts into snow water equivalent (SWE) was also studied. The thesis also conducted a school project to raise awareness about avalanche safety using drones and education in the Krkonoše Mountains.

The aims were:

1. to analyse the avalanche type changes and meteorological and snow drivers
    a) analyse **changes in avalanche activity (wet and slab avalanches)** via assessment of **frequency, magnitude and aspects of avalanche paths** over 59 winter seasons (1962–2021);
    b) determine the **main meteorological and snow drivers** governing snow avalanche activity of (1) **wet avalanches** and (2) **slab avalanches** for a daily timescale of winter seasons from 1979 to 2020 within a low-altitude mountain range in Central Europe, specifically the Krkonoše mountains.
2. Testing the snow data collection methods: snow depth spatial variability by manual, UAS and neutron-based methods
    a. to assess the feasibility of UAS-SfM for capturing flat Graswang and steep Krkonoše terrain and estimation of SD variabilities with low-cost Phantom 4 Pro (P4P) V2.0 camera (visible wavelength) in comparison with manual SD and Trimble Global Navigation Satellite System device (GNSS);
    b. extend the station network, maintain existing sites, and collect in situ snow data in Ammer and Isar river catchments in Bayern region (south Germany);
    c. study the CRNS method observation theory for SWE and generalize and investigate if it is possible to find a universal approach to translate the observed above snow CRNS measurements into SWE dynamics for different altitudes and the environments in Northern Limestone Alps. The amount of water stored in the snowpack is key information for regulating the Sylvensteinsee and Achensee reservoirs in spring .
3. Model simulation of the avalanche release
    a. reconstruction of Žlab Úpičky avalanche release using RAMMS model and compare it with the UAS results
4. Public awareness and enlightenment, school project: hands on, the use of drones and education on Krkonoše Mts. avalanche terrain.

1.5 Introduction

Avalanche hazard is a threat to winter recreationists in the Krkonoše Mountains, a popular ski and hiking destination in the Czechia. Although snow avalanches in low to medium-height mountains may not frequently make international headlines, they pose a hazard, particularly in Krkonoše, where there have been 11 reported victims since 2005 to 2021 (Mountain Rescue Service, 2021[1]). However, its essential to recognize that snow avalanches are not just a danger; they also play a vital role in the unique ecosystem of the Krkonoše Mts, influencing local flora and fauna, as well as contributing to crucial environmental processes. A snow avalanche is a sudden downhill movement of a huge mass of snow from mountains top to the valley bottom. It is important to note that the terms 'hazard' and 'risk' are often misused therefore, we provide clear definitions for their use in this thesis. In this context, 'hazard' refers to the spatial and temporal probability of a specific event occurring with a defined magnitude (Blahut & Klimeš, 2011). Conversely, 'risk' pertains to the potential for the loss of property or human resources. Traditionally, avalanche hazard assessment has relied on subjective assessments made by experienced observers. This approach can be limited by the availability of trained observers and the inherent subjectivity of human judgment. In recent years, there has been a growing interest in using objective data collection methods to improve avalanche forecasting accuracy.

The prediction of avalanche release from a mountain slope is a highly complex task, as it depends on various factors, including:

a) **Terrain parameters:** terrain-related factors also play a significant role, including slope, elevation, curvature, aspect, roughness, and the extent of vegetation cover in the region (Bühler et al., 2013).

b) **Snowpack parameters:** These include factors such as the presence of weak layers, bonding between layers, SD, liquid water content, and grain size.

c) **Meteorological parameters:** These encompasses elements like windspeed, wind orientation, air temperature, precipitation, and more.

d) **Analysis of historical data:** knowledge of avalanche historical records

One approach is to use ground-based sensors to measure snowpack properties, such as SD, snow density, and temperature. These sensors can provide real-time data that can be used to develop avalanche forecasts. However, the placement and maintenance of ground-based sensors can be expensive and time-consuming and not densely distributed in mountain environments. Despite having a relatively dense network[2] of station data in Czechia, this network may still be inadequate, particularly in areas with complex terrain. Spatial interpolation methods can be employed, however they may not provide a sufficiently accurate representation of the snowpack, Thus, a more comprehensive approach is often

[1] https://www.horskasluzba.cz/cz/pocasi-na-horach/lavinova-predpoved/krkonose
[2] https://www.chmi.cz/files/portal/docs/poboc/OS/stanice/ShowStations_CZ.html

required for accurate avalanche prediction and assessment. Another approach is to use airborne sensors to collect data on snowpack conditions.

To effectively manage avalanche risk, it is necessary to have a comprehensive understanding. Therefore, we deal with these factors in the individual chapters of this thesis. Meteorological and snow parameters are investigated in (Chapters 5 and 6). Snow weak layer is partly mentioned in Chapter 7.3.2. We did not analyse all terrain parameters influence on avalanches in this dissertation (only aspect within wet and slab avalanches changes, DEM as the input of RAMMS model, and few terrain parameters of avalanche paths displayed in Zenodo xlsx in Součková, M. et al., (2022). Analysis of the historical avalanche data helps to understand the changes in time (Chapters 6.1.1, 6.2.1). RAMMS model helps to back calculate or predict avalanche release and estimate avalanche length, area, and volume (Chapter 8.2). SD is easy to measure snowpack characteristic in comparison with SWE, and snow density. Thus, we focus on measuring SD with multiple methods such as: manual, UAS and CRNS based methods.

SD (in cm, m) serves as a critical input variable for hydrological models. SD is also the input RAMMS parameter. It is defined as the vertical distance from the base to the surface of the snowpack (Fierz et al., 2009) and can exhibit significant variability over short distances and horizontally within a meter-scale (Dong, 2018). SD measurements are typically collected as point data, either manually or automatically at weather stations or through snow pillow. Point measurements do not fully capture the high spatial variability of SDs (Nolan et al., 2015).

In this context, one of the most meaningful indicators is the Snow Water Equivalent (SWE, in mm w.e. or mass of snow kg m^{-2}), which quantifies the volume of water held within the snowpack and refers to the water depth that would exist if the snow mass of a particular area would melt completely. In other words, it is the product of snow depth in meters and the vertically integrated density (the mass per unit volume [$kg.m^{-3}$]), in kilograms per cubic meter, typically expressed in millimetres of water equivalent [$kg.m^{-2}$]. This information holds exceptional importance for hydrologists, especially in the context of predicting floods during snow melting periods. Since SWE data may not always be readily available at monitoring stations, having spatial information on SD becomes imperative.

In regions where gridded SWE and SD data are either lacking or too sparse, photogrammetry methods, especially Structure-from-Motion (SfM), provide a viable solution for acquiring this essential information in regional scale. The concept behind photogrammetry-based SD estimation involves comparing the actual surface model of the snow cover with a reference model representing the terrain without snow. A common approach is to generate the snow-free surface model using the same technique, namely UAS photogrammetry, during periods when there is no snow cover (Adams et al., 2018; Avanzi et al., 2018; Buhler et al., 2016; Bühler et al., 2017; Cimoli et al., 2017; Vander Jagt et al., 2015). Another option is to utilize national terrain models, typically created through LiDAR measurements, which are generally available in many countries. The important UAS photogrammetry resolution parameter is

the Ground Sampling Distance[3] (GSD) which is the distance between two consecutive pixel centers measured on the ground and can be calculated by GSD calculator[4]. The bigger the value of the image GSD, the lower the spatial resolution of the image and the less visible details.

To georeference means to determine a real-world spatial position of photogrammetry images ground Global Navigation Satellite System (GNSS). GNSS satellites transmit electromagnetic signals in the radio spectrum which are reflected by many objects on the Earth's surface. The GNSS structure consists of a space, control, and user segment. The space segment consists of individual navigation systems such as NAVSTAR GPS, GLONASS, Galileo, Beidou. Control segment consists of observation ground stations and performs corrections of atomic clocks and satellite positions. User segment consists of passive receiver that receives signals from individual satellites. Based on the received data, the receiver calculates its position (Tesař, 2007). Traditionally, accurate surveying required two GPS receivers. Modern reference station networks eliminate the need for a second receiver. Instead, a known point with precise x, y, z coordinates is established as a reference station. This reference station is connected to the receiver via an internet connection, typically using a Global System for Mobile Communications: GSM module, allowing for real-time positioning (Tesař, 2007). Georeferencing of UAS imagery can be achieved using GCPs (negating the benefits of rapid and efficient mapping in remote areas (Tomaštík et al., 2019). Instead of network connection and collection of multiple GCPs we might use base station placed over a known control point and to choose between:

a) Real-Time Kinematic (RTK) positioning which can be incorporated into base station, receiver or can be mounted on drone.

b) Post-Processed Kinematic (PPK) positioning

Kinematics is a term in traditional Global Position System: GPS surveying methods where receivers are in motion. To process the data Base Station and Rover are needed. RTK does not require post processing to obtain accurate positioning (Van Sickle, 2015). A radio at the reference receiver, either a local base station or a network base station, broadcasts its position to the rover in real time (Fig. 1-a). The PPK positions are not corrected in real time. It involves placing stationary base station over a known control point or using of the geolocated monument. GPS data is simultaneously collected by the base station and the drone as it flies. Afterwards, the data are downloaded from both the base station and the rover (UAS-drone) and post processed in a GPS software. The RTK workflow enables a very quick way to obtain accurate imagery but relies on a real-time connection to produce accurate maps. A PPK solution takes more time to set up, however relies on its signal backup data to ensure positional accuracy of the flight. In general, horizontal RMSEs of the RTK/PPK method do not exceed 10 cm and vertical RMSEs 20 cm (Tomaštík et al., 2019).

The CRNS method was originally introduced for soil moisture measurements. Epithermal neutrons produced by cosmic radiation in the soil and widely used to determine soil

[3] https://support.pix4d.com/hc/en-us/articles/202559809-Ground-sampling-distance-GSD-in-photogrammetry

[4] https://support.pix4d.com/hc/en-us/articles/202560249-TOOLS-GSD-calculator

moisture in the upper decimetres of the ground. Neutrons are sensitive to all sources of hydrogen at the land surface. Therefore, the CRNS method has the potential to measure SWE. The application of CRNS for snow monitoring is based on the principle that snow water moderates the epithermal neutron intensity, which can be directly related to the snow water equivalent of the snowpack (Bogena et al., 2020).

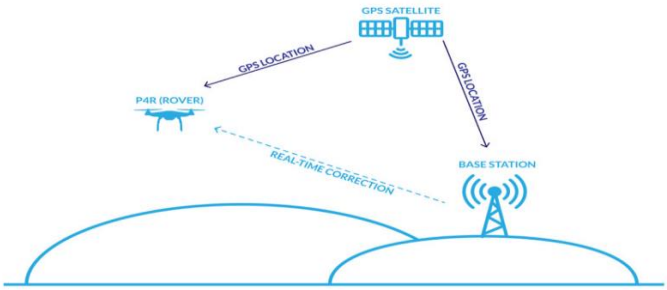

Fig. 1-a: RTK workflow of base station, GPS satellite and rover. Reused from Heliguy [5].

[5] https://www.heliguy.com/blogs/posts/dji-phantom-4-rtk-accuracy-confirmed

I.PART

LITERATURE REVIEW

LITERATURE REVIEW

This part of the dissertation thesis contains the literature review. The first part focuses on Snow avalanche changes and their drivers (Chapter 2), and the second focuses on Snow monitoring (Chapter 3).

2 Snow avalanche changes and their drivers

2.1 Climate change impact on snowpack freshwater supply and snow avalanches

The amount of water stored in a snowpack is crucial for freshwater supply in mountainous regions, which are regarded as water towers, of their adjacent lowlands (Viviroli et al., 2007). With the ongoing climate change (CC), there are more extremes like heavy rainfall, and snowfall are less frequent and intense at lower altitudes, resulting in a thinner, wetter snowpack with a higher average density according to Intergovernmental Panel on Climate change (IPCC) special report (Hock et al., 2019). Information of small-scale evolution of snowpack may be useful for avalanche prediction (Barnett et al., 2005), (Sweizer, 2008) and snow drift modelling around buildings (Tominaga et al., 2011). Furthermore, climate change impacts the snowline position and in the high mountain areas shifts it upwards (Beniston et al., 2018; Giacona et al., 2021a; Marty et al., 2017) which in turn affects the flood generation and determines water level thresholds for dam regulation. The management: filling and releasing of reservoirs is important for the vulnerable ecosystems as well as human infrastructure further downstream. What remains unclear is the CC effect on snow avalanches (Strapazzon et al., 2021) especially in low to medium high altitudes. Moreover, more attention should be paid to monitoring snow distribution: spatial-temporal variability (Miller et al., 2022), as it has implications for both risk management and water resources management civil engineering applications (Cimoli et al., 2017).

2.2 Snow avalanche trend in low to medium altitudes

Large snow avalanches are major natural hazards. As rapidly moving snow masses, snow avalanches pose a serious threat to people, property, and infrastructure. The growth in popularity of winter tourism has led to an increase in numbers of avalanche accidents (Techel et al., 2016). It is said that the frequency and types of snow avalanches may change (Hock et al., 2019). A wetter, warmer climate could exacerbate the consequences of burial (Strapazzon et al., 2021). This is why, it is vital to analyse how a changing climate has impacted avalanches in low altitudes in Central Europe.

The overall number and runout distance of snow avalanches will reduce in regions and elevations experiencing a significant reduction in snow cover. There is medium evidence and high agreement that observed changes in avalanches in mountain regions will be exacerbated in the future (Hock et al., 2019), with generally a decrease in hazard (Martin et

al., 2001) at lower elevations. However, less snow does not necessarily result in fewer avalanches (Ballesteros-Cánovas et al., 2018; Reuter et al., 2020; Peitzsch et al., 2021). At higher elevations, mixed changes are expected, with more wet-snow avalanches.

Wet-snow avalanches will occur more frequently even in winter, which has already been shown for recent decades from December to February (Naaim et al., 2016). Since wet-snow avalanches are more likely to occur early in the season, spring avalanche activity at lower elevations is likely to decrease, while avalanche activity at higher elevations is likely to increase (Castebrunet et al., 2014; Strapazzon et al., 2021). There is no clear direction in the trend for overall avalanche activity (Hock et al., 2019); however, at a local scale (e.g. NE France, Vosges mountains) there is observed upslope migration of snow avalanches in a warming climate with release areas > 1200 m a. s. l. (Giacona et al., 2021). Ballesteros-Cánovas et al. (2018) reported increased frequency of wet-avalanche activity on some slopes of the western Indian Himalaya over recent decades. In the European Alps and Tatra mountains, avalanche mass and runout distance as well as powder avalanches have decreased at lower elevation. Avalanche numbers have decreased below 2000 m a. s. l. and increased above this elevation (Eckert et al., 2013; Lavigne et al., 2015; Gądek et al., 2017).

Mountain regions worldwide are susceptible to wet-snow-avalanche and slab-avalanche types (Soteres et al., 2020). Focusing on wet-snow avalanches, three triggering mechanisms exist (or combinations thereof) due to loss of strength, overloading, and gradual weakening (Baggi and Schweizer, 2009). More specifically, loss of strength can be caused by infiltration and accumulation of water at capillary barriers. Overloading can occur due to precipitation of partially wet and weakened snowpack. Lastly, the gradual weakening of the basal snowpack can occur as the snowpack becomes isothermal, causing failure of the basal layers. This can be caused by heat stored in the ground that melts the lowermost snow layer.
The most frequent are slab avalanches (Schweizer and Föhn, 1996), which are wet or dry. Natural slab avalanches are triggered either due to gradual uniform loading by precipitation and wind (or by a combination of both) or due to a non-loading situation that changes the snowpack properties, such as surface warming (Schweizer et al., 2003).

Climate change influences mountain snow cover by increase in air temperature and rainfall during the winter. Depending on elevation, air temperature increases may cause changes in the type, intensity, and frequency of snowfall (Strapazzon et al., 2021). At higher elevations, air temperatures will rise, and rain will occur more often. At high elevations (high mountain areas, distinct regions where snow is a prominent feature of the landscape, without an exact and quantitative separation line), the likelihood of more dynamic changes in temperature and precipitation is higher, with accelerated fluctuations between extremes and with less prominent trends because of local effects (Hock et al., 2019). The avalanche regime may be less impacted at higher elevations, where snowfall is still abundant and may increase in intensity (Laute and Beylich, 2018; Hock et al., 2019; Le Roux et al., 2021). At high altitude, trends in extreme snowfall are increasing above 2000 m in the French Alps (Le Roux et al., 2021) but with a spatially contrasting pattern amplified at around 2500 m in the north and south part of France, possibly resulting from climate warming and circulation patterns. The observed shift from solid to liquid precipitation is likely to move the position of seasonal

snow lines to higher elevations and shorten snow seasons (Marty et al., 2017; Beniston et al., 2018; Giacona et al., 2021). At lower elevations, snowfall is less frequent and intense, resulting in a thinner, wetter snowpack with a higher average density according to an Intergovernmental Panel on Climate Change (IPCC) special report (Hock et al., 2019). When snow cover decreases, avalanche hazard areas also decrease (Strapazzon et al., 2021).

Globally, snowfall has reduced as a result of increasing temperatures, especially at lower elevations (Hock et al., 2019). Regional trends of increasing liquid precipitation during winter have been confirmed (Feng and Hu, 2007; Bintanja, 2018). Moreover, a decrease in the snowfall fraction (SF) of −5.5 % per decade in low-altitude mountain catchments (> 900 m) in Czechia and Slovakia has been observed since 1966 (Blahušiaková et al., 2020). From SYNOP (surface synoptic observations) reports the precipitation phase in the cold season has partially shifted from solid to mixed precipitation, with the most substantial decrease in snowfall in February (−10.5 % per decade) and January (−6.3 % per decade) from 1983–2018 in Czech meteorological stations (Hynčica and Huth, 2019).

2.3 Snow characteristics

Snowpack properties such as snow depth (SD), snow water equivalent (SWE), and snow characteristics (e.g. snow cover extent (SCE) and snow cover duration (SCD)) are used as indicators or proxies to assess and understand snow avalanche activity and behaviour in various regions. The trends, on the other hand, are the long-term patterns or changes observed in these parameters over time, which can provide valuable insights how snow avalanche activity may be affected by climate change or other factors. Changes projected for the mountain cryosphere indicate a decrease in SCE and SCD (Notarnicola, 2020). SWE and SD have declined in nearly all regions by −5 % per decade on average. This trend is apparent especially at lower elevations, although year-to-year variation is high (Hock et al., 2019). Overall, snow cover duration has shortened in Czech mountain catchments over recent decades by up to −6.8 d per decade, principally due to earlier melt-out (Blahušiaková et al., 2020). Results of Nedelcev and Jeníček (2021) have shown that snowpack at elevations below 1200 m a.s.l. seems to be more sensitive to changes in air temperature, while precipitation influenced the snowpack more at elevations above 1200 m a.s.l. In Central Europe snow depth has been declining by 1 % at higher elevations (~ 2300 m) and 6.3 % at lower elevations (~ 800 m) since 1966 (Blahušiaková et al., 2020).

2.4 Drivers of the avalanche risk and avalanche activity

Zgheib et al. (2020) suggests that social–economic, environmental changes and anthropogenic drivers may be the primary factors driving the spatiotemporal evolution of the **risk** rather than just changes in **hazard** (meteorological conditions = variable factors; snow parameters such as snow stratigraphy; and terrain characteristics = permanent). Changes in land use and land cover, such as deforestation (García-Hernández et al., 2017) and reforestation (Zgheib et al., 2020, 2022), as well as changes in demographics (Giacona et al., 2018), will affect avalanche risk.

Avalanche activity is governed by both variable and permanent factors (Quervain et al., 1973). Whereas variable factors are attributed to meteorological conditions (for instance rain, air temperature, wind, snowfall) that progressively build the snowpack, permanent factors are attributed to terrain features (elevation, slope, aspect, roughness of the ground, etc.; Sielenou et al., 2021). Avalanche types and avalanche frequency are affected by a combination of precipitation amounts and air temperatures during storms and prior snow stratigraphy (Schweizer et al., 2009). Winter recreationists face a significant risk due to the presence of persistent weak layers (Techel et al., 2015; Statham et al., 2018).

2.5 Snow avalanche hazard in Krkonoše

Snow avalanche hazard in Czechia is mainly constrained to Krkonoše and Jeseníky mountains. Although snow avalanches do not present a significant risk to the population and settlements in Czechia (there are approximately twenty snow avalanche releases every year), the rising popularity of winter sports (off-piste skiing and ski touring) in recent years has led to an increase in social exposure to snow avalanches and thus a growing number of victims (11 fatalities, 15 injured, and 28 people pulled down since 2005). (Mountain Rescue Service, 2021) and, rarely, road accidents. Krkonoše was one of the first non-Alpine regions that established regular snow monitoring and avalanche records in 1961 (Vrba and Spusta, 1975, 1991; Spusta and Kociánová, 1998; Spusta et al., 2003, 2006; Juras et al., 2013; Blahůt et al., 2017).

2.6 High spatial resolution of snow depth

Monitoring snow distribution: spatial-temporal variability has implications both risk management and water resources management civil engineering applications (Cimoli et al., 2017). Information of small-scale evolution of snowpack may be useful for avalanche prediction (Barnett et al., 2005), (Baggi and Schweizer, 2009), and high-resolution spatial-temporal snow depth information is required for many purposes:

a) to **detect avalanche release zones** to **estimate and mitigate avalanche hazard** (Eberhard et al., 2020; Singh et al., 2022); in particular, snow depth mapping (a key input parameter for modelling) enables rapid documentation of avalanche accidents (Korzeniowska et al., 2017; Lato et al., 2012; Singh et al., 2022);
b) mapping the **mass balance of avalanches using numerical avalanche dynamic simulation** tools such as Rapid Mass Movement Simulation: RAMMS (Bartelt, 2022; Christen et al., 2010)

c) **ski resorts** would also benefit from high-resolution snow depth maps to better redistribute snow on slopes throughout the season (Hanzer et al., 2020; Spandre et al., 2017);

d) to **snow drift accumulations** (Schön et al., 2015); snow drift modelling around buildings (Tominaga et al., 2011).

f) for **snow water equivalent** (SWE) modelling in **snow hydrology** (Steiner et al., 2018)

3 Snow monitoring

Snow monitoring involves various methods, including point or line measurements, airborne (Deems et al., 2013) and terrestrial Light Detection and Ranging (LiDAR), and photogrammetry. With the advancement of technologies like laser scanning, these platforms can generate snow depth maps, both actively and passively, which are used for monitoring SD over time. Both active and passive sensors can be used. Active platforms actively send out a signal, usually a radio wave or pulse of light, and then measure the reflected signal to gather information about the object or environment. Passive platforms detect/sense and measure objects or phenomena using energy that is naturally reflected or emitted by them (Kupfer and Emerson, 2005). Active sensors are LIDAR, RaDAR, SoNAR. Passive are RGB cameras, thermal sensors. Different platforms exist terrestrial, air-borne, and spaceborne. We focused on airborne, specifically UAS method combined with traditional manual probing and snow pits method.

SD is often measured with manual probing and SWE with snow pits (Fierz, 2009), which are both time consuming and risky in avalanche-prone, remote areas. While SWE is commonly estimated using snow pillows (Johnson and Marks, 2004) or recently by cosmic neutron rays (Fersch et al., 2020; Schattan et al., 2017), SD can also be measured using ultrasonic (Avanzi et al., 2014) or laser (Morin et al., 2012) sensors and UAS (Buhler et al., 2016).

3.1 Techniques for snow depth monitoring and their advantages and disadvantages

Point measurements of snow depth and SWE provide valuable data, however they often suffer from spatial incompleteness, as they represent only specific locations within a larger area and do not represent the high spatial variability (Nolan et al., 2015). Snow pillows rely on hydrostatic pressure. They can be influenced by various factors that disturb the measurements. Factors such as energy transport into the snowpack or ice layer, and wind fields can affect the accuracy and representativeness of snow pillow measurements. These factors might introduce uncertainties and lower quality of the estimated snow cover and SWE. Therefore, while point measurements and snow pillows have their utility, it is important to consider their limitations and potential sources of error when interpreting the data.

Complementary approaches, such as airborne LiDAR (actively sends pulsed laser light and measures the backscatter signal reflected from the target) mapping (Deems et al., 2013) and other techniques can help to overcome these limitations and provide a more comprehensive understanding of snow distribution and characteristics. However, LiDAR terrain field and software requirements skills are indeed more demanding and expensive for small-scale areas. Furthermore, the TLS method requires multiple stationing points to map snow depth

over irregular terrain, is time-consuming and require careful planning to complete the survey. Additionally, TLS results differ with altitude (Prokop, 2008), with accuracies typically below 0.10 m beyond 1000 m a.s.l. The absolute maximum and mean errors for spatially distributed snowpacks up to 3000 m range from 0.5-0.6 m and 0.2 – 0.3 m, respectively (López-Moreno et al., 2017). While, Airborne laser scanning (ALS) can provide higher spatial resolution (typically 1 m) and achieve a vertical accuracy of 0.1 m (Deems et al., 2013) it requires the use of an aircraft, which adds to the cost and complexity (López-Moreno et al., 2017) and requires expertise in handling different snowpack conditions (dry or wet) since only certain wavelengths can provide satisfactory results.

Techniques such as GPS-reflectometry (Jin et al., 2016);, Terrestrial Laser Scanner (TLS) (Jaakkola et al., 2014), or satellite-based sensors (Dietz et al., 2012), Ground Penetrating Radar (GPR) (Machguth et al., 2006), digital photogrammetry (Bühler et al., 2015; Nolan et al., 2015), time-lapse photography (Farinotti et al., 2010; Parajka et al., 2012), tachymetry (Prokop et al., 2008) exist and might provide more comprehensive approaches. However, these techniques are of high costs (e.g., airborne or helicopter flights) or only useful supplements to weather stations and manual measurements (Lendzioch et al., 2016). All of them present a list of advantages and disadvantages.

Other method: SfM is a technique that reconstructs 3D models of topography using a collection of overlapping photographs taken with a consumer-grade digital camera (Smith et al., 2016; Westoby et al., 2012). It simultaneously solves for camera pose and scene geometry by using a highly redundant bundle adjustment process. The process involves identifying matching features in the images and determining their corresponding 3D positions (Westoby et al., 2012) to determine characteristic points. By triangulation these positions, a detailed 3D model of the terrain can be generated. At least three images are needed for SfM to reconstruct 3D models of the topography. There are two existing methods used to accurately georeference the SfM-generated 3D models: 1) GCPs with known geographic positions and 2) UAS with Real-time kinematics (RTK) were one to three GCPs are needed (Cho and Lee, 2023). These GCPs serve as reference points to align the model with the real-world coordinates. One of the outputs of the georeferenced 3D model is the creation of a Digital Elevation Model (DEM; Fonstad et al. 2013). The DEM represents the topography of the area in a gridded format, providing elevation information for each point in the model.

Digital photogrammetry presents a relatively cost-effective method for data acquisition compared to laser scanning, especially in most applications except dense vegetated areas. UAS have the potential to enable timely, flexible, cost-effective, and safer data acquisition in inaccessible and dangerous mountain terrain (Boesch et al., 2016). Therefore, we used UAS-borne SfM techniques in this thesis. Moreover, different platforms such as high-resolution satellites (e.g., Pléiades), airplanes (e.g., Ultracam), UAS (e.g., eBee+), and ground-

based systems (e.g., single-lens reflex cameras) may yield different levels of accuracy (Eberhard et al., 2020).

3.2 UAS potential of for snow depth monitoring

UAS is a suitable tool for obtaining spatial information about snow depth, especially in hard-to-access, risky mountain terrain. UAS also offers enhanced safety compared to traditional point methods. With UAS, it is possible to generate high-accuracy Digital Surface Model (DSM), Digital Elevation Model (DEM), Digital Terrain Model (DTM), and orthophoto maps with accuracy levels ranging from mm to dm. The method involves subtracting an underlying topography Digital Terrain Models (DTMs) from the snow surface cover DEMs (DSMs) generated through SfM techniques. This allows for mapping snow depth in avalanche-prone areas and detecting the extent and volume of avalanche depositions. By improving the reliability of input data for snow avalanche models like RAMMS, it becomes possible to enhance hazard estimation and prediction of avalanche extent, thereby minimizing potential risks. Previous studies conducted by Bühler et al. (2017) and Adams et al. (2018) have presented comparisons between UAS and TLS for assessing snow conditions under different illumination conditions. These studies have shed light on the performance of UAS in capturing high-density datasets in snowy environments. However, most studies evaluating the effectiveness of UAS in snow assessments have utilized datasets at low density. These studies including those by (Bühler et al., 2016), De Michele et al., (2013), Harder et al., (2016), Lendzioch et al., (2019, 2016); Vander Jagt et al., (2015) have provided valuable insights into the potential of UAS in collecting snow-related data, but their datasets may not achieve the same level of density as TLS.

The results from previous studies that estimated snow depth using UAS (Table 1) show significantly higher errors compared to the findings Lee et al (2021). Lee et al., (2021) investigated the accuracy of fresh snow measurements and reported a **median of residuals** ranging from −2.30 cm to 5.90 cm and a **Normalized Median Absolute Deviation (NMAD)** ranging from 1.78 cm to 4.89 cm under optimal condition (50 m flight altitude and 80% overlap ratio). Lee's result also suggests that the controlling factors for the precise measurement of snow depth are **GCP abundance, accuracy, and spatial configuration**, not sensor and drone performance.

Table 1: Summary of studies that estimated snow depth using UAS. Adopted after source Lee et al., (2021) and Adams et al., (2018).

Author(s)	Area (km^2)	UAS type and camera (1)	Flight Method (2)	GSD (3)	MP (4)	Result (SD) and (RMSE) [cm]	Use of RTK (5)
Vander Jagt et al., (2015)	0.007	SkyJiB2 (MC); VIS	~29 m 85–90%	0.6	20	RMSE = 18.4 cm 9.6 cm	-
De Michele et al., (2013)	0.03	Swinglet (FW); VIS	130 m 80%	4.5	12	SD = 0.13 m 14.3 cm	-
Marti et al., (2016)	3.1	eBee (FW); VIS	150 m 70%	10–40	343	SD < 0.63 m NMAD <38 cm	RTK
(Lendzioch et al., 2016)	0.26 (site A); 0.005 (site B)	Phantom 2 (MC); VIS	35 m 60–80%	~1	10	SD = 0.22 m, 0.36 m RMSE = 22 cm, 42 cm	-
Harder et al., (2016)	0.65 (site A); 0.32 (site B)	eBee (FW); VIS	90 m 70%; 90 m 85%	3	34 83	SD = 6–8 cm RMSE = 8–12 cm, 8–9 cm	RTK
Bühler et al., (2016)	0.29	AscTec Falcon 8 (MC), Sony NEX-7 camera, VIS and NIR	157 m 70 %	3.9	22	RMSE from 7-15 cm (meadows, rocks) to 30 cm (bushes, tall grass	-
Miziński and Niedzielski, (2017)	0.005	eBee (FW); VIS and NIR	151 m	5.3	42	RMSE = 41-58 cm NMAD = 37–55 cm	-
Goetz and Brenning, (2019)	0.05	Phantom 4 (MC); VIS	65 m 75%	2.1	80	15 cm	-
(Avanzi et al., 2017)	0.0067	hexacopter; VIS	80 (summer)-90 (winter) %	about 0.02 m.	A regular grid of points ~5 m	SD = 5.6-2.5 cm; RMSE = 6.9-3.6 cm	-
(Bühler et al., 2017)	0.12 (site A) 0.12 (site B)	site A: AscTec Falcon 8 octocopter (MC) site B: Multiplex Mentor Elapor (FW); VIS =λ = 400–700 nm and NIR, λ = 700–830 nm))	approx. 100 m, 70 %	0.02-0.05	-	SD = 0.11–0.19 m; RMSE = 0.17–0.23 m RMSE = 0.18–0.77 m	-

(1) Camera spectrum Visual: (VIS) and near infrared (NIR), UAS type – fixed wing (FW), multicopter (MC). (2) Flight Method: numbers represent flight height and forward overlap, respectively. (3) GSD: ground sample distance (cm/px). (4) MP: number of ground measurements of snow depth. (5) RTK: Real-time kinematic positioning.

3.3 Accuracy of UAS results

Accuracy of results is influenced by:

1) **mission planning**: it is recommended to include both **nadir + oblique** images (James et al., 2020); lower UAS flight altitude (Lee et al., 2021)

Low flight altitude of UAS and high overlap ratio increases the number of the tie-points, which enhances the accuracy of the snow map. According to (Tekeli and Dönmez, 2018) the higher SD values the bias in SD calculation is lower.

2) **percentage of image overlap**; greater photograph overlap lower the NMAD and median of residuals: QΔD (Lee et al., 2021), however forward image overlap higher than 95 % is also not recommended (Seifert et al., 2019)

3) **resolution of land surface**: ground sample distance (GSD)

4) **number and placement of GCP**; greater number of GCPs lowers NMAD and QΔD; spatial configuration and accuracy of GCP coordinates influenced the accuracy of the snow depth distribution map (Lee et al., 2021)

Ideally, GCP should be distributed around the edge of the study area to lower planimetry errors and inside use **stratified** distribution with density of around 0.5-1 GCP. ha^{-1} to minimalize altimetry error, as suggested by Martínez-Carricondo et al. (2018). This led to more accurate results than regular grid placement according to Martínez-Carricondo et al., (2018) results. GCPs should also be evenly distributed evenly across the entire study area and different altitude bands, as recommended by Bühler et al. (2015). While increasing the number of GCPs generally improves accuracy, this strategy can be challenging in hazardous and inaccessible areas, as noted by Tomaštík et al. (2019). To achieve high accuracy in the final products, it is advisable to maintain a GCP density of at least 1 GCP/ 200 m^2 (0.02 ha^{-1}), as recommended by Oniga et al. (2018).

5) **meteorological conditions** temperature change of the device, wind, not sufficient/ ambient light conditions, foggy, sharp sunlight; avoid overcasted sky or shadows (Bühler et al., 2017).

To achieve plausible results, it is recommended to ensure:

1. Direct sunglight, avoid overcast sky or shadows as they cause higher noise (Bühler et al., 2017)

2. Validated UAS results with in-situ or TLS data (accuracy of approximately ± 0.3 m and a root mean square error of 0.23 - 0.32 m), GNSS method (Bühler et al., 2017b); RMSE - 0.036, UAS and MultiStation data; or manual probing (UAS data and manual probing - 0.31 m) (Avanzi et al., 2017).

3.4 Processing of UAS limitations - Photogrammetry of snow covered terrain

3.4.1 Choice of image format and issues with image saturation

For accurate orthophotos, low-compression JPEG or TIFF images (level 12) are recommended instead of DNG images. JPEG images with compression level 12 preserve image detail, minimize artifacts, and are especially suitable for UAV photogrammetry (Alfio et al., 2020). For flat or slightly flat surfaces, the differences between TIFF, JPEG, and DNG images may be less noticeable. However, for complex 3D models, the choice of image format becomes more critical in preserving fine details and ensuring accurate representations of the terrain (Alfio et al., 2020).

Shadows and bright, homogenous areas can introduce noise into the DSM. Fresh snow is less suitable for photogrammetry, than an older weathered surface with developed features like sastrugi or wind ripples. Insufficient light reduces image contrasts which might affect the accuracy and utility of SD estimates (Tekeli and Dönmez, 2018). Problems might occur if reflections of the sun on the snow saturate the camera sensor. Two things are recommended: setting up the proper camera exposition and to store imagery in raw format using the full bit depth of the sensor, typically 10 to 14 bits (Bühler et al., 2016). We may also apply enhanced algorithms for image matching and orientation specialized to resolve image saturation, such as Semi-Global Matching (Lee et al., 2021). Another alternative is to scatter tiny colour papers using the UAS before taking photographs (Lee et al., 2021). Furthermore, using NIR could help to disreveal fine structures as snow absorbs more energy in the near-infrared (NIR) part (760–2500 nm) of the electromagnetic spectrum than in the visible part (400–700 nm) and the reflection is sensitive to snow grain size (Warren, 1982) at the snow surface.

Reconstructing snow surfaces using SfM can be difficult due to several factors:

1) Limited texture and image contrast in the acquired images: snow surfaces often lack distinct features and visible contrasts, making it challenging for image-matching algorithms to identify corresponding points across multiple images.

2) Varying lighting conditions (luminance): changes in lighting intensity and direction can significantly alter the appearance of snow, further complicating the feature-matching process. Light plays a crucial role in the SfM workflow as it improves the ability to distinguish fine details by increasing image contrast (Gaiani et al., 2016). The SFM method's performance can be affected by different sky conditions, such as flat lighting due to an overcast sky, which may necessitate further testing and evaluation (Nolan et al., 2015; Vander Jagt et al., 2015).

3) Homogeneous surfaces: snow surfaces often exhibit a uniform texture, making it difficult to distinguish between homologous points in different images (Gindraux et al., 2017).

4) Lack of image contrast impact on feature tracking: the lack of image contrast can hinder the ability of SfM algorithms to track features across images (Barnett et al.,

2005; Westoby et al., 2012), particularly for large focal length images where each frame captures only a small area.

Further research is needed to determine the effect of snow's physical characteristics on surface DEM reconstructions, as the image texture can vary significantly depending on the type of snow surface (e.g., fresh, wind-packed, etc.) (Bühler et al., 2016; Vander Jagt et al., 2015).

3.4.2 Influence of surveying time and shadows

A significant positive bias, which represents a measure of how far the expected value of the estimate deviates from the true value, is evident for the surveying times of 9 a.m. and 3 p.m. This bias is likely attributable to time-dependent accuracy issues with the shadows cast by objects. Generally, the accuracy of photogrammetry results tend to decrease as shadow sizes increase, and this effect is more pronouced the further the surveying time is from noon. For example, the time gap between images taken in different swaths can be several minutes, and even within those few minutes, the size of the shadows can change significantly during the early morning and late evening hours (Bühler et al., 2016). According to the photogrammetric data, **SD appears noticeably greater in areas with shadows.** Furthermore, areas with high brightness contrast are more prevalent in the morning and evening, which can introduce additional bias into the overall results of photogrammetry (Lee et al., 2021). Areas with animals tracks or wind features help with brighter image contrasts (Fig. 3-a).

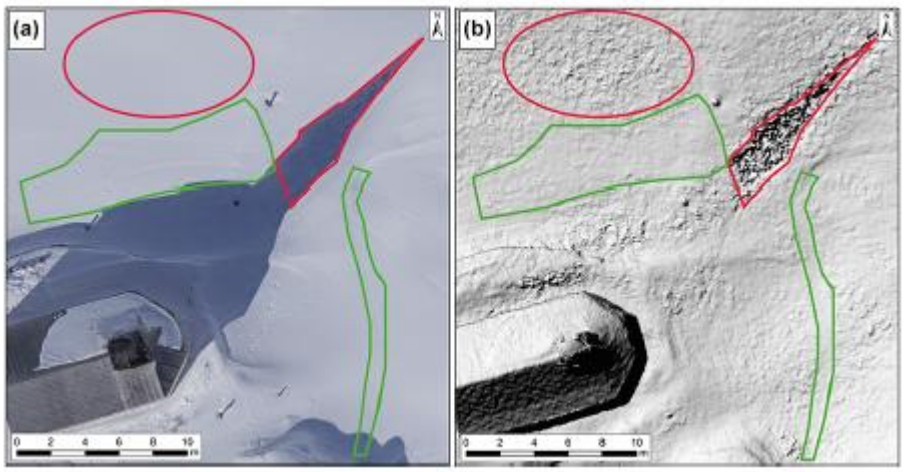

Fig. 3-a: Influence of shades (a) and hillshade of the derived DSM (b). Areas in red show very homogeneous snow surfaces either in cast shadow or nearly saturated areas. Areas marked in green are areas with better contrast at the snow surface due to tracks of animals or wind features. Reused from (Buhler et al., 2016).

3.4.3 Camera processing limitations and bundle adjustment

Processing UAS limitations are:

1) camera calibration and bundle adjustment,
2) stability of internal orientation – radial lens distortion is affected by camera distance from the screened object/ area,
3) In general, smooth fresh snow does not provide features for detection (known as tie points), which might result in a significant error (Lee et al., 2021).

Camera calibration plays a significant role in determining the internal parameters and lens distortion of the camera (Fig. 3-b). The placement of GCPs is crucial for accurately estimating reverse calibration.

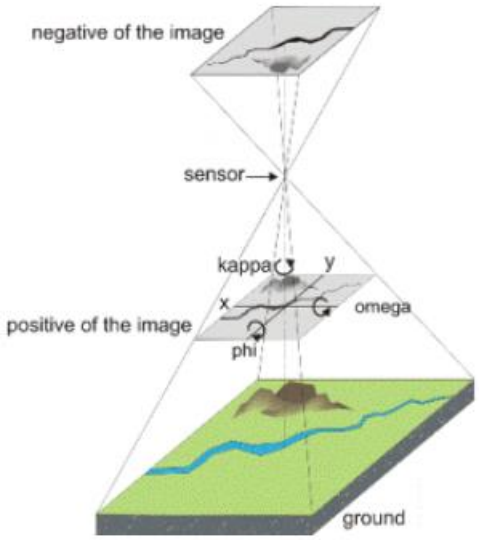

Fig. 3-b: Understanding omega, phi, and kappa parameters. Adapted from: Wolf et al., 2014.

The bundle adjustment process aims to optimize both exterior and interior orientation, s well as correct lens distortion. To achieve accurate results, it is essential to ensure that the input parameters of bundle adjustment have minimal noise. The internal orientation elements define the geometry of the rays within the cameras image coordinates, while the outer orientation elements define the position (centre of the input pupil $X0$,$Y0$,$Z0$) and inclination (ω,φ,κ) of the cameras measuring chamber (Sedlina, 2021). Considering the various instabilities, it is advised to use reverse camera calibration (Sedlina, 2021). Additionally, re-processing techniques can improve point cloud density and accuracy, accounting for different image qualities and lighting conditions in the snow environment.

3.4.4 Methods of DEM's orthorectification

The UAS-based photogrammetry snow depth extraction method involves subtracting an underlying topography DEM (DTM) from the snow surface cover DEMs (DSM) generated using SfM. Accurately aligning the two Digital Surface Models (DSMs) is crucial for determining snow height (snow-covered DSM minus snow-free DSM). Even minor displacements in the x and y directions can lead to significant changes in the z-direction, especially on steep slopes. Several referencing approaches are available to achieve the necessary precision.

Three main methods for referencing digital surface models (DSMs) exist:

1. **Artificial reference points** (RPs): This method involves placing artificial markers, such as targets or monuments, at known locations within the study area. These markers are then precisely measured using differential GNSS to establish a reference for the DSM. While this method is the most accurate, it also requires the most fieldwork, which can be time-consuming and expensive.

2. **Reference one DSM and compare to another**: This method involves referencing one DSM to the real world using differential GNSS and then comparing it to a second DSM. This is done by identifying and matching points in both DSMs that are clearly visible in both snow-free and snow-covered imagery. While this method is less accurate than the first method, it requires less fieldwork.

3. **Natural RPs**: This method involves identifying and matching natural landmarks, such as buildings or rock formations, in both snow-free and snow-covered imagery. These landmarks are used to establish a reference for the DSM, but their coordinates are not as precise as those of artificial RPs. This method is the least accurate but requires no fieldwork (Bühler et al., 2016).

Methods 2 and 3 are only applicable in areas with distinct terrain features that are not completely covered by snow. The identifying and matching reference points is difficult or impossible in areas with uniform terrain or complete snow cover.

3.5 UAS DEMs types of errors and manual probing uncertainty

The produced DEMs obtained from UAS data are subject to two types of error.
1) The first type is a georeferencing error, which can be affected by factors such as the quality of the GNSS post-processing, the allocation and identification of GCPs in the images, and accuracy of the antenna height.
2) The second type of is a photogrammetric reconstruction error, which is influenced by the overall quality of the photosets.

One of the validation method can be manual probing which is influenced by the type of surface: icy layers in snow profile, peat bogs, dwarf pines, blueberry bushes, rocks. The comparison between the UAS map and manual samplings obtained the RMSE of 0.31 m (Avanzi, 2017), SD below 30 cm is also reported in previous works using UAS on snow or glaciers (Bühler et al., 2016; De Michele et al., 2013; Harder et al., 2016; Lendzioch et al.,

2016; Vander Jagt et al., 2015). Often, **larger errors are attributed to vegetated areas** (Bühler et al., 2016; Lendzioch et al., 2016). When areas of potential outliers, such as vegetation or riverbeds, are excluded, the RMSE between UAS data and manual probing drops to 0.06-0.17 m from the range of 0.20-0.30 m (Avanzi et al., 2018). The average difference between **UAS-estimated** and measured **snow depth**, checked with conventional snow probing, ranged from **0.015 to 0.16 m** in (Cimoli et al., 2017).

3.6 Potential of CRNS snow monitoring

The CRNS monitoring for snow is a method of using cosmic ray neutrons to measure the snow water equivalent (SWE). SWE is the amount of water contained in a snowpack. The CRNS technique measures the interaction of cosmic ray neutrons with the snowpack. The hydrogen atoms in snow water slow down cosmic ray neutrons. The more snow water there is, the more neutrons there are to slow down. The SWE can be calculated using this change in neutron count rate. The principal of the method is that snow water moderates epithermal neutron intensity which is directly related to snow water equivalent (Fig. 3-c).

The CRNS method is still under development, however it has shown great potential for water management practices, particularly in soil environment and monitoring mountain snowpacks. They can bridge the gap between traditional in-situ measurements such as snow surveys and remote sensing by providing both spatial and temporal resolution: more accurate and timely data on SWE, in the context of water management in snow-dominated regions. One of the advantages of CRNS is their larger measurement footprint compared to labour-intensive methods like snow pits and snow cores. This allows for more extensive coverage and higher repeat frequency of the surveys, providing valuable data for both gauged and ungauged mountain basins. Other pros are it is a non-invasive method and enables real-time monitoring.

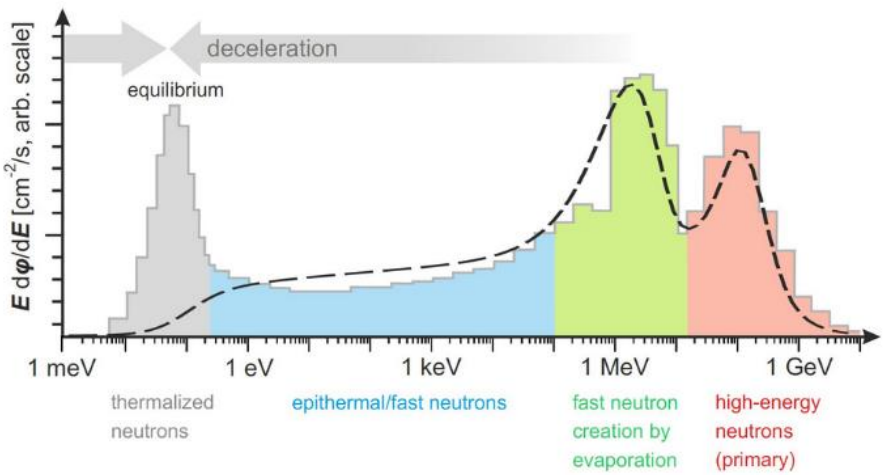

Fig. 3-c: Types of neutrons and energy. Source: The picture is copied from Heildelberg university.[6]

The first application of monitoring a mountain snowpack using above-snow CRNS was done by (Schattan et al., 2017). They were able to detect SD and SWE for Alpine snowpacks. However, the sensitivity of CRNS decreases with higher SWE levels (up to 600 mm). Nevertheless, CRNS can still be valuable for monitoring snow accumulation, as neutron count rates display a sharp decrease with the onset of snow accumulation compared to

[6] https://www.physi.uni-heidelberg.de/Forschung/PAT/Cosmic-Sense/Method/#:~:text=Cosmic%2DRay%20Neutron%20Sensing%20(CRNS,epithermal%2Ffast%20neutron%20albedo%20flux

snow-free conditions, as shown in studies by Delunel et al. (2014), Mark J. P. Sigouin and Si, (2016).

The signal of neutron counts from CRNS can be distinguished between snow and soil environments since the decrease of neutron intensity in the snow is more evident than in wet soil. However, there are limitations to CRNS snowpack monitoring, particularly when dealing with deeper snowpacks. Studies by Mark J. P. Sigouin and Si, (2016), Zweck et al., (2013) suggest that CRNS measurements of snowpack is limited to shallow snowpacks where a mixed signal of snow and soil moisture is observed. Even in the case of small amounts of snow, the concentrated hydrogen layer effectively absorbs fast neutrons reflected from the ground (Desilets et al., 2010; Guidicelli et al., 2021; Mark J.P. Sigouin and Si, 2016). For example, 1 cm of SWE can reduce the neutron count rate by∼10% depending on the soil moisture under the snow cover (Andreasen et al., 2017). Desilets (2017) proposed an upper limit of 100-150 mm SWE, suggesting that beyond this range, the sensitivity of CRNS decreases, and it becomes challenging to accurately distinguish the signal from deeper snowpacks due to the increased attenuation of cosmic-ray neutrons by thicker snow layer. On the other hand, Schattan et al., (2017) showed that CRNS could still detect snow-induced signals even in snowpacks with 600 mm of SWE, especially in high elevation areas where, in general, higher neutron intensities are reached.

The results of CRNS monitoring for snow can be influenced by various factors:
1) The amount of snow water equivalent (SWE) in the snowpack. The more SWE, the more neutrons are slowed down, and the higher the neutron count rate.
2) The depth of the snowpack. The deeper the snowpack, the more neutrons are scattered and the lower the neutron count rate.
3) The density of the snowpack. The denser the snowpack, the less neutrons are slowed down, and the lower the neutron count rate.
4)The presence of other materials in the snowpack, such as ice, firn, or vegetation. These materials can scatter neutrons and reduce the neutron count rate.
5)The ambient temperature. The temperature of the snowpack can affect the scattering of neutrons and the neutron count rate.
6)The geographic location. The latitude and altitude of the snowpack can affect the amount of cosmic rays reaching the Earth's surface and the neutron count rate
7)The type of neutron detector used. Different neutron detectors have different sensitivities to neutrons, which can affect the results.
8)The background radiation level. The background radiation level can affect the neutron count rate, and it is important to correct for this in the analysis.
9)The calibration of the neutron detector. The neutron detector must be calibrated to ensure that it is measuring neutrons accurately[6].

3.7 Avalanche numerical model: RAMMS

Avalanche hazard mapping studies frequently employ numerical models. Numerical model serves for verification of terrain monitoring – area and volume quantification. The diverse methods such as point snow measurements, UAS and gravimetry based, remote sensing methods are used for accurate snow depth measurement that serves as an input data to hydrological models. Both the effects of potential hazard scenarios can be forward calculated as well as back-calculated: the documented avalanche events at a specific site in RAMMS.

RAMMS (Rapid mass movement system) is a 2-D model on a 3-D terrain. Although RAMM´s hydraulic principle, employs a Voellmy-fluid friction model based on Voelmy-Sam approach (Salm, 1993), is now slightly outdated, the model can numerically express the slab avalanches flow. A beneficial feature of this model is the possibility of full user control on the friction parameters. If it is well-known avalanche path – it enables to define areas with different friction parameters which enables real situation approximation. It has a user-friendly environment (Christen et al., 2010).

Mostly, RAMMS was used in the Alps, however, was also verified in Modrý důl (Racek and Blahůt, 2016) (low altitude Krkonoše mountains, the highest peak is 1602 m a.s.l.) and in limited usage in Beskydy (Richnavský et al., 2010). Therefore, for the purpose of this dissertation thesis, we used it for the study site: Žlab Úpičky avalanche path.

II. PART

WET SNOW AND SLAB AVALANCHES IN THE KRKONOŠE MOUNTAINS

WET SNOW AND SLAB AVALANCHES IN THE KRKONOŠE MOUNTAINS

The following section describes the study area and their data in the Krkonoše mountains, a low-altitude mountain range in Central Europe. We report on the avalanche activity dataset, meteorological and snow data preparation.

4 Krkonoše Mountains (NE Czechia) study area and data preparation

In the following section, we present Krkonoše's geology, geomorphology, and land cover. The Krkonoše mountains (Mts.) (internationally known as the Giant Mountains), with the highest peak Snežka at 1603 m a.s.l., comprise the area with the most frequent snow avalanche activity in Czechia. The Krkonoše Mts. extends between Czechia and Poland, with the larger part located in north-east Czechia. Most of the mountain range belongs to Krkonoše National Park (KRNAP), which covers an area of 550 km^2 and has been protected since 1963.

As part of the Variscan and Hercynian Mountain ranges in Europe, Krkonoše is mainly comprised of crystalline schists with several quartzites and crystalline limestones. The central part (border with Poland) is formed of granites, with Alpine orogeny and Quaternary glaciations that carved out several plateaus at an elevation between 1300 and 1450 m a.s.l. (Blahůt et al., 2017). The plateaus host several headwaters (e.g., Elbe River) and glacial cirques (Engel et al., 2010), where small brooks originate in the vicinity of several avalanche-triggering areas and might affect avalanche activity mainly in the snowmelt period. The mean slope of avalanche release areas is 31°, and mean elevation ranges between 1072 m and 1575 m a.s.l.; the avalanche paths are mostly facing east, south-east, and south (Fig. 4-a) (mean aspect is 168°). Released areas were vectorized over the orthophoto and camera photos were collected in the field and delimited by Krkonoše National Park (KRNAP).

The biogeographical location of the Krkonoše mountains consists of a varied mosaic of montane spruce and mixed forests, tall herb meadows, dwarf pine communities, Nardus grasslands, subarctic peat bogs, and lichen tundra. According to the KRNAP Green Infrastructure map, the avalanche release areas consist mainly of alpine meadows (39.7 %), natural cypress (32.7 %), and rocks and scree (21.0 %) (MaGICLandscapes, 2020). A few spruces, peat bogs, and springs are spread in avalanche release areas (< 3 %). The treeline lies between 1200–1350 m a.s.l. (Štursa et al., 2010). Prevailing westerly winds (resulting in

relatively low snow accumulation on the west-facing, windward slopes, while steep, leeward slopes accumulate much more snow) (Blahůt et al., 2017) favour cornice avalanches.

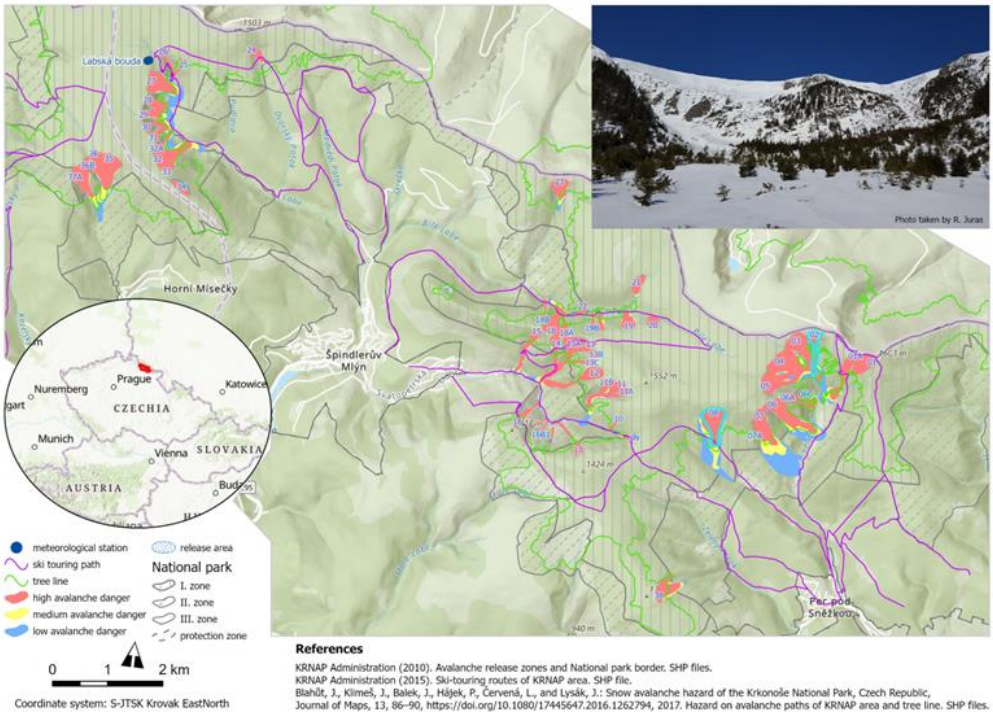

Fig. 4-a: Study location of avalanche activity in the Krkonoše Mts. The investigated Aval paths are marked with azure line.

4.1 Avalanche activity dataset (frequency, magnitude and aspect) over 59 winter seasons (1962–2021)

Avalanches, as rapidly moving snow masses with a minimum length of 50 m, have been systematically monitored on 60 avalanche paths in the Czech part of Krkonoše since the 1962 winter season (the first record was on 13 January 1962) (Spusta et al., 2020) (Fig. 4-a) by the KRNAP administration, Krkonoše Mountain Rescue Service. During 59 winter seasons (from 1962 to 2021) 1246 avalanches were recorded on the Czech site of the Krkonoše avalanche dataset. We define the winter season from 1 October to 31 May; i.e. 1 October 1961–31 May 1962 is assigned to 1962. Snow avalanches are classified by international codes (Quervain, 1973), with a little modification for the Krkonoše mountains. The dimensions of each avalanche are listed in, for example, (Vrba and Spusta, 1975), 1991), Spusta and Kociánová (1998), Spusta et al. (2003, 2020) and (Součková, Markéta et al., 2022).

4.2 Meteorological and snowpack data preparation

Daily data are freely accessible through the Czech Hydrometeorological Institute (CHMI). We used meteorological data from an automated weather station: Labská bouda (LBOU, 1320 m; Fig. 4-a). For the purpose of the study, we created two wet- and slab-avalanche datasets with the variables listed in Table 2 which are also in Table 1 in NHESS article (Součková, M. et al., 2022). Besides the measured values, we calculated two additional variables representing two different rainfall estimates. There are more methods to determine rainfall from total precipitation. First we used rainfall (Rain_Tw) based on single-threshold wet-bulb temperature (T_t= −0.5 °C) calculated according to the Stull (2011) formula. Second, we used rainfall separated from the total precipitation (Rain_Ta) based on single-threshold air temperature (T_t= +0.46 °C), which was calibrated for the Elbe catchment (Juras et al., 2021). Apart from station-measured variables, we generated 3 d moving-average windows of the input variables and sums of selected variables (Table 2). By using a moving average, the curve is smoothed, and it helps to better identify a trend or trend change; sums highlight the effect. Even though snow water equivalent would be a promising predictor of avalanches, we excluded it from the dataset as it is, unfortunately, measured only weekly in Czechia, and the interpolated data could be misleading. The winter season was considered a period from 1 October to 31 May when snow can be observed at the study site.

For the purpose of machine learning analysis, the wet and slab datasets contain the avalanche days (ADs) and non-avalanche days (NADs) and are linked to meteorological data available since 1979. An AD was defined within the winter season as when at least one avalanche was recorded and a NAD as when no avalanche was recorded. We explored the occurrence of avalanches based on the course of hydroclimatic variables during the previous 6 d. NADs that occurred 6 d after an avalanche record were deleted to minimize the dependency on preconditions between ADs and NADs. Datasets should not contain any missing values as some machine learning algorithms do not deal with them correctly. Therefore, we excluded them using 38-year-long data time series (1979–1999 and 2002–2020 data periods; 2000–2001 was omitted) as the station Labská bouda (LBOU) did not operate during 2000–2001. For the trend variable analysis 1999 and 2002 were also excluded

as the variables had fewer than 50 % of data. For nonlinear models, colinear variables can remain.

5 Method

This chapter includes changes in frequency, size, and aspect of wet and slab avalances since 1962 by statistical means: trend analysis. Next, the chapter suggest a method suitable for balancing avalanche and nonavalanche datasets. Lastly, it detects the main weather and snow variables for these types of avalanches using machine learning over the period 1979-2020 to understand the variables: their development in time and determine primary drivers.

5.1 Filtering avalanche types and avalanche activity changes

In order to know the trends of wet- and slab-avalanche activity, we filtered two types of avalanches from the avalanche dataset according to the following criterias: zone of origin (known as release area) (a) manner of starting (A2 line release zone, 271 avalanche records ("Aval"); A3 soft slab, 514 Aval; A4 hard slab, 45 Aval; 4 no value, NA, of avalanche length) and (b) liquid water in snow (C = 2, 186 Aval; 1 NA of avalanche length) according to the avalanche classification (Quervain, 1973). We chose two avalanche types. First, the wet-avalanche dataset, defined by wet snow (liquid water presence) in a release area, was chosen as an indicator of changing climate and, second, slab avalanches were chosen as the most frequent and dangerous avalanche type for skiers on the Krkonoše mountains (Schweizer and Föhn, 1996). The selection of these two avalanche types is also based on avalanche danger models suggested by (Mair and Nairz, 2020).

Long-term trends in frequency, size, and aspect as well as basic weather parameters were analysed for both selected groups. We processed avalanche data characteristics for wet-snow and slab avalanches: count, magnitude (avalanche size) of avalanche length, and aspect. Avalanche activity trends in the avalanche dataset were explored over periods (1962–1991 and 1991–2021) by the Mann–Kendall τ. Kendall's Tau is a non-parametric measure (meaning there is no underlying assumption made about the normality of the data) of relationships between columns of ranked data. The Tau correlation coefficient returns a value of 0 to 1, where:

0 is no relationship,

1 is a perfect relationship.

To compare changes in avalanche size. Each recorded avalanche path length was related to the potential maximum avalanche length – 100-year return period (RP) output from the Rapid Mass Movement Simulation Avalanche module (RAMMS:: Avalanche, considering the topography and terrain roughness; Christen et al., 2010) – and were computed by (Blahůt et al., 2017; Fig. 5 a). This method enabled us to compare avalanche sizes among paths of different lengths objectively.

The aim was to compare changes in avalanche size. Each recorded avalanche path length was related to the potential maximum avalanche length – 100-year return period (RP) output from the Rapid Mass Movement Simulation Avalanche module (RAMMS:: Avalanche, considering the topography and terrain roughness; Christen et al., 2010) – and were computed by (Blahůt et al., 2017; Fig. 5 a). This method enabled to compare avalanche sizes among paths of different lengths objectively.

5.2 Balancing avalanche and non avalanche data

We analysed the explanatory power of several meteorological and snow variables (Table 2) to explain avalanche triggers for the daily timescale (1979–1999, 2002–2020). We applied tree-based models (decision tree, DT; random forest, RF) to (a) determine the set of the most relevant combinations of explanatory variables for the avalanche occurrence represented as ADs and NADs in the model and (b) quantify how important each variable is and test the model's performance.

A severely imbalanced dataset of wet/slab ADs and of NADs) makes the learning process difficult. Hence, we created balanced datasets to enhance the skill of the model. We tried to balance the datasets by upscaling avalanche records and synthetic data generation; the latter method was more successful in evaluating model efficiency; hence we used the approach for RF – see further in Sect 6.1.3 and 6.2.3. The former upscaled method was better for descriptive purposes, and we used it for only one DT – see further in Sect. 6.1.2 and 6.2.1. The synthetic data generation method (Lunardon et al., 2014) overcame imbalances by generating artificial data via the synthetic minority oversampling technique (SMOTE) (Chawla et al., 2002). A SMOTE algorithm creates artificial data based on feature space similarities from minority samples. It uses bootstrapping and the k-nearest neighbours (KNN) algorithm and works as follows:

- KNN takes the difference between the feature vector (sample) under consideration and its nearest neighbour.
- Differences between neighbours are multiplied by a random number ranging from 0 to 1 (can be adjusted to maintain dispersion in data – our case).
- New data are added to the feature vector under consideration.

Synthetic data had much higher dispersion than the original dataset (after application of aforementioned SMOTE approach); therefore, we generated data closer to our input data by adjusting the natural-neighbour algorithm with kernel density (ranging in our case from 0 to 0.5). Thanks to the SMOTE method, we can generate data with a similar statistical distribution along with the two classes of avalanche types. For further details on checking distributions of initial datasets of weather variables of original and synthetic data see more details in Appendix A: named „Exploratory dataset analysis of original and synthetic data“ in NHESS article (Součková, Markéta et al., 2022).

Prior to evaluation of the models, we split datasets into training (0.75) and test sets (0.25). For evaluation we used confusion matrices (CMs), the receiver operating characteristic (ROC) curve, and area under the curve (AUC). A CM makes a two-way frequency table and compares predicted versus actual classes (Table A1 in NHESS) in (Součková, M. et al., 2022). The ROC curve is the ratio of the sensitivity and specificity; by increasing one measure, the other is decreased. The AUC coefficient is defined as an area under the ROC curve and is a single-number summary of a model's predictability, ranging from 0 to 1; when AUC = 1 it

means that the model is correct all the time at predicting (Biecek and Burzykowski, 2021; James et al., 2021).

Table 2: Description of the weather variables used for machine learning.

Variable	Abbreviation	Model	Explanation
Snow depth [cm]	SD	SD_value	Daily mean snow depth
		SD_value3	3 d moving average of snow depth before avalanche release (day when Aval occurred)
		SDdif2, SDdif3, SDdif4	2, 3, 4 d snow depth difference from the day when avalanche released; SDdif = SD_value − SD_value2, SD_value3, or SD_value4
New-snow sum [cm]	NSS	NSS_value	New snow fallen in a day
		NSS_value3	3 d moving average of new snow before avalanche release (day when Aval occurred)
		NSSsum3	Sum of 3 d new snow before avalanche release
Relative humidity [%]	RH	H_value	Daily relative humidity
		H_value3	3 d moving average of relative humidity before avalanche release (day when Aval occurred)
Air temperature [°C]	Tair	Tair_value	Daily mean air temperature [°C]
		Tair_value3	3 d moving average of air temperature before avalanche release (day when Aval occurred)
		Tmin3	3 d minimum air temperature [°C]
		Tmax3	3 d maximum air temperature [°C]
		Tamp3	Thermal amplitude the day before and up to 3 d before the avalanche release [°C]; Tamp3 = Tmax3 − Tmin3
Sunlight duration [h]	SLd	SLd_value	Daily sunlight duration
		SLd_value3	3 d moving sum of sunlight duration before avalanche release (day when Aval occurred)
Precipitation [mm]	P	P_value	Daily total precipitation
		P_value3	3 d moving sum of daily precipitation
Rainfall [mm]	Rain_Tw	Rain_Tw_value	Daily rainfall separated from total precipitation (P) based on single-threshold ($T_t = -0.5\,°C$) wet-bulb temperature (calculated according to Stull, 2011, formula).
		Rain_Tw_value3	3 d moving average of Rain_Tw_value
Rainfall [mm]	Rain_Ta	Rain_Ta_value	Daily rainfall, separated from the total precipitation (P) based on single-threshold air temperature ($T_t = +0.46\,°C$) T_t was calibrated by (Juras et al., 2021).
		Rain_Ta_value3	3 d moving average of Rain_Ta_value
		Rain_Ta_sum3	3 d sum of Rain_Ta_value prior to the avalanche event
Wind speed [$m\,s^{-1}$]	WSavg	WSavg_value	Daily mean wind speed
		WSavg_value3	3 d moving average of wind speed before avalanche release (day when Aval occurred)
Wind direction [°]	WD	WD_value	Daily circular mean of wind direction
		WD_value3	3 d moving circular average of wind direction before avalanche release (day when Aval occurred)

5.3 Snow avalanches drivers assessed by machine learning

In our analysis, both the Decision Tree (DT) and Random Forest (RF) methods were employed to analyse avalanche data. The DT (Therneau and Atkinson, 2019) method to find some variable threshold separating ADs and NADs to obtain the most significant variables determining wet and slab avalanches. DTs are a useful tool to comprehend the identification and assessment process of avalanche problems because they present relationships in a way that is resembling to human decision-making processes, as discussed by (Horton et al., 2020). On the other hand, the RF method, proposed by Liaw and Wiener (2002), focuses on predictive performance.

The RF method was used to predict a binary target variable, specifically the occurrence of unique ADs and NADs, with multiple predictor variables, in this case, weather and snow variables. RF is known for its robustness against overfitting and its ability to generate accurate, nonlinear models. It achieves this through bootstrapping observations from the dataset (bagging), which generates the out-of-bag (OOB) error rate, and by randomly selecting variables for comparison during the classification process. By training a sufficient number of trees, the RF model stabilizes the OOB error and produces reliable results. This eliminates the need for additional cross-validation to prevent overfitting.

RF classifiers can improve prediction accuracy but at the cost of interpretability (Sielenou et al., 2021). However, RF allows for feature (variable) importance analysis by conducting permutations on all variables, enabling us to assess the influence of each variable on the accuracy of the decision-making process. Therefore, we can distinguish what influence each of the variables has on the accuracy of the decision classifier process if we exclude a variable. The variable importance is quantified using mean decrease in accuracy (MDA), where a higher value indicates a more important predictor, as described by (Gregorutti et al., 2017). To gain better performance of the RF, we fine-tuned the hyperparameters. Hyperparameters impact the model fit and can vary across different datasets (Probst et al., 2019). By employing a grid search technique, we explored various combinations of hyperparameters and evaluated the models performance through cross-validation. Based on the area under the curve (AUC) metric, we selected the best-performing hyperparameters.

6 Results

This chapter focuses on statistical analyses of the avalanche datasets and relates meteorological and snow variables to wet and slab avalanches. Firstly, we show the trend analysis results of the avalanche activity in the study location. We investigate changes in wet and slab avalanches over the winter seasons (1962–2021). We assess the explanatory power of the weather variables concerning wet- and slab-avalanche activity using two methods – DT and RF. To highlight the potential effect of climate change on avalanche activity, we investigate the meteorological and snow variable trends for the LBOU meteorological station.

In the Krkonoše mountains, on average of 20 snow avalanches are reported each year. This number varies greatly year to year and ranges from 0–77 records (no record in winter 2011, 77 records in 2005). We focus on wet avalanches (185 records, 14.8 % of all snow avalanches in the avalanche cadastre) and slab avalanches – the most frequent avalanches (826 records, 66.3 %) – in the Krkonoše mountain range. The percentages of avalanche activity are related to 1246 avalanches recorded over the period 1962–2021.

6.1 Wet snow avalanches changes and their drivers

6.1.1 Long-term wet-avalanche activity

It was revealed that the number of wet avalanches classified in the cadastre as wet, i.e. $C = 2$ (185 Aval), increased during the period 1962–2011. However, it has slightly decreased in the last decade, 2011–2021. The highest number of wet avalanches was observed in 2005. Over the last 3 decades there were about 7 times more wet avalanches (163 total wet avalanches, annual mean 5.6) than in 1961–1991 (22 total avalanche releases, annual mean 0.7) (Fig. 6-a). The wet-avalanche activity also changed within the winter season, when we observe increases in avalanche occurrence in March, followed by February, in the last 3 decades (Fig. 6-b). Conversely, decreases are observed in December, January, April, and May.

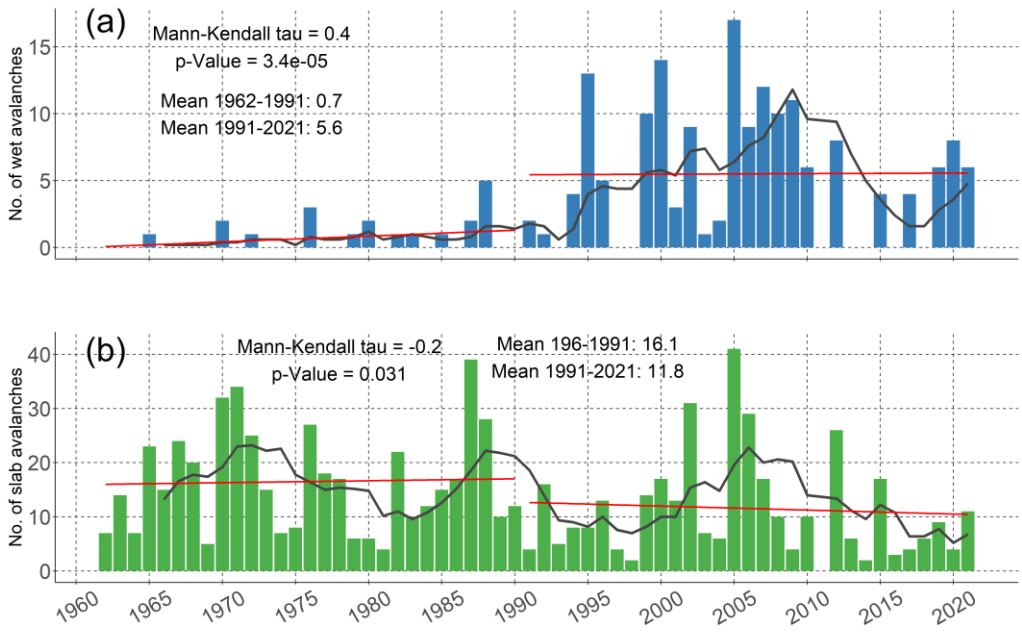

Fig. 6-a: Occurrence of wet and slab avalanches over the winter seasons 1962–2021. Each year represents the winter season (1 October–31 May). The trend was analysed by Mann–Kendall τ; its significance was estimated by the p value for two periods, 1962–1991 and 1991–2021 (red line), and the five-season moving average (black line). The count of avalanches for each subperiod is calculated as a seasonal mean.

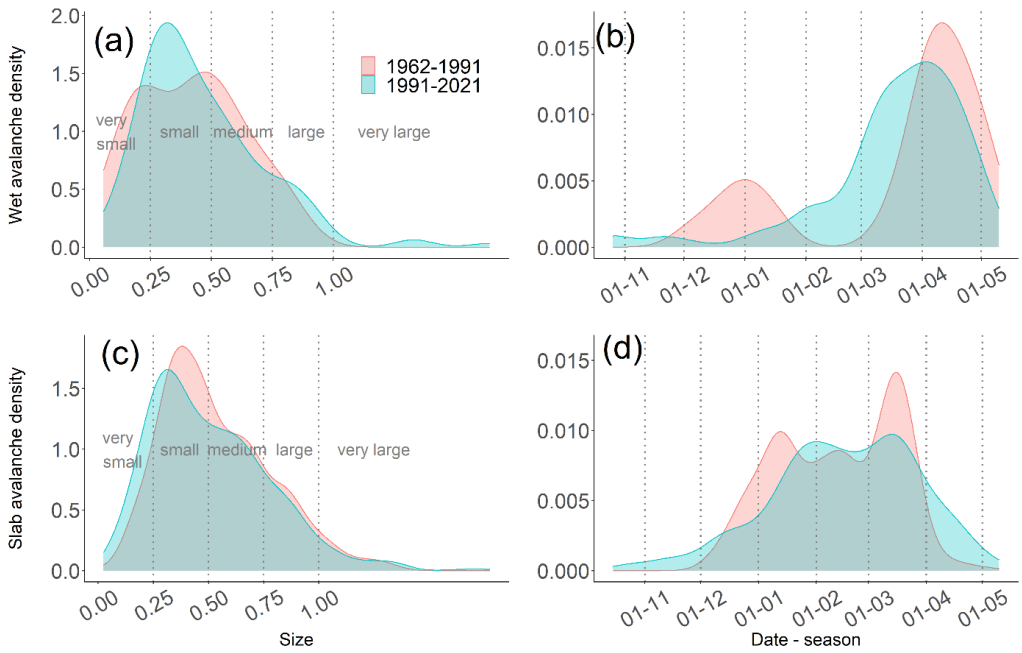

Fig. 6-b: Wet-snow and slab-avalanche characteristics split into two winter season periods, 1962–1991 and 1991–2021. (a) Proportional sizes of avalanche length related to the RAMMS 100-year return period output. (b) Winter season distribution of avalanche occurrences.

The avalanche length magnitude (size) denotes a moderate rise on a proportional scale (0.2–0.4) and large and very large avalanches (> 0.8) from 1991 to 2021. More very large wet avalanches appeared during the period 1991–2021 in comparison with 1961–1991. We observe a rise in the number of wet-snow avalanches in the last 30 years and a shift in the peak of avalanche releases towards earlier in the year, from the middle of April to the beginning of April during the winter season (Fig. 6-b). In general, wet avalanches mainly occur in March and April; however, more wet-avalanche releases are present in February in the last 30 years (Fig. 6-b).

The most wet-avalanche releases were in the eastern (E), south-eastern (SE), north-eastern (NE), and south (S) in the period 1961–1991, whereas, in the last 30 years, the highest number of avalanches have been on the SE, E, S, and NE sides. The greatest change (24 percentage points – pp) in wet-avalanche activity can be seen on the SE slopes, while the proportion of wet avalanches increased from 23 % (1962–1991) to 47 % (1991–2021). On the other hand, the highest decrease (9 pp) was observed on the E slopes, when the proportion changed from 36 % (1962–1991) to 27 % (1991–2021) (Fig. 6-c).

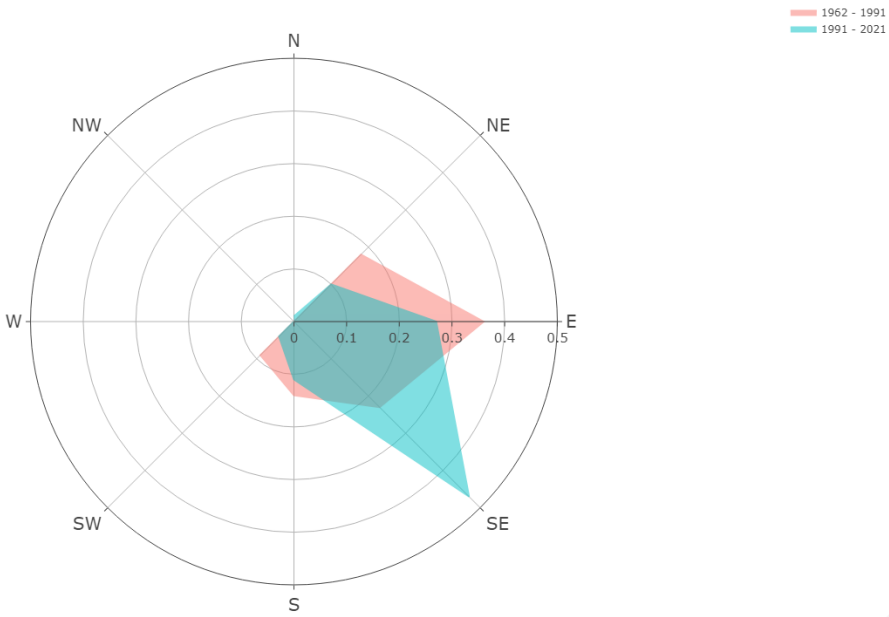

Fig. 6-c: The avalanche occurrence distribution per path orientation for wet-snow avalanches. Radial axis represents the avalanche proportion for each cardinal direction.

6.1.2 Decision tree of wet avalanches

We analysed weather variables determining triggering of wet and slab avalanches in the period 1979–2020. The wet-avalanche dataset contains 91 unique wet-snow-avalanche days, and the slab-avalanche dataset contains 271 avalanche days.

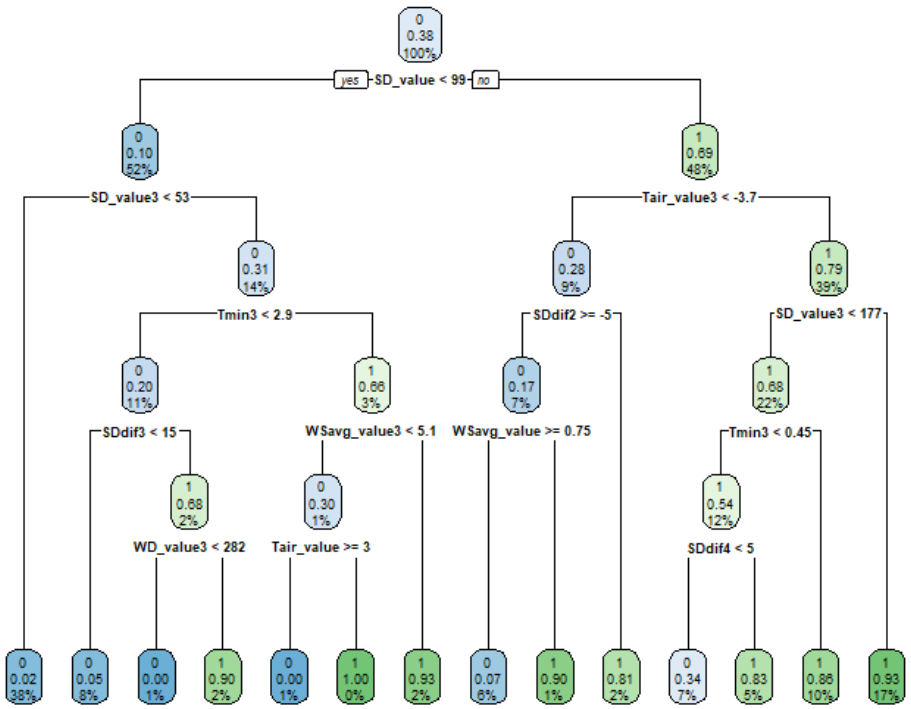

Fig. 6-d: The decision tree of weather variables triggering wet avalanches. Numbers 1 and 0 denote avalanche day and non-avalanche day. The single value means the probability of occurrence/non-occurrence of avalanche release. The percentage signifies what percent of data are influenced by the split node from the wet SMOTE avalanche dataset.

The daily mean snow depth was the primary split in the decision tree of wet avalanches that splits days with and without slab avalanches (Fig. 6-d). The group of days with more than or equal to 99 cm had a probability (p) of 0.38 that an avalanche would occur. If 3 d moving-average air temperature (Tair_value3) ≥ −3.7 °C, we obtain a 0.69 likelihood of avalanche trigger, using 48 % of the observational data. If SD_value3 is higher than 177 cm, there is a high probability of avalanche release (p=0.79). When SD_value3 < 177 cm is slightly above a zero 3 d minimum air temperature, an avalanche is likely to be triggered (Tmin3 ≥ 0.45 °C, p=0.68). Other significant splits (p > 0.9) are mean wind speed (WSavg_value3 ≥ 5.1 m s^{-1}) and wind direction (WD_value3 ≥ 282)Fig. 6-d) The higher the snow depth, the higher the probability of avalanche trigger. This might be because of the fraction of wet snow compared to dry within the snowpack.

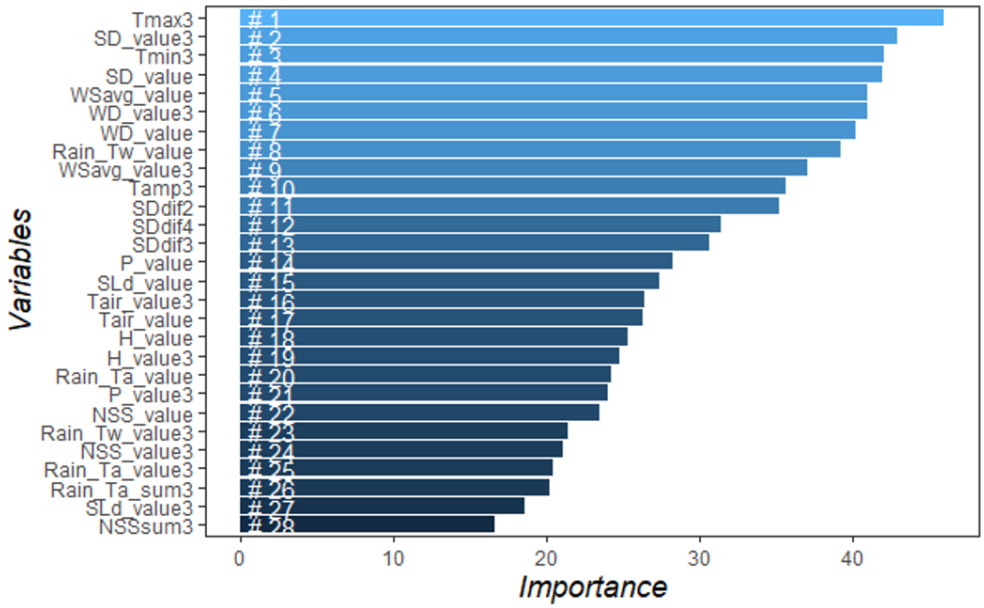

Fig. 6-e: Variable importance using the mean decrease in accuracy (MDA) for each variable of the wet-avalanche dataset (winter seasons 1979–2020) in the random forests. Variables are described in Table 1 in NHESS.

6.1.3 Meteorological and snow variables driving the wet-avalanche activity using the random forest model and trend analysis

The random forest model ranked the most important variables based on variable importance (VIP) using MDA. The most important variables for wet avalanches seem to be 3 d maximum and minimum air temperature (Tmax3, Tmin3), snow depth (SD_value3, SD_value), wind speed (WSavg_value, WSavg_value3), wind direction (WD_value3, WD_value), and rainfall based on wet-bulb temperature (Rain_Tw_value) (Fig. 6-e). Sunlight duration (SLd_value) and precipitation are almost 1.6 times less important than 3 d maximum air temperature. From snow depth difference variables, the most important is when it is 2 d different from the avalanche day (SDdif2) (Fig. 6-e). Wet-bulb temperature is calculated from humidity, so humidity also plays a role; however, its importance is 25. The wet-avalanche model predicts 84 of 91 avalanches (92.3 %) and 6555 of 6588 non-avalanches (99.5 %). There were 33 false-alarm wet-snow avalanches (Fig. 6-f), which means that the model tends to falsely predict wet avalanches that are non-avalanches in real-world scenarios. This would falsely

imply that there is a high probability of avalanche occurrence. The models perform well according to the AUC criterion with 0.992 (Fig. 6-f).

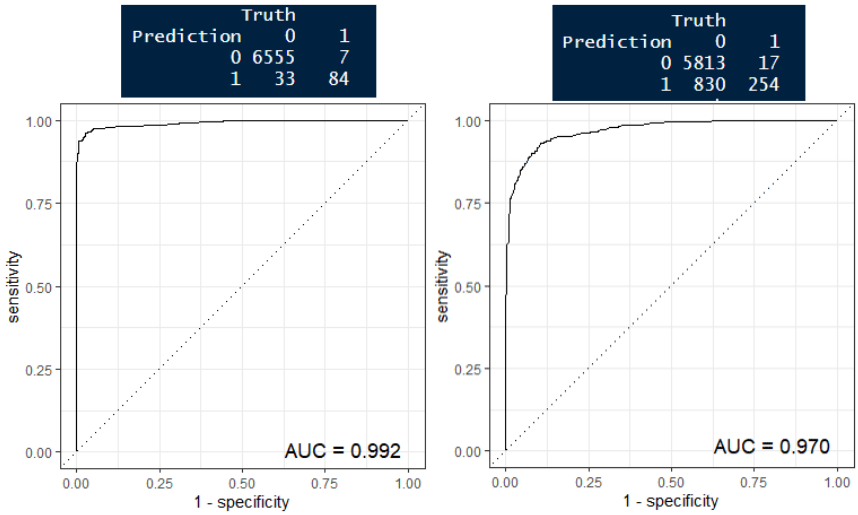

Fig. 6-f: Random forest model fit on original wet- and slab-avalanche datasets using CM, ROC, and AUC metrics.

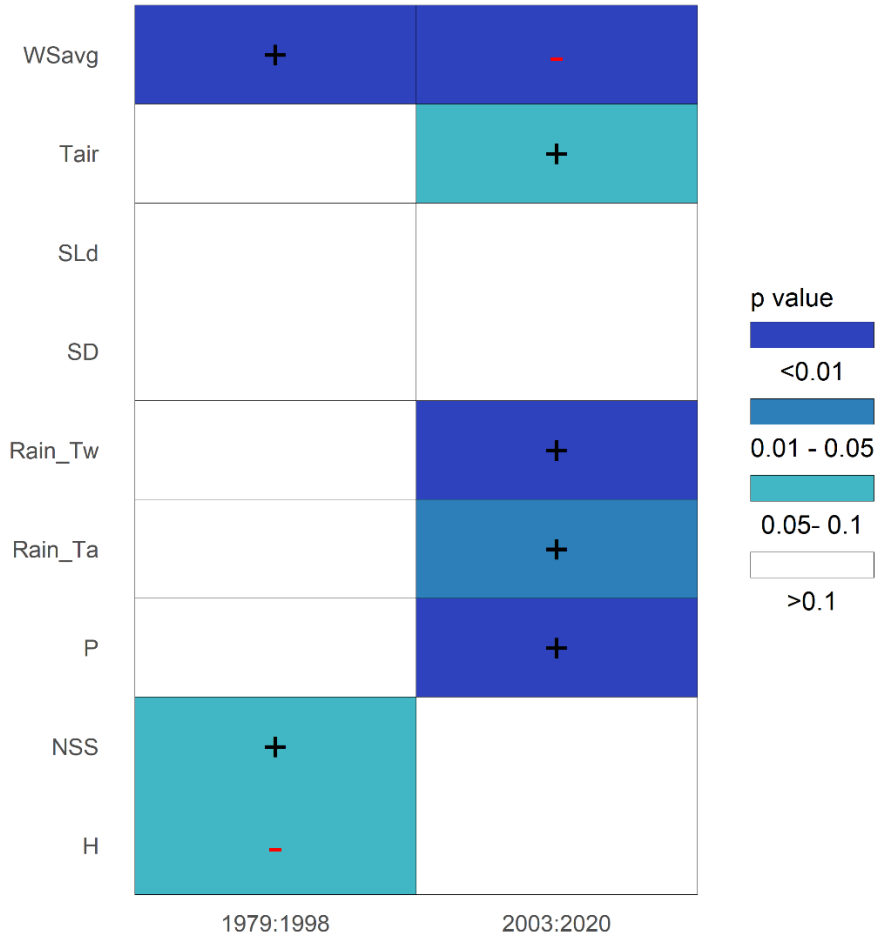

Fig. 6-g: Trends at the LBOU meteorological station for meteorological and snow variables (mean values) in the winter season (1 October–31 May). The values represent Theil–Sen slopes. Significant Mann–Kendall trends are expressed by shades of blue ($p < 0.01$, dark blue; $p < 0.05$, medium blue; or $p < 0.1$, light blue). An increasing trend is displayed by "+" and decreasing by "–".

From meteorological and snow variables, the wind speed was the variable with the most significant trend in both observed periods, 1979–1999 and 2002–2020. In the recent period, precipitation (solid and liquid – *P*, Rain_Tw, Rain_Ta) has shifted from a non-significant to a significant positive trend. Air temperature has also changed from non-significant to positively significant trends, and wind speed has changed to a negative trend. New snow was significant in the older period but not in recent 20 years (Fig. 6-g).

6.2 Slab avalanches changes and their drivers in the Krkonoše mountains

6.2.1 Long-term slab-avalanche activity

There might be a slight decreasing trend in slab-avalanche records (826 records) (483 total avalanche releases, annual mean of 60) in the 1961–1991, and there have been 343 total avalanche releases (annual mean of 43) in the last 30 years (Fig. 6-a). The mean value of slab avalanches decreased from 16.1 (1961–1991) to 11.8 (1991–2021) significantly ($p < 0.05$) according to a Wilcoxon non-parametric paired test.

Avalanche size (small, medium, large, and very large, 0.3–1.6 of a proportional scale) has declined in the last 30 years in comparison with the 1961–1990 period. Very small avalanches have risen in the last 30 years. Slab-avalanche releases dominate in March and mainly occur from December to April. In the last 3 decades, slab avalanches have also occurred in April, which was not that typical in the older period (Fig. 6-b).

Most of the slab-avalanche releases were related to SE, E, S, and SW slopes in the 1961–1991 period and SE, S, NE, and E slopes in the last 30 years. In the last 30 years more slab-avalanche releases are present on NE sides. The greatest change (9 pp) in slab-avalanche activity can be seen on the E slopes, while the proportion of slab avalanches decreased from 23 % (1962–1991) to 14 % (1991–2021). On the other hand, the highest increase (5 pp) was observed on the SE and NE slopes, when the proportion changed from 32 % (1962–1991) to 37 % (1991–2021) and from 10 % (1962–1991) to 15 % (1991–2021), respectively (Fig. 6-h).

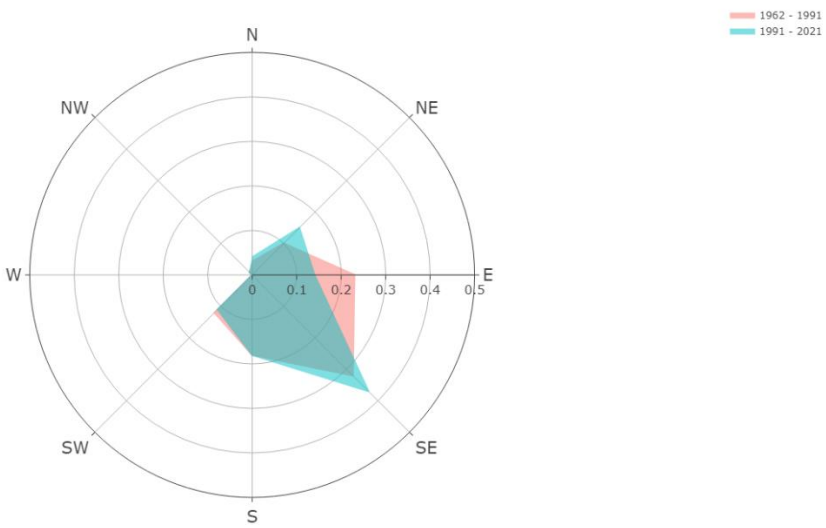

Fig. 6-h: The avalanche occurrence path distribution per orientation for slab avalanches. The radial axis represents the avalanche proportion for each cardinal direction.

6.2.2 Decision tree of slab avalanches

Snow depth was the primary split in the decision tree that splits days with and without slab avalanches (Fig. 6-i). In the group of days that had an SD_value more than 47 cm, there is a 0.36 probability that an avalanche will occur. However, if SD < 47 cm, not releasing an avalanche is uncertain (p=0.05 – low value). The second split node (using 61 % of observation data) separates with 0.57 likelihood ADs and NADs. When 3 d mean new snow (NSS_value3) ≥ 3.8 cm, an avalanche might occur (p=0.77), but when it is lower, an avalanche is not likely to be released. The higher the 3 d mean snow depth SD_value3 is (≥ 134 and 195 cm), the higher probability of avalanche release. If the snow depth difference over the 4 d before the avalanche record (SDdif4) is higher than 13 cm, the avalanche hazard increases. Avalanches occur when the 3 d wind direction (WD_value3) ≥ 108°. Conversely, they are not released when wind speed is lower than 11 m s^{-1} (p=0.24) and 3 d air temperature amplitude (Tamp3) < 6.6 °C in the Krkonoše mountains.

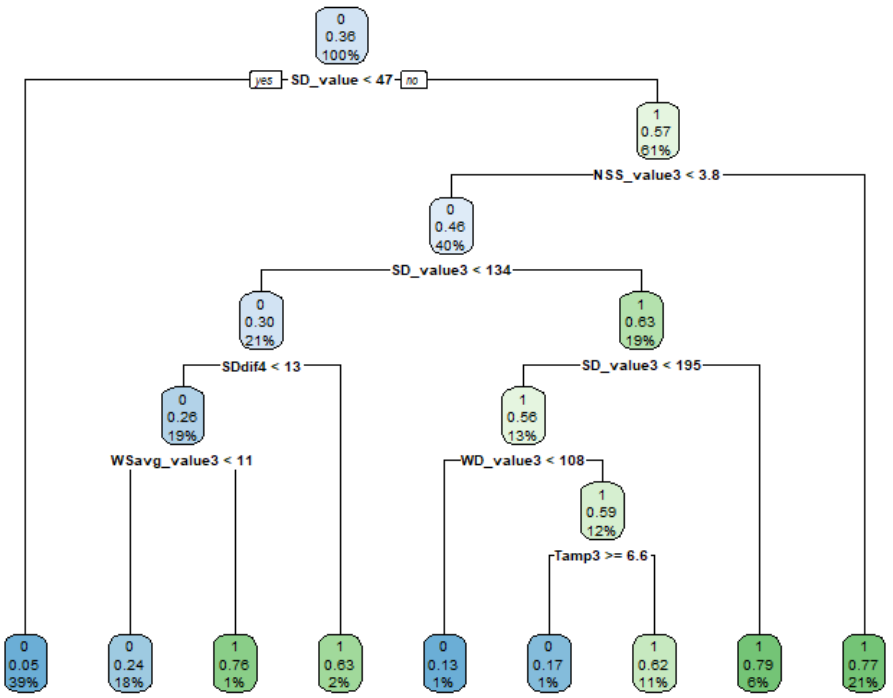

Fig. 6-i: The decision tree of weather variables triggering slab avalanches. Numbers 1 and 0 denote avalanche day and non-avalanche day. The single value means the probability of occurrence/non-occurrence of avalanche release. The percentage signifies what percent of data are influenced by the split node from the wet SMOTE avalanche dataset.

6.2.3 Meteorological and snow variables driving the slab-avalanche activity using random forest modelling and trend analysis

The most important variables for slab avalanches in the daily random forest are the most likely snow depth (SD_value, SD_value3), rainfall variables based on the air temperature threshold (Rain_Ta_sum3, Rain_Ta_value, Rain_Ta_value3), new snow (NSS_value3, NSS_value), wind speed (WSavg_value3, WSavg_value), and air temperature (Tair_value). Daily mean air temperature was about 1.3 times less important than daily mean snow depth (Fig. 6-j). The results show that rain- and snow-related variables are more important than air temperature (Tair_value). The RF model correctly predicts slab avalanches on 254 (true positives) 271 (93.7 %) and 5813 (true negatives) 6643 (87.5 %) slab-avalanche days. There were 830 false-alarm slab-avalanche days (Fig. 6-f), which means that the model tends to falsely predict slab avalanches that did not happen in a real-world scenario. The performance of the model according to AUC values is very good: 0.97 for slab avalanches (Fig. 6-f). From meteorological and snow variables, snow depth is insignificant in both observed periods, 1979–1998 and 2003–2020. In recent years, precipitation (solid and liquid – *P*, Rain_Tw, Rain_Ta) and air temperature have had a significant positive trend and wind speed has had a significant negative trend (Fig. 6-g).

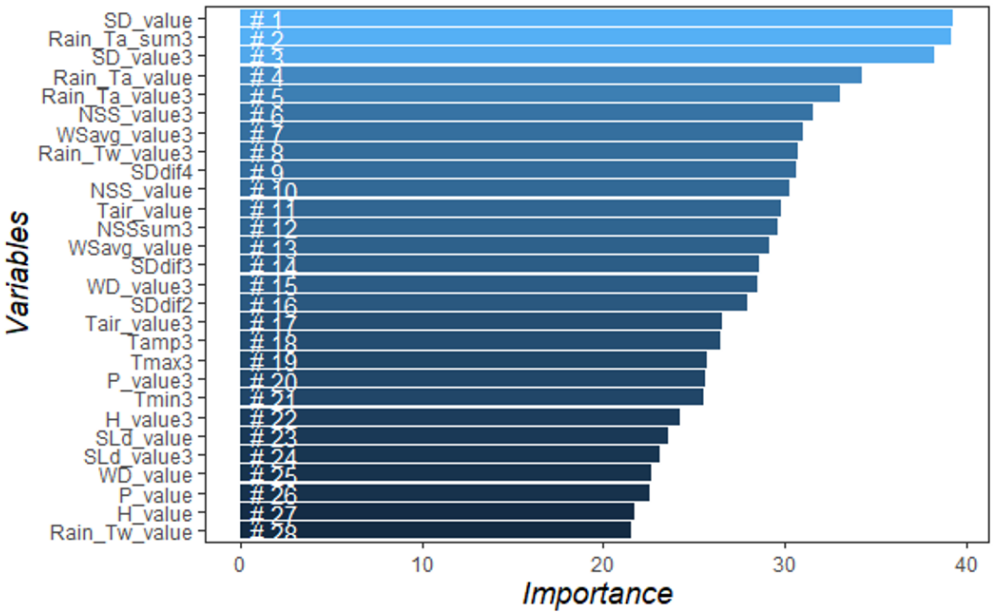

Fig. 6-j: Variable importance using the mean decrease in accuracy (MDA) for each variable of the slab-avalanche dataset in the random forests. Variables are described in Table 1 in NHESS.

6.3 Changes in weather conditions influencing avalanche activity

A rising trend in wet-avalanche occurrence over the last 4 decades and a slightly decreasing trend in slab avalanches are also accompanied by changing trends in meteorological variables. There was an apparent rising air temperature (1.8 °C), reduced wind speed (from 5 to 2.5 m s^{-1}), and slightly decreasing trend of max snow depth (from approximately 210 to 180 cm) in the first decades of the 21st century, when there were an enormous number of avalanche releases in Krkonoše (Fig. 6-k).

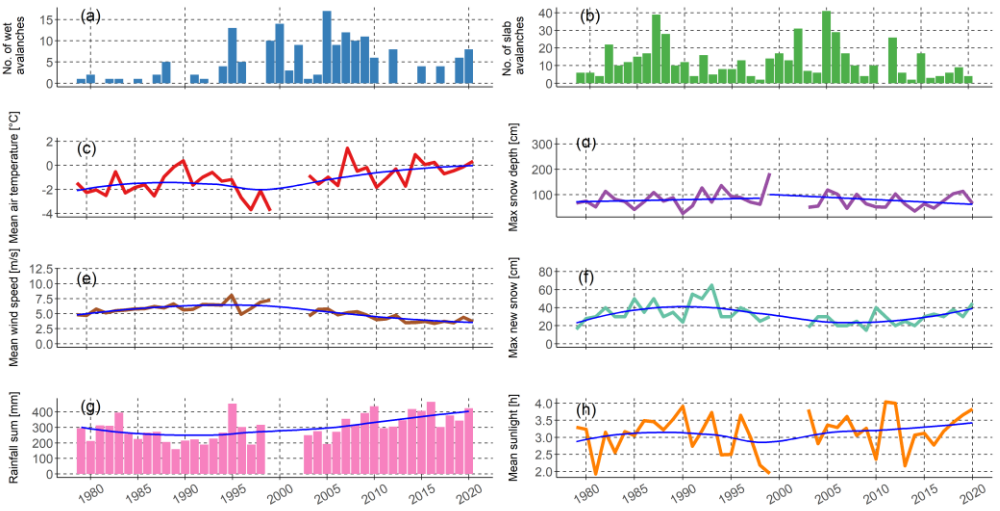

Fig. 6-k: Avalanche occurrence distribution and meteorological and snow variable conditions at the Labská bouda automated weather station (1320) from 1979 to 2020. Horizontal axes represent winter season daily data aggregation from 1 October to 31 May. The time series includes a data gap from winter seasons 1999–2002 for all weather variables. Blue line shows local polynomial regression for two compared periods (1979–1998, 2003–2020). Air temperature, wind speed, and sunlight subplots represent mean daily values over the given winter season.

III. PART

MONITORING SPATIAL SNOW DISTRIBUTION

MONITORING SPATIAL SNOW DISTRIBUTION

Monitoring of spatial snow distribution is important for climate change research, avalanche and flood forecasting, and water resource management. Monitoring snow distribution over time helps us to understand how snowpacks are changing and how these changes are likely to impact water resources, flood risk, and avalanche hazard. By monitoring snow distribution, we can understand how much water is stored in the snowpack and how it is likely to be released over time. This information can help us to effectively manage water resources, predict snowmelt, issue flood warnings and develop flood mitigation strategies. Additionally, monitoring snow distribution can help us to identify areas that are at risk of avalanches and develop avalanche warning systems. We chose one testing area and few study areas.

The Map of the Republic in the Krkonoše National Park (KPN) served as a testing ground for familiarizing ourselves with the measurement devices, conducting terrain reconnaissance, and preparing for subsequent aerial missions. To evaluate the feasibility of UAS for SD estimation in diverse terrain and environmental conditions, two sites were chosen: the Žlab Úpičky avalanche path in Krkonoše, Czech Republic, and the Graswang station in Bayer, Germany. The UAS-derived data has the potential to validate and verify RAMMS avalanche runout simulations in the Krkonoše mountain range. UAS technology offers a versatile tool for multi-temporal landscape assessment, enabling the monitoring of snow extent and the quantification of snow water equivalent (SWE) throughout the snowmelt and accumulation periods. These capabilities hold promise for enhanced snowpack monitoring and improved avalanche forecasting. Lastly, we examined Northern limestone Alps - Ammer and Isar river catchments to assess the feasibility of UAS for snow depth estimation in a flat terrain.

7 Testing sites, study areas and data collection

7.1 Testing site: Map of the Republic in Modrý důl avalanche path

Within UAS testing we focused on monitoring a snow patch located in „Modrý důl“ near a place known as the Map of the Republic in the northeastern part of the Krkonoše Mts (Fig. 7-a). The snowpatch, Map of the Republic, is situated in a nivation niche on a south-facing slope benath and between Studniční Mountain (Mt., 1554 m a.s.l.) and Luční Mt. (1555 m a.s.l.) in altitudes of 1420 - 1455 m a.s.l. Snow depth can reach up to 20 m (Hejcman et al., 2006). The map of the country is a popular tourist destination. Its shape is clearly visible from a distance and thus easily recognizable. The primary objective was to familiarize ourselves with the measurement devices, conduct terrain reconnaissance, and prepare for upcoming aerial missions. Throughout this process, we encountered both advantages and disadvantages. These included variations in UAS flying heights, changes light conditions and shading throughout the day, limited network coverage, windy conditions, and low cloud cover, and icing on UAS propellers.

By addressing these factors and gaining experience through this initial phase, we aimed to optimize future UAS flights and improve the quality and reliability of our data collection in the study area. The map of the Czech Republic which is located in Modrý důl avalanche path (southerly oriented aval path) was screened on 26/06/2020 (Fig. 7-b). This site was previously screened by Gabrlik's et al. (2019). They utilized UAS-based snow field mapping and achieved an RMSE of approximately one decimetre and a spatial resolution of the photogrammetric products at a centimetre level through direct georeferencing.

Fig. 7-a: Monitoring site in Modrý důl avalanche path in NE Krkonoše mountains monitored by the drone oktokopter on 26/06/2020. Photos were taken by M. Součková and T. Lendzioch.

Fig. 7-b: Snow field: Map of the Czechia, the illustrative photo was taken on the 26/06/2020 by T. Lendzioch.

7.2 Testing site: Ski area Alšovka in Krušné mountains (NW Czechia)

Ski area Alšovka[7] is in Krušné mountains (NW Czechia) and served for testing and multitemporal screening of snow cover extend (SCE) within winter season. The principal investigator of this thesis made five campaigns during winter 2021 on the following dates: 12/02, 20/02, 28/02, 28/03, 02/04 using UAS: P4P V2.0 and Trimble R8s for snow monitoring and obtained a snow free DEM which was screened on 30/05/2021. Flight mission was preplanned in Litchi application (its interface is displayed in Fig. 7-c). Snow free DEM of the Alšovka ski slope was the required output (Fig. 7-d) within a small cooperation project with Alšovka ski resort.

[7] https://alsovka.cz/

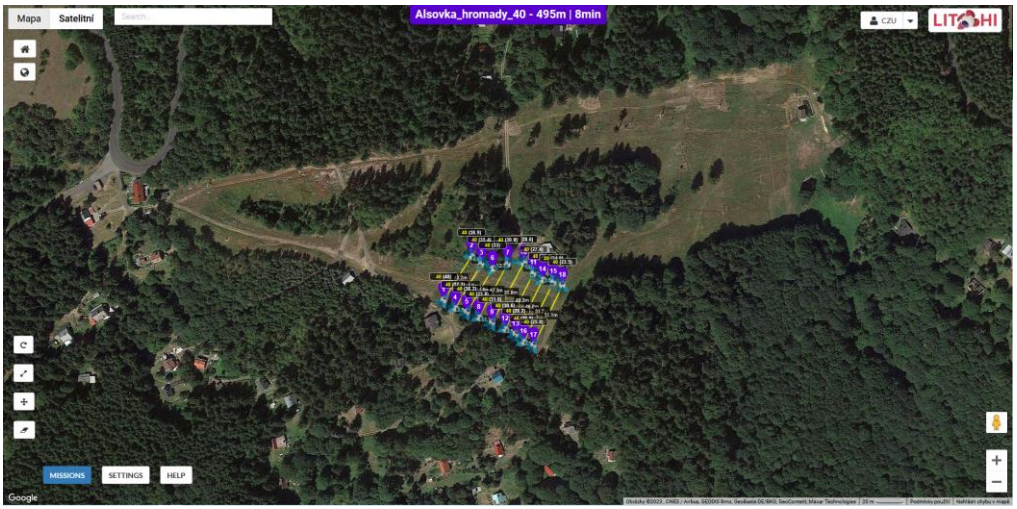

Fig. 7-c: Example of preplanning Litchi application and winter scheme of Alšovka ski slopes.

Fig. 7-d: Alšovka ski resort. Images were taken for the purpose of creating orthophotos and DEM was created by M.Součková. The white places signify DEM holes – the flight was not preplanned to fly over the forests. Coordinate system: S-JTSK / Krovak East North (EPSG::5514).

7.3 Žlab Úpičky avalanche path in Krkonoše Mts (NE Czechia)

Žlab Úpičky avalanche path was monitored to assess the feasibility of UAS for spatial variability of snow depth in steep Krkonoše terrain and older snow conditions (screened six days after avalanche release: on the 21/02/2021). Specifically, we focused on the avalanche that was released on 15/2/2021 located in Obří důl in Krkonoše mountains (cadastre number 02). Žlab Úpičky avalanche characteristics were reported or estimated by Mt. Rescue (MR) Krkonoše and are displayed in Fig. 7-f and Fig. 7-g Žlab Úpičky GCP data were collected by UAS: low-cost standard P4P V2.0 camera (visible spectrum) and GNSS – Trimble R8s device (Fig. 8-d).

The snow profile was analysed at the location of the avalanche release on 15/02/2021. Extended Column Test (ECT) revealed the avalanche detach 52cm on the edge of the coarse-granited snow that was on the ice layer. The abbreviation means ECTN 5@135cm – fracture do not propagate across the entire column. ECTP 12@52 cm - fracture initiates and propagates across the entire column. The temperature differs a lot within the snow profile from -0.4 °C to -14.1 °C (Fig. 7-e).

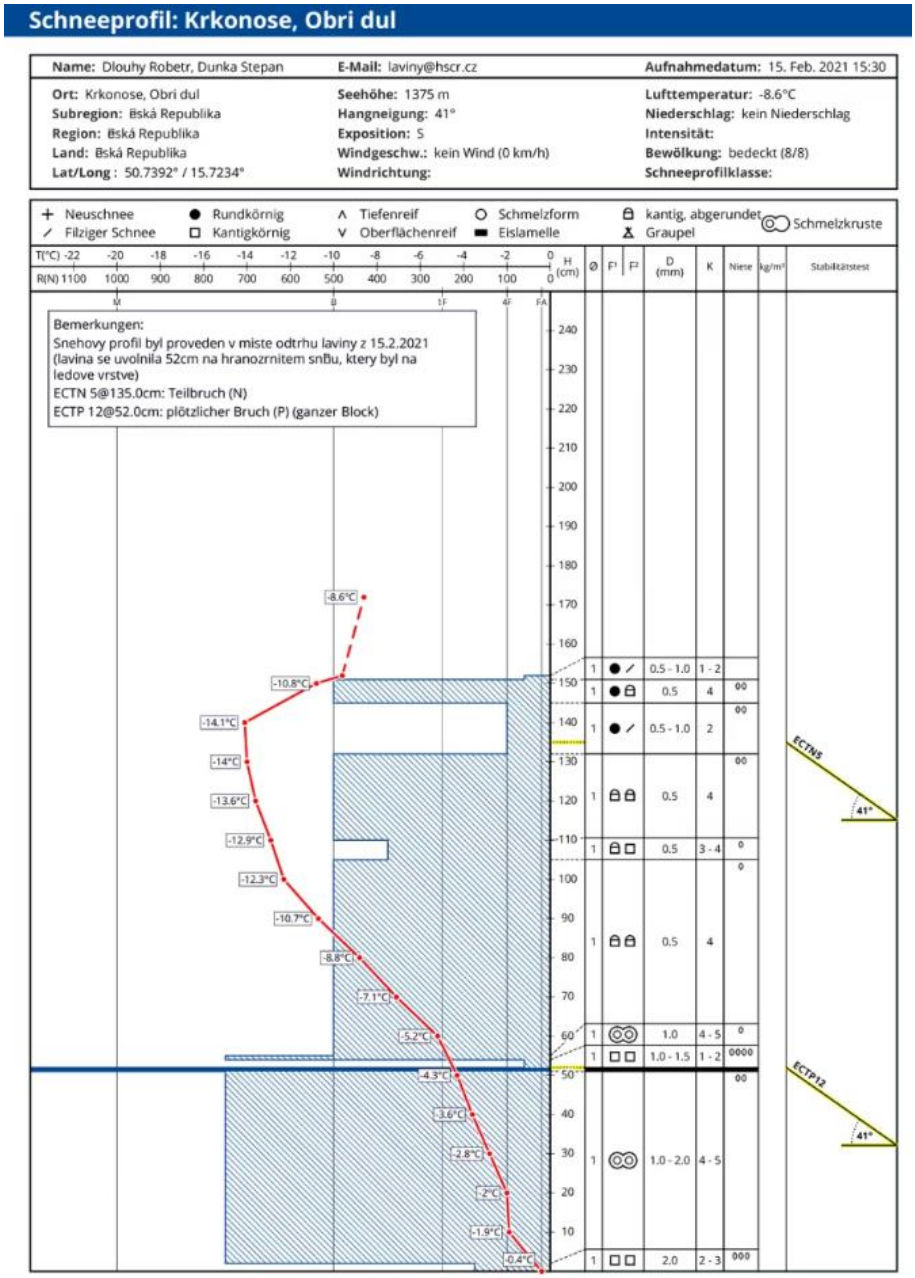

Fig. 7-e: Snow profile analysed in Žlab Úpičky avalanche release zone on 15/02/2021 by MR Krkonoše.

Žlab Úpičky characteristics

Avalanche (Aval) danger level: 2
time of avalanche release: approximately 12:30
approximate Aval length: 400 m
height of avalanche release: 0.3-1.7 m
Aval release width: approximately 60 m
accumulation width: 20 m
accumulation height: it was estimated 7 m (not measured)
exposure: south
slope: 42 °
type of avalanche: slab Aval (line release)

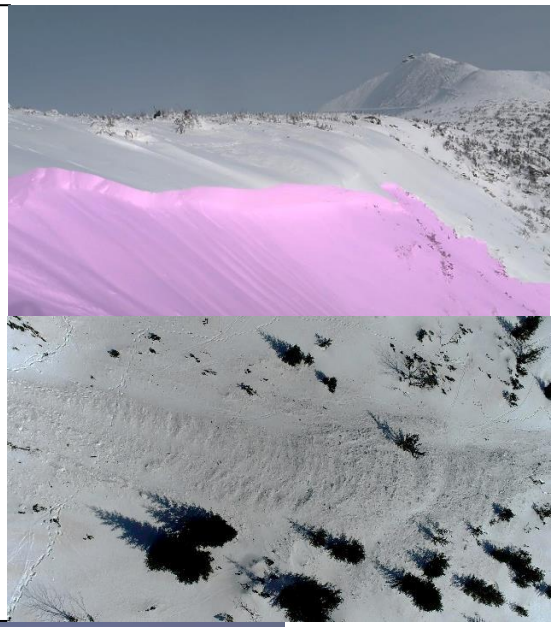

Fig. 7-f: Žlab Úpičky release area (upper right photo taken by R. Dlouhý: Mt. Rescue Krkonoše) and accumulation area = runout zone (bottom right photo taken by T.Lendzioch) in the Krkonoše Mts. The release area of winter Žlab Úpičky avalanche path in Krkonoše Mts and Sněžka peak (1603 m a.s.l.) in the background.

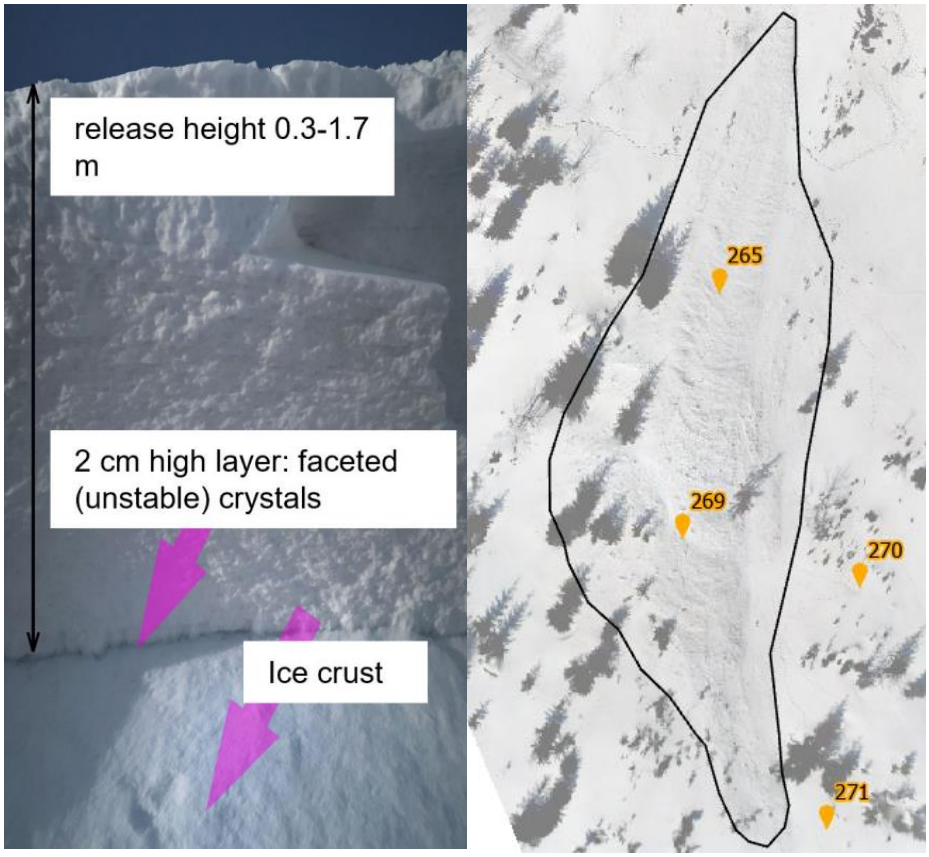

Fig. 7-g: Snow profile at the day of avalanche release: 15/02/2021, digged by Mt. Rescue Krkonoše (photo taken by R. Dlouhý) and Žlab Úpičky accumulation area (orthophoto was processed in Agisoft Photoscan). Orange points and numbers signify GCPs.

Fig. 7-h: Summer (upper) and winter (bottom) Žlab Úpičky avalanche path (Upic02) photo taken by M. Součková (summer) and T. Lendzioch (winter).

7.3.1 Meteorological conditions before the Žlab Úpičky avalanche release

Meteorological conditions prevailing before the avalanche release are described in Table 3 and their evolution from 14/02 to 16/02/2021 is displayed in Fig. 7-i.

Table 3: Meteorological conditions before Žlab Úpičky avalanche release reported by Krkonoše Mt. Rescue Team.

Date	Meteorological condition
4-5/2/2021	Warming and rain, with mixed precipitation at altitudes above 1 400 m above sea level. Subsequently it cooled down and a significant ice crust formed on the surface.
6-14/2/2021	New snow fell (40 cm), initially wet, then dry. The wind blew strong westerly at first and strong northerly gusts for the last three days. The wind-displaced snow was deposited on the leeward slopes to the SE, S, and SW gullies and in the release zones. In addition, the temperature cooled down sharply on 7 Feb and fluctuated between -10 and -17°C. Due to moisture in the snow profile and strong, long-lasting frosts above and below the crust, construction metamorphosis of the original snow crystals acted on. This process created several layers of unstable coarse-grained snow. The dangerous layer is about 2 cm thick and occurs exactly between the ice crust formed in the previous days and the layers of newly accumulated snow seen in Fig. 7-g.

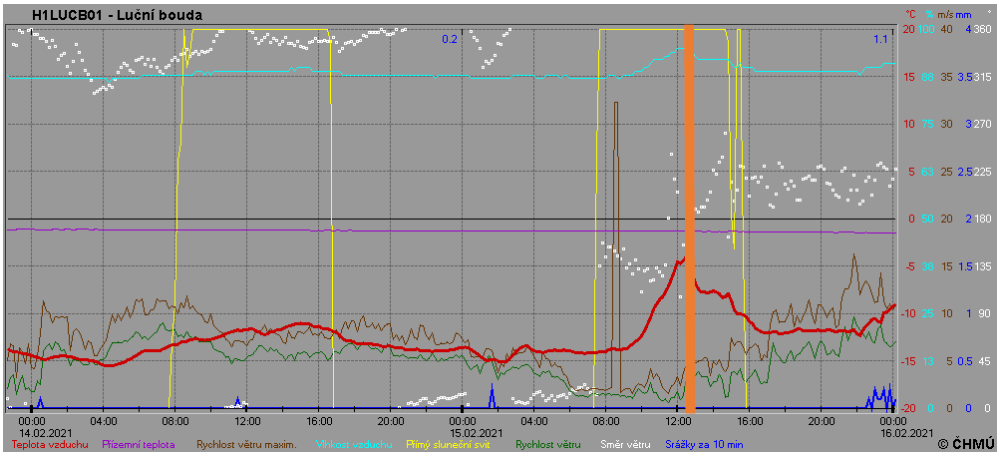

Fig. 7-i: Illustrative data of weather course from Luční bouda meteorological station from 14/02 to 16/02 2021. Meteorological variables: air temperature (red line), ground temperature (purple line), maximum wind speed (brown line), air humidity (azure blue line), direct sunlight (yellow line), wind speed (green line), wind direction (white line), rainfall [mm/ 10 min] (blue line) (from left to right from the readers view). Reused from ČHMÚ.

7.3.2 Snow profile and avalanche release measurement

A detailed measurement of the snow profile and avalanche release area is a standard activity conducted by Moutain Rescue Krkonoše (MR) in response to any snow avalanche accident. This practice is essential for providing a comprehensive understanding of the incident and serves to educate others who wish to comprehend the causes of avalanche releases. MR Krkonoše regularly conducts multiple snow profiles each week in the proximity of potential avalanche areas. The avalanche was released on 52 cm deep coarse-grained snow which laid on ice crust (Fig. 7-e). These profiles are included in the main accident reports. In general, you can find uploaded snow profiles on the Czech MR organization website (1), and the international website which cover various snow profile measurements (2), following these two links:

1) https://www.horskasluzba.cz/cz/pocasi-na-horach/lavinova-predpoved/krkonose
2) https://www.lawis.at/profile/

Similarly, mainly southly oriented paths in Obří důl or Modrý důl area can give us a clue about snow profile compactness of the Žlab Úpičky avalanche path.

7.3.3 The probable cause of the Žlab Úpičky avalanche release

The avalanche release was a caused by a combination of human overloading and previous changing weather condition with unstable layer in a snow profile. The avalanche released near the edge of the gully, where the snow pillow had not yet reached sufficient thickness. As a result, it was relatively easier to trigger the release of the avalanche by breaking the supporting layer of north windblown snow. This layer was situated on top of a 2 cm high, unstable layer composed of loose, coarse-grained snow crystals, which rested on an ice crust (Fig. 7-g). Additionally, the activity of skiers previously ascending and skiing in the area may have contributed to disturbing the overall stability. The influence of sunlight around midday could have had a minor effect on the stress between the individual layers, although this effect was considered negligible. However, given the prevailing conditions in the Krkonoše Mountains during that period, it was said it was not possible to remotely trigger an avalanche[8]. According to the assessment by MR, the propagation of a longitudinal crack within the unstable layer was insufficient to cause such an avalanche. The overall avalanche danger level and specific avalanche problems associated with the avalanche release are depicted in Fig. 7-j.

[8] https://avalanche.ca/glossary/terms/remote-triggered-avalanche

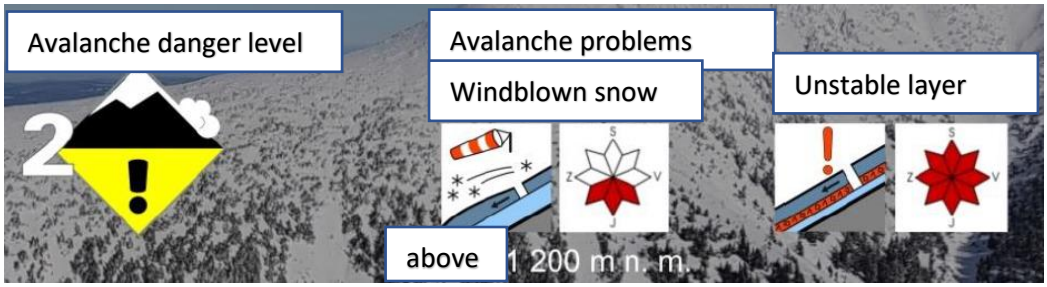

Fig. 7-j: Avalanche danger level and types of avalanche problems of Žlab Úpičky avalanche release on the 15/02/2021.

The rescue process, snow profile analysis, release zone measurements, meteorological forecast, and weather conditions on the day of the avalanche release can all be found in the avalanche report[9]. In particular, it highlights that the largest avalanche occurred on 08/03/1956 and other big avalanches were recorded in Žlab Úpičky in 1976, 1987 and 1996. The longest Žlab Úpičky run out length was 1100 m in 2012. The avalanche broke trees 35 cm in diameter and cleared trees to a height of 4 - 6 m (50-year avalanche) (Spusta et al., 2020).

7.3.4 Survey specification in the Žlab Úpičky avalanche path

Surveying conditions such as luminance, and surface type are displayed in Table 4. Meteorological conditions at the day of the field monitoring were: temperature from -2 to 2 °C, wind speed was ranging from 6 to 1 $m.s^{-1}$, with air pressurea approximately 1021 hPa.

Table 4: Žlab Úpičky terrain surveying conditions.

Aval path	**survey date**		**luminance conditions**		**snow surface type**	**physiography descriptors**	**number of GCP**	
info	DEM summer (s)	DSM winter (w)	DEM s	DSM w	DSM w	DEM s	DSM w	DEM s
Upic02	27.06.2020	21.02.2020	morning: sunny; afternoon: partly cloudy	morning: sunshine; afternoon developing clouds	morning: frozen, icy afternoon: wet	**release zone**: steady grassy, rocky parts **transport zone:** steep slope 35-42 ° and narrow gully, lots of dwarf pines, **accumulation zone**: flat and spruce forests (Fig. 7), constantly "cut" by the descending avalanches at a height of about 2 m	9	10

[9] https://www.alpy4000.cz/lavinove-nehody/krkonose-upicka-obri-dul-detail-1752

7.4 Northern limestone Alps

To accomplish the aims of the dissertation, a comprehensive approach was undertaken involving various research activities and methodologies. The following steps were undertaken to address the research objectives:

1. Extended Station Network and In-Situ Snow Data Collection:

In order to gather valuable data, the station network was expanded within the Ammer and Isar river catchments located in the southern region of Bayern, Germany. Existing sites were also maintained to ensure the continuity of data collection. To obtain precise snow measurements, in-situ snow data was collected utilizing gravimetry and neutron methods.

2. Assessment of UAS-SfM for Snow Depth Variability:

The study area, characterized by flat terrain and varying fresh snow depth, was selected to assess the feasibility of employing UAS with SfM techniques. A standard Phantom 4 V2.0 camera operating in the visible wavelengths range was utilized for image capture. The objective was to investigate the potential of creating spatial maps of SWE through UAS scanning and subsequent generation of derived snow maps. This method aimed to provide valuable insights into the variability of snow depth within the study area.

3. Study of Cosmic-Ray Neutron Sensor (CRNS) Method Observation Theory for SWE:

To enhance the understanding of SWE dynamics, the research initiated a study on the observation theory of the CRNS method. The goal was to develop a universal approach to interpret CRNS measurements obtained above the snow surface at different altitudes and under varying environmental conditions. Dr. Benjamin Fersh, an esteemed researcher, actively contributed to this project.

Moreover, the knowledge of water melting from snow is paramount importance for effective dam manipulations. In the dissertation study area, this translates to the regulation of Syvensteinsee and Achensee, which are critical water bodies for the region. Fig. 7-k provides an illustration of the relevant features.

Fig. 7-k: Sylvensteinsee (upper image) in Bayer region (Germany) and Achensee (lower image) (Austria). The Sylvensteinsee image is copied from Bergfex[10] and Achensee websites[11].

[10] https://www.bergfex.cz/sommer/toelzer-land/seen/sylvensteinsee/

[11] https://www.achensee.com/en/

7.4.1 Graswang UAS and CRNS data and devices

UAS and GNSS data were collected using the Phantom 4 V2.0 drone and the Trimble R10 receiver (Fig. 8-d). The Phantom 4 drone was employed for capturing aerial imagery, while the Trimble R10 receiver was used for ground-based measurements. The captured images were taken in Pix4D Capture and Litchi apps and were utilized for photogrammetric processing, generating orthomosaic maps, digital surface models (DSMs), and other derived products using a commercial software for photogrammetric reconstruction. Pix4D Capture application allows users to configure forward and side overlaps, ensuring optimal image coverage and data quality during the flight missions.

UAS based monitoring of snow characteristics (snow depth) was performed at Cosmic Ray neutron sensor (CRNS) Graswang station in the Northern limestone Alps. The reason of choosing this site was that there is a clear terrain not encroaching on the National Park, which would require a permit to fly from the German Aviation Authority. Moreover, the site enabled us to compare CRNS, UAS and manual snow depth results. CRNS data were processed with GNU R, raster results in Geographic Information System (GIS), specifically ArcPro environment, and UAS data in Agisoft.

7.4.2 Bayern region– Ammer and Isar river catchments

The third study area lies in the southern Bavarian region of Germany. During the past winter season of 2021, a total of nine CRNS stations were deployed within the Ammer and Isar river catchments. These stations were strategically placed at various altitudes, ranging from 600–1550 m a.s.l. (Fig. 7-l).

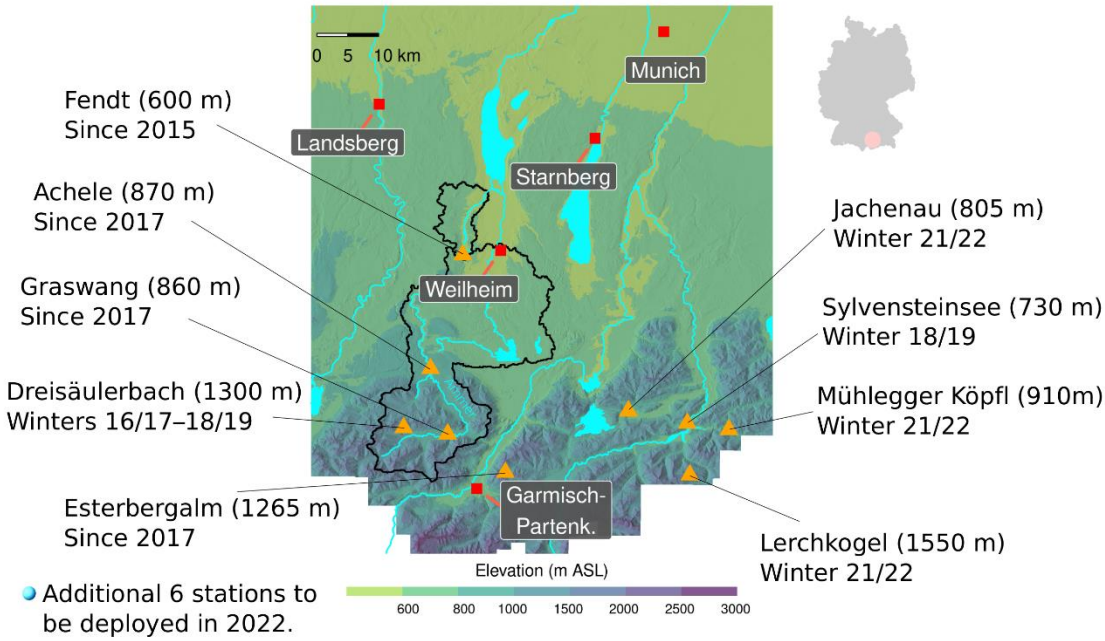

Fig. 7-l: Nine CRNS stations located in Ammer and Isar river catchments.

Table 5: CRNS stations in the Ammer and Isar river catchments monitored in 2022, sorted by altitude in ascending order, with the start of data collection.

Station Name and abbreviations	Altitude [m]	Data collection
Fendt (fen)	600	since 2015
Achele (ach)	870	since 2017
Graswang (gwg)	860	since 2017
Jachenau (jac)	805	2021/2022
Sylvensteinsee (syl)	730	2018/2019
Esterbergalm (est)	1265	since 2017
Lerchkogel (lek)	1550	2021/2022

8 Methods

8.1 Advances in snow monitoring

This thesis focuses on selected methods of spatial snow depth measuring: UAS photogrammetry using a visible spectrum of the camera, manual snow probe measuring and CRNS monitoring of SD and SWE. Also, it reconstructs the released Žlab Úpičky avalanche in avalanche numerical model: RAMMS. To assess the feasibility of UAS screening for snow assessment, two study areas were selected: Krkonoše Mts., and monitoring stations in the Ammer and Isar river catchments located in the Northern Limestone Alps. Firstly, we provide a workflow of the UAS flight procedure and the subsequent processing of the acquired UAS data. Secondly, we explain the process of snow depth extraction from the collected UAS imagery. Additionally, we explain how the Žlab Úpičky snow avalanche release is reconstructed using RAMMS. Furthermore, we introduce the above-ground CRNS method for snow assessment. This method involves using cosmic ray neutrons to estimate SWE and provides valuable information about the snowpacks properties. We collected in-situ SWE data at different elevation altitudes within the study areas, enhancing our understanding of snow dynamics and variations across different elevations.

8.1.1 UAS workflow and data processing

The UAS workflow involved five main steps in surveyed areas: mission planning and setting up flying parameters, terrain work and data acquisition, data processing, extracting outputs and error analysis and validation. This workflow (Fig. 8-b a) was designed to ensure a systematic and efficient process for UAS data collection and analysis.

1. Mission Planning and Setting Up Flying Parameters (Fig. 8-b a):

In the first step, careful mission planning was conducted, taking into consideration the study objectives, flight area, and specific requirements. Flying parameters such as altitude, speed, and flight path were determined to optimize data collection. This planning stage ensured that the UAS flights were conducted in a controlled and effective manner. To georeference UAS models, two methods can be applied: direct and indirect georeferencing. Direct georeferencing involves the integration of onboard positioning and orientation sensors within the UAS system. These sensors, such as Global Positioning System (GPS) and Inertial Measurement Unit (IMU), provide real-time measurements of the UASs position and orientation during the flight. By synchronizing the sensor data with the captured imagery, each image can be directly georeferenced to a specific location on the Earths surface. This allows for accurate positioning of the UAS model without relying on additional Ground Control Points (GCPs) using RTK in UAS. Direct georeferencing is particularly useful for rapid deployment and small-scale mapping applications. Indirect georeferencing involves referencing the UAS model to known GCPs after the data acquisition phase. GCPs are specific locations on the ground with known coordinates obtained through conventional surveying techniques. During the UAS flight, the GCPs are visible in the captured imagery. By accurately identifying the GCPs in the imagery and matching them with their known ground coordinates, a transformation can be applied to georeference the entire UAS model. This process accounts for any systematic errors or distortions in the UAS imagery. Indirect georeferencing is commonly used for large-scale mapping projects where higher accuracy is

required. In our project, where indirect georeferencing was primarily used for UAS models, the distribution of GCPs over the entire area becomes crucial during the planning phase, particularly in hilly and steep terrain. This terrain can introduce challenges such as variation in elevation, topographic features, and perspective distortions in the imagery. To account for these challenges, it is important to strategically distribute the GCPs across the entire area of interest.

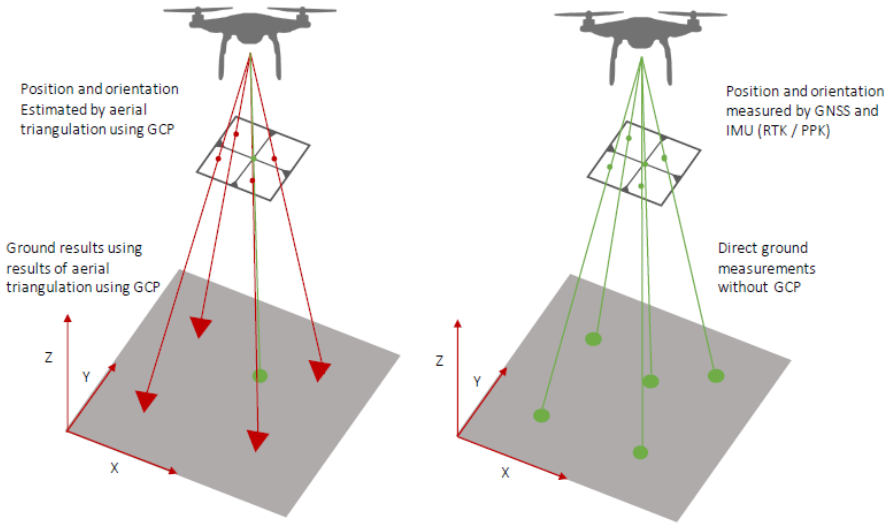

Fig. 8-a: Direct and indirect georeferencing principle. Reused from (Cignoni et al., 1998) and (Maier et al., 2022).

2. Terrain Work and Data Acquisition (Fig. 8-b b):

Once the mission plan was finalized, the UAS was deployed to the study area. The UAS was flown over the designated terrain, following the predetermined flight parameters to cover the desired area thoroughly. These flight parameters include variables such as altitude, speed, overlap, and grid pattern. Before the UAS flight mission, GCPs were strategically placed throughout the entire study area. After the completion of the UAS flight, the GCPs were measured using high-precision RTK receiver.

3. Data Processing (Fig. 8-b c,d):

After the data acquisition phase, the collected data underwent a series of processing steps (in total 5). The typical UAS processing data pipeline, as depicted in Fig. 8-b c.d, involves several key steps to transform the acquired imagery into useful outputs. A) To ensure the quality and consistency of the imagery, a selection process is undertaken. This involved the preprocessing of the snow imagery, including removal of any artifacts or noise from the images or even delete blurry, similar, and low-quality images that may hinder the subsequent processing steps. B) The selected imagery is then subjected to an imagery alignment process. This step aims to align the images accurately, accounting for variations in camera position and orientation during the UAS flight. Sophisticated algorithms, such as those implemented in Agisoft Photoscan (1.7.4 version of Agisoft Metashape), were used to match corresponding features in the images, enabling precise alignment. During the image

alignment process, the software analyses the captured images and identifies common features or points of interest present in multiple images. These features can include distinctive landmarks, texture patterns, edges, or corners. The algorithms then establish correspondences between these features across the images, allowing for accurate alignment. Usually, the software's algorithm use various techniques such as scale-invariant feature transform (SIFT), speeded-up robust features (SURF), or other advanced matching algorithms that are designed to be robust to changes in lighting conditions, viewpoint variations, and image noise, ensuring accurate feature matching even in challenging conditions. Once the image alignment is completed, the software creates a virtual sparse cloud and determine the position of the points in space of the scene by triangulating the matched features.

C) Sparse point cloud represents a collection of 3D points that correspond to the features captured in the images. It provides a rough representation of the surveyed area, with fewer point and lower density compared to the final dense point cloud. D) The sparse point cloud is then densified, resulting in a depth maps of dense point cloud. This process involves interpolating additional points to increase the density of the point cloud, providing a more detailed representation of the surveyed area. The dense point cloud captures the fine-scale features of the terrain, structures, and objects present in the imagery. E) Based on the dense point cloud, various raster outcomes can be generated. The first outcome is the Digital Surface Model (DSMs) or Digital Elevation Model (DEMs), which represents the elevation of the Earth's surface, including natural and man-made objects. The second outcomes are the Digital Terrain Model (DTMs), which specifically depicts the bare ground surface, excluding above-ground objects. Lastly, an orthophoto mosaic can be created, which is geometrically corrected aerial image that eliminates distortions caused by the terrain and camera perspective.

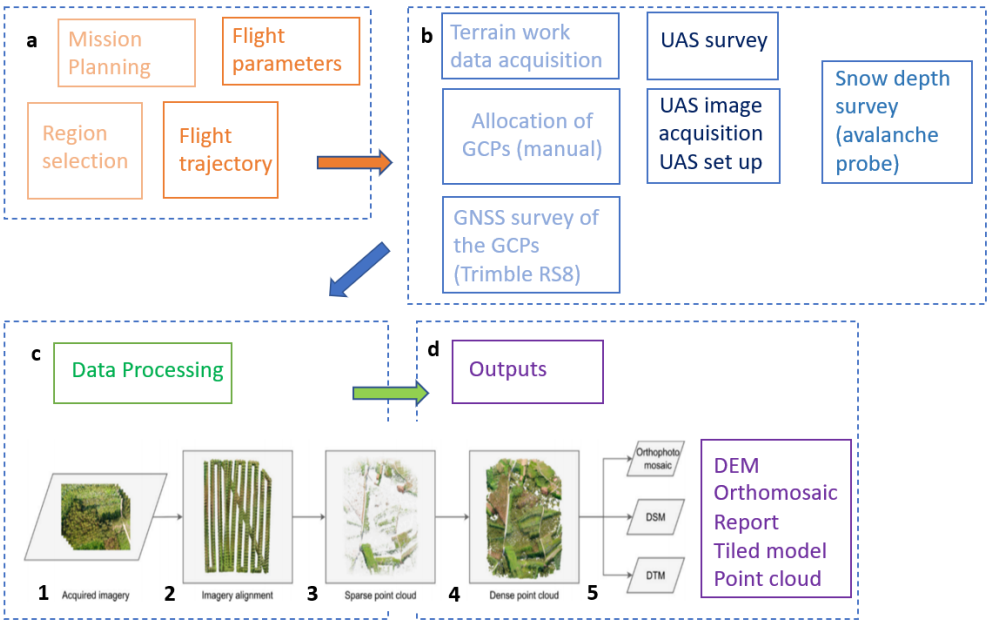

Fig. 8-b: Typical photogrammetric concept pipeline. Small image was reused and from Guimarães et al., 2020.

4. Snow Depth Calculation:

Once the elevation models were generated in ArcPro using Minus or Raster functions, the snow depth calculation was performed. This step involved comparing the elevation models before and after the snowfall to estimate the snow depth. By subtracting the pre-snowfall elevation from the post-snowfall elevation, the snow depth values at different locations within the surveyed areas could be determined.

5. Error Analysis and Validation:

The final step contained analysing and validating the processed data. Error analysis was conducted to assess the accuracy and precision of the derived outputs. This step involved comparing the processed data with ground truth measurements or other reference datasets to identify any discrepancies or error. By conducting validation, the reliability of the generated outputs could be assessed.

8.1.2 Survey Instrument Specification (UAS and GNSS Receiver)

Data collection in all study areas was conducted using UAS and GNSS: Trimble R8. For gathering snow depth information, a Phantom 4 Pro V2.0 drone, manufactured by DJI, was employed (Fig. 8-c). This drone has a maximum flight time of 30 minutes and can operate in wind speeds of up to 10 m/s. It utilizes a GPS/GLONASS positioning system and offers a hovering vertical accuracy of ±0.1 m (with Vision Positioning) or ±0.5 m (with GPS Positioning), as well as a horizontal of ±0.3 m (with Vision Positioning) or ± 1.5 m (with Vision Positioning). The camera lens on the drone have a viewing angle of 84°, with focal lengths of 8.8 mm and 24 mm (35 mm format equivalent) and an aperture range of f/2.8 – f/11. It supports autofocus from 1 m to infinity. The onboard camera captures images with dimensions of resolution 5472 × 3648 pixels for a 3:2 aspect ratio. The sensor size is 13.2 mm (width) × 8.8 mm (height). The cost of the Phantom 4 Pro V2.0 drone is approximately 3000 euros.

Fig. 8-c: Phantom DJI: P4P V2.0.

To measure the three-dimensional coordinates of the GCPs and in-situ snow depth locations, a Trimble R8 GNSS receiver was utilized (Fig. 8-d). This instrument incorporates advanced technologies such as Real-Time Kinematic (RTK), Virtual Reference Station Networks (VRSN), and Real Time eXtended (RTX) to ensure precise measurements. Virtual Reference Station: VRS Now™Network use RTK solutions for survey, and mapping and reaches the accuracy better than 2 cm. Trimble receivers using RTK (Trimble RTK[12]) can calculate their relative position with an accuracy of up to 1 cm ± 1 parts per million (ppm). It leverages the tracking capabilities of multiple satellite systems, including GPS, GLONASS, Galileo, BeiDou and QZSS, to enhance the accuracy and reliability of the measurements. The Trimble R8s can achieve a maximum precision of 8 mm (horizontal) and 15 mm (vertical) when utilizing post-processing kinematic methods (PPK). We used Trimble VRS Now Correction Service[13].

Fig. 8-d: Trimble Rs8 (left) and R10 devices (right).

[12] https://www.youtube.com/watch?v=QDeNnwJrTpM

[13] https://www.youtube.com/watch?v=Y0s84qTuvQY

8.1.3 GCP placement

GCPs are essential for georeferencing the reconstructed 3D model (Smith et al., 2016; Westoby et al., 2012). In our study, GCPs were distributed across the surveyed area, taking into consideration the terrain characteristics, such as steep slope, rock levee with waterfall and dense dwarf pines in Žlab Úpičky terrain. Each GCP had a distinctive mark on its surface to precisely pinpoint the GCP on the imagery. The GCPs were represented by black-and-yellow rectangular targets (in winter) and black-and-white rectangular 12 bit targets[14] (generated from Agisoft program). These targets were printed on lightweight, folded Tenstex DK 280g/m2 material with hydrophobic treatment and PU coating (Fig. 8-e). Typically, co-ground control points (CGCPs) are selected from snow-free areas, such as overlying boulders, rocks, and ground patches, to support the co-georeferencing of the TDEMs (Bühler et al., 2016). However, due to time constraints and limited daylight during a day, we were unable to collect CGCPs. The number of GCPs and control and check points for the Žlab Úpičky area are listed in Table 12, and their positions can be seen in Fig. 9-b.

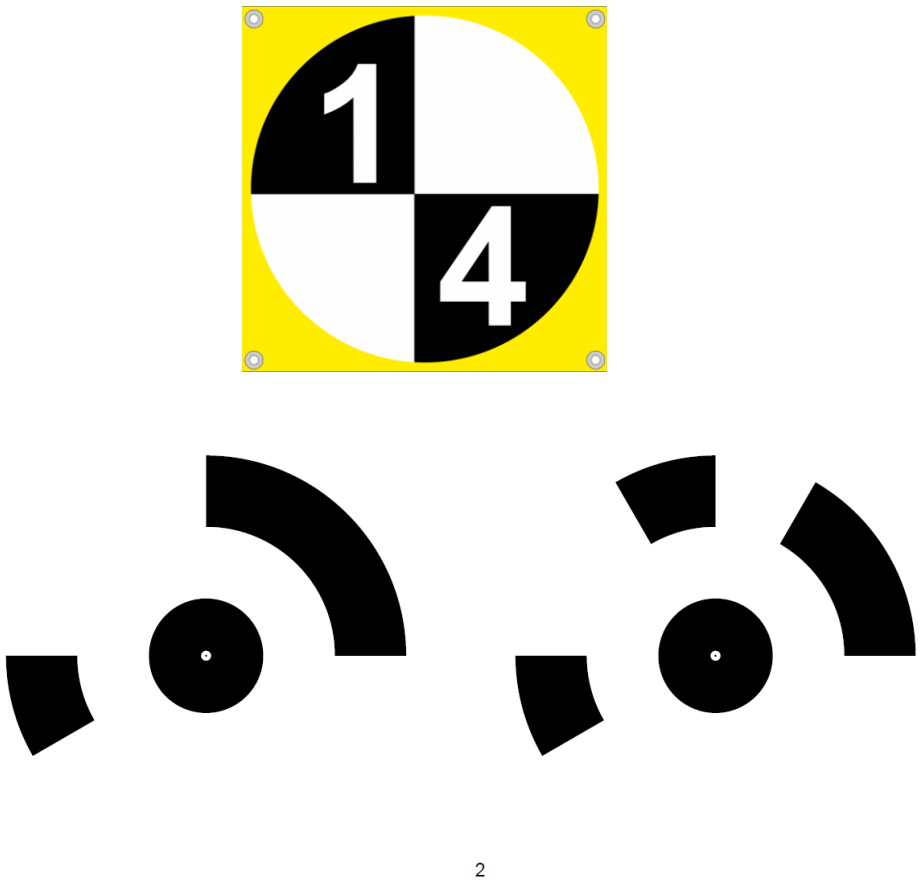

Fig. 8-e: Examples of targets: winter campaign (upper part), Agisoft targets for automatic detection (bottom).

[14] https://agisoft.freshdesk.com/support/solutions/articles/31000148855-coded-targets-and-scale-bars

Due to the challenging terrain conditions, the positions of the winter and summer GCPs were situated in different places. The accessibility of the terrain was limited by features such as dwarf pine and waterfall levees situated in the middle of the avalanche path. In the winter, our strategy was to reach the accumulation zone first and then climb up towards the release zone. On the other hand, during the summer, we had to approach the upper part of the avalanche release area, where narrow paths exist amidst relatively dense and difficult-to-penetrate dwarf pines. These factors influenced the selection and placement of GCPs, ensuring their suitability and practicality in each respective season.

We used the Trimble Rs8 GNSS receiver with the assistance of VRS-NOW (Virtual Reference Station Network) technology. This system utilizes satellites from both the GPS and the GLONASS systems to enhance the accuracy of positioning. In our measurements, we employed the “measure detailed points” function, which provided accurate horizontal and vertical position measurements in approximately 5 seconds.

8.1.4 UAS image acquisition

The UAS flight was conducted using a typical systematic mapping pattern, with the camera positioned at an orthogonal angle 87-89° to the surface. The mission planning was done in the Litchi application for the Žlab Úpičky study site, which provided cost-effective solutions and included ground elevation data, crucial for our steep terrain area to ensure consistent flight altitude. However, it was necessary to be cautious about overlaps (missing places in DEM), as the app did not automatically plan for horizontal and side overlaps, potentially resulting in missing areas in the DEM. The flight height was verified in Google Earth (GE), where the KLM format was uploaded from Litchi. The Graswang mission was preplanned in both applications – Litchi and Pix4D Capture. To georeference the photogrammetric images, we utilized 9 GCPs for the winter dataset and 10 GCPs for the summer dataset. The images were processed using Agisoft Metashape Professional Software version 1.7.4 build 13028) (www.agisoft.com). The winter datasets consisted of 622 images, while the summer dataset comprised 1173 images.

8.1.5 Agisoft processing parametres

The processing parametres for both study sites, the Žlab Úpičky and Graswang, recpectively are displayed in Table 6 and Table 7.

Table 6: Processing parameters of the Žlab Úpičky avalanche path. Coordinate system: S-JTSK / Krovak East North (EPSG::5514). Source: Agisoft Photoscan.

Point Cloud	Snow period	Snow free period
Alignment parameters		
Accuracy	High	High
Generic preselection	Yes	Yes

Reference preselection	Source	Source
Key point limit	100 000	100 000
Tie point limit	40 000	40 000
Guided image matching	No	No
Adaptive camera model fitting	No	No
Depth maps generation parameters		
Quality	Medium	Medium
Filtering mode	Mild	Mild
Texturing parameters		
Mapping mode Adaptive	orthophoto	orthophoto
Blending mode	Mosaic	Mosaic
DEM	17.7 x 16.3	14.3 x 13.2

Table 7: Processing parameters of Graswang site. Coordinate system: ETRS89 / UTM zone 32N (EPSG::25832). Source: Agisoft Photoscan.

Point Cloud	**snow period**	**snow free period**
Alignment parameters		
Accuracy	High	High
Generic preselection	Yes	Yes
Reference preselection	Source	Source
Key point limit	40,000	40,000
Tie point limit	8 000	8 000
Guided image matching	No	No
Adaptive camera model fitting	No	No
Depth maps generation parameters		
Quality	Medium	Medium
Filtering mode	Mild	Mild
Texturing parameters		
Mapping mode Adaptive	orthophoto	orthophoto
Blending mode	Mosaic	Mosaic
DEM	17,7 x 16,3	14,3 x 13,2

8.1.6 Manual snow probe and UAS SD measurement

SD was probed at the GCP positions and positions displayed in Table 11 for the Žlab Úpičky and Table 14 for Graswang study site. SD was measured four times (four square points) with 10 cm minimal distance with Arva Pro+ 280 cm snow probe in Žlab Úpičky avalanche path. The output value was counted as a mean of four measurements. SD in Graswang was measured five times and the average value was taken for comparison with UAS SD estimation Table 14.In this study, snow depth was calculated by subtraction of surface: snow cover DEM and snow free DEM snow free (Fig. 8-f).

(Lee, Park, Choi, & Kim, 2021)

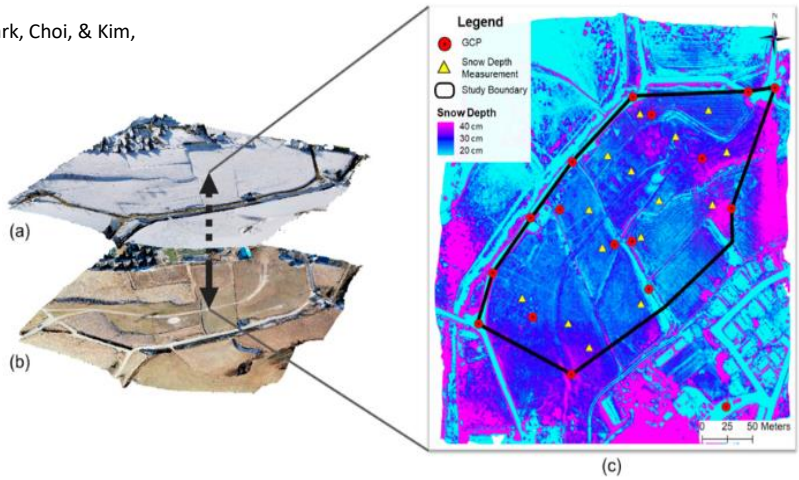

Fig. 8-f: (a+b) Orthophotos of DSM (snow surface) and DEM (without snow cover) (c) The snow depth map that was obtained by subtracting the DSM of ground from that of the snow surface. Images were reused from Lee et al., 2021.

8.2 RAMMS model

The RAMMS numerical avalanche dynamics simulation software (Christen et al., 2010), version 1.8.0, was used to model the documented Žlab Úpičky avalanche in Obří důl in the Krkonoše Mountains in order to compare the measured snow depths of the accumulation zone by UAS. This model, developed by the WSL Institute for Snow and Avalanche Research SLF, allows the modelling of two-dimensional runout distances.

The examined avalanche released on 15/02/2021 in the avalanche path Žlab Úpičky (cadastre number 02). We can classify it as a small avalanche < 400 m partly gully/ channelled avalanche according to the RAMMS software classification explained in (Christen et al., 2010). The highest recorded Žlab Úpičky avalanche length was 1100 m since 1962 according to Vrba and Spusta (1975, 1991), Spusta and Kociánová (1998), Spusta et al. (2003, 2020) and (Součková et al., 2022).

Avalanche flow heights and velocities were calculated on three-dimensional digital terrain models. Information of simulations: the release area (mean slope, total volume), flow behaviour (max flow velocities and heights) and stopping behaviour (mass flux) are provided in avalanche simulation.

RAMMS avalanche model **inputs** are: 1. DEM; 2. release height, 3. extent of forest, 4. friction parameters (Mu, Xi). Possible **outputs** are: heigh of accumulation, velocity flow, bedrock pressure; 2D, 3D maps and simulations; line and cross sections profiles; and trace log (Fig. 8-g).

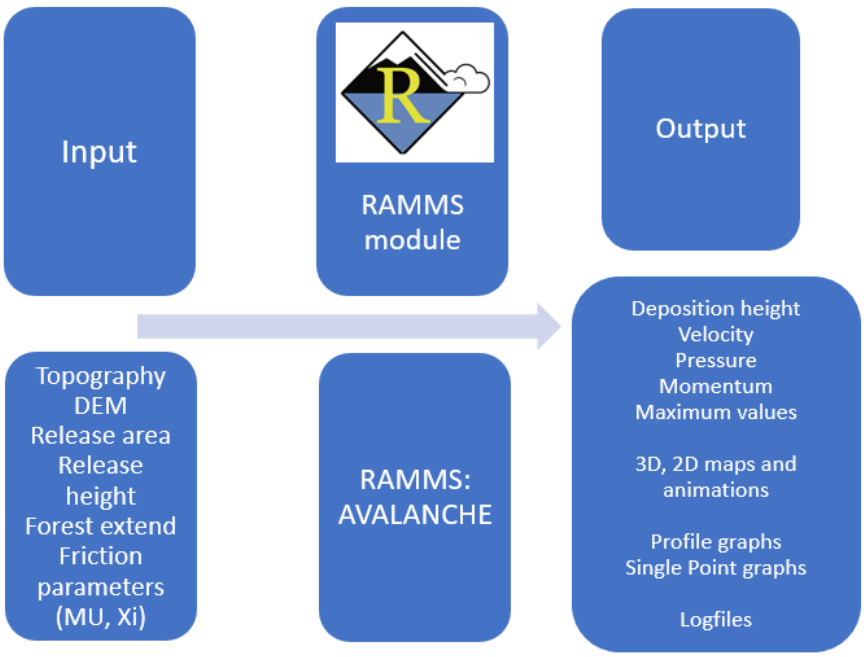

Fig. 8-g: RAMMS avalanche module and its input and output data scheme.

Within RAMMS solutions we considered three scenarios:

1) different DTM resolution (1m and 5m)

2) including forest layer – to consider roughness (no forest, forest values) without ability to distinguish in between dense and sparce forest/ bush types

3) cohesion – 150 Pa recommended by RAMMS manual.

8.2.1 Input variables: topography, release area, and forest extend

The best simulation included DTM resolution of 1 m extracted raster of Obří důl from KRNAP LIDAR data. The airborne LiDAR data for the Czech part of the Krkonoše Mountains study area were collected, using a Riegl LMSQ680i scanner. The data were collected in July and August, during the leaf-on season. Over the course of 16 days, 553 flight lines with a 20% flight line side overlap were flown at 700 meters above the ground. The obtained LiDAR point cloud density was 5 points per m^2. The vertical datum of the LIDAR point cloud is Baltic Vertical Datum—after adjustment (EPSG: 5705), and the horizontal datum is the Datum of Uniform Trigonometric Cadastral Network (EPSG: 5514).

Release area is divided into two snow depth values 0.3 and 1.7 m (release heights were measured at the day of Žlab Úpičky avalanche release by Mt. Rescue Krkonoše. Release area shape and its upper boundary was delimited over UAS orthophoto from Agisoft Photoscan (Fig. 8-h). The average release width was set up to 60 m, Mt. Rescue Krkonoše reported this value in their report. Lower boundary of the release area was set up at the same level as KRNAP administrative deliminated. The release area was 3599.1 m^2 and release area volume: **5006.1 m^3** counted by RAMMS.

We considered roughness, as Žlab Úpičky is covered by grassy, forestry, and dwarf pine vegetation. RAMMS model enable to classify between no forest and forest values. The forest polygon was vectorised over UAS orthophoto created by the principal investigator of this thesis and ArcPro background orthophoto vectorised by Podaný, (2023) (Fig. 8-h). Dwarf pine vegetation is classified as no forest as it is usually covered by snow in the winter.

Fig. 8-h: Vegetation classification of land cover of the Žlab Úpičky avalanche path (UAS screened in summer 2021).

8.2.2 Friction parameters, Cohesion and Curvature

The RAMMS model relies on the well-established Voellmy model (Salm, 1993) to simulate the frictional resistance of avalanches. This two-parameter model separates friction into two types:

1. Viscous-turbulent friction: represented by the coefficient ξ,
2. Dry-Coulomb friction: represented by the coefficient μ,

Both a constant and a variable friction mode are available in the Avalanche module. Naturally, calculations based on constant friction values do not consider forest areas or terrain that is undulating. It is suggested to use the variable friction values to prevent it. An automatic RAMMS procedure classifies the friction values and based on the analysis of topographic data (slope angle, altitude, and curvature), forest data, and global parameters return period and avalanche volume. Values are kept in ASCII files called MuXi-files, which can be easily imported into GIS applications (like ArcGIS). Each cell of the DEM-based calculation was calculated during the automatic process. Although the altitude is known, it is still necessary to calculate the slope angles and curves. Automatic computation classifies the "track type" as flat, open slope, channelled, or gully (Bartelt, 2022)

To handle materials with yield stress (e.g., snow, mud), RAMMS additionally incorporates a cohesion parameter N_o. This prevents unrealistic flow initiation on gentle slopes when normal stress is insufficient to overcome the yield stress (Bartelt, 2022). The strength of the cohesive bonding between granules is determined by snow temperature and moisture content. Strong, cohesive interactions reduce the free mechanical energy in the avalanche core and therefore influence the avalanche flow regime (Bartelt et al., 2015).

RAMMS also accounts for the terrain's curvature through a dedicated parameter. This influences the calculation of the centrifugal force, impacting the normal stress and ultimately affecting the flow's friction and deceleration, especially in winding paths. For detailed formulas and further explanations, we refer to the RAMMS avalanche website[15] or the provided RAMMS avalanche user manual 1.8.0 (Bartelt, 2022).

[15] https://ramms.slf.ch/en/modules/avalanche/theory/friction-parameters.html

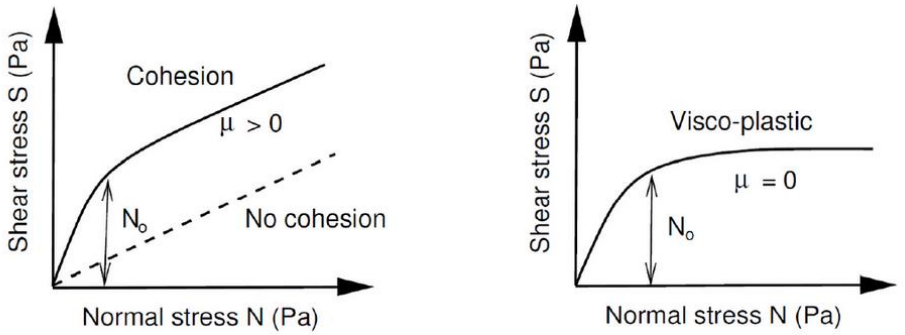

Fig. 8-i: Relation between shear and normal stress. Left: yield stress No serves to increase the shear stress for higher normal pressure. At low normal pressure (small flow heights) the shear stress increases rapidly from S=0 to S = No. The slope of the "S vs. N" relation remains μ when the normal pressure is large. Right: If μ = 0 it is a visco-plasic behaviour. Reused from: RAMMS theory[16].

[16] https://ramms.slf.ch/en/modules/avalanche/theory.html

8.3 CRNS method, its footprint and CRNS workflow

For continuous detection of spatially averaged snow depth and snow water equivalent we used a method of Cosmic-Ray neutron sensing in alpine environments. We compared CRNS sensors derived snowpack characteristics (unweighted calibration) with in-situ observations of SWE by weighing and snow probe SD measurements, and we performed UAS screening and derived snow depth from UAS digital elevation models (Fig. 8-j).

Recently, it has been shown that Cosmic-Ray Neutron Probes (CRNP) are a promising technique to monitor snowpack development (Bogena et al., 2020). and to measure snow depth (Schattan et al., 2019, 2017) with a horizontal footprint radius in the order of 200 m (Schrön et al., 2017). CRNS provide SWE derivation of a medium scale footprint 12-18 ha (Bogena et al., 2020) and minor maintenance requirements (Fersch et al., 2020). CRNS can be placed a few meters above the snow surface (Desilets, 2017; Desilets et al., 2010; Schattan et al., 2017; Mark J.P. Sigouin and Si, 2016). A CRNP placed above the snow cover is influenced by snow up to more than 150 m away from the sensor (Zweck et al., 2013), thus enabling the characterization of medium scale and heterogeneous snow cover dynamics. Manual in-situ SWE and SD were collected in three lines about 120 m long, under angle of 120°. In each line four SWE measurements are taken and five snow probe snow depth measurements at every sampling site (Fig. 8-k).

Fig. 8-j: Cosmic-Ray Gauge in Graswang (upper left), and in Lechkogel (lower left) and Snow tube (right).

Fig. 8-k: In situ SD and SWE collection methodology: three lines under 120 ° at Lechkogel station.

Preliminary tasks before focusing on processing in-situ and CRNS data in R software is to make correction which was done through the first phase of Cosmic Sense project available at https://www.uni-potsdam.de/de/cosmicsense/. Cross border cooperation brings together scientists from nine institutes and universities from Germany and Austria investigated for example by Dr. Benjamin Fersch (KIT IFU). The aim of the corrections are to normalise the Neutron Count rates to a number of reference conditions (Bogena et al., 2020) and it is necessary to correct:

1. barometric pressure,
2. incoming cosmic radiation - corrected neutron counts,
3. atmospheric water vapour.

For CRNS data we adopted two approaches to relate gravimetric samples with above-snow neutron measurements. We tried to a) rescale the N_o parameter (a range of values of N_o: 3500-6000) and the observed intensities b) level the pressure (same reference conditions). Next, we changed N_o calibration function parameters according to (Bogena et al., 2020). For fitting neutron counts and SWE relation, at first, we used idea of (Desilets et al., 2010), later modified by (Howat et al., 2018) method. However, (Köhli et al., 2021) assumed that the equation is mathematically over defined with four parameters (hyperbolic) relationship between neutron intensity and soil moisture for the purpose of unique fitting solutions and suggested to reduce the hyperbolic part to three parameters.

Different methods are used for converting neutron rates into snowpack characteristics, some performed better such as a) N_O Calibration function b) physically based calibration function, and other results like c) linear regression, and d) thermal, epithermal ratio indicated worse results in Bogena et al., (2020) study. We worked with the N_0 function

which we had to fit manually for each station. The function for relating neutron counts with SWE is:

(1)

$$SWE(N) = \Theta(N) = a_0 \frac{1 - N/N_{max}}{a_1 - N/N_{max}}$$

(Köhli et al. 2021)

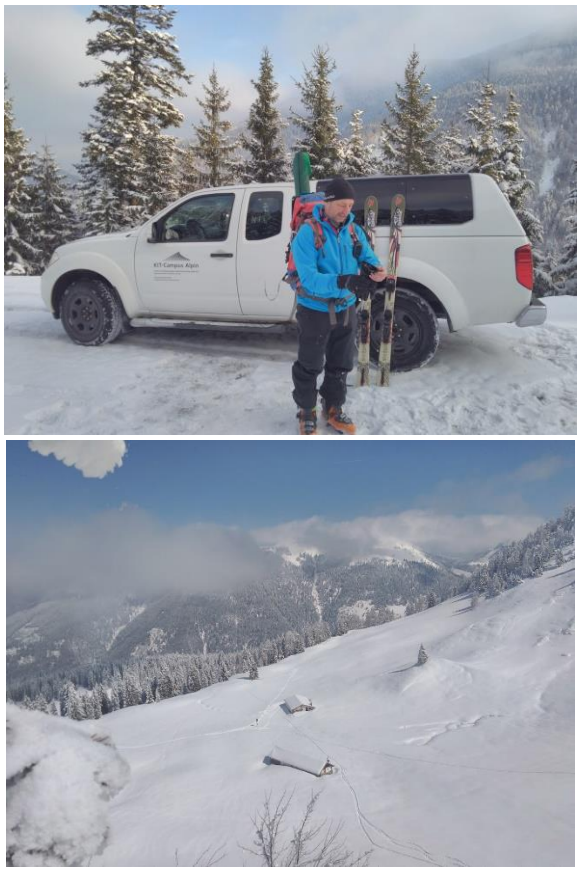

Fig. 8-l: Terrain work using ski-tours to Lerchkogel CRNS station. Photo taken by M. Součková.

9 Results

This section presents results from manual, UAS and CRNS monitoring of snow:

1. DEMs of the Žlab Úpičky avalanche path and its difference raster (NE Czechia) see in 9.1
2. DEMs snow cover and snow free of Graswang study site and CRNS results from different elevation study sites in Ammer and Isar catchment (Bayer region), see in 9.2.
3. RAMMS simulation, see 9.3
4. elevation dependent SWE monitoring, see 9.4.

This chapter assess snow depth distribution in 1) steep avalanche terrain, specifically the Žlab Úpičky avalanche path in low attitude Krkonoše mountain range in NE Czechia 2) flat terrain in low altitude study site in Graswang, Bayern region in south Germany. Within the results, there are different methods or combination of methods used such as UAS monitoring and image processing, manual snow probe measurements and CRNS monitoring of snow. Furthermore, UAS snow depth results from the Žlab Úpičky are compared with RAMMS snow depth output. The outputs from UAS might serve as the input or verification data to RAMMS model simulating. Lastly, elevation dependent SWE to neutron counts was analysed within DBU Fellowship in Ammer and Isar river catchments where CRNS stations are installed, and data have few years of measurements displayed in Table 5.

9.1 UAS monitoring of steep Žlab Úpičky avalanche path (Krkonoše) terrain

We conducted UAS monitoring of the Žlab Úpičky avalanche path and obtained snow cover and snow free orthophotos through post-processing in Agisoft Photoscan version 1.7.4 build 13028 (Fig. 9-a). Fig. 9-a shows the different zones of the avalanche path, including the release area, transport zone, and accumulation zone. The GCPs in snow cover period coordinates errors X = 1.3; Y = 1.8, Z= 0.6 cm of control points and coordination errors X=3.1, Y= 2.2, Z = 12.0 cm of check points are displayed in Table 9. XY coordinates are satisfactory till 5 cm error, however Z coordinate error could be lower. The total error: RMS of marker errors is 12.8 cm for snow covered period.

The GCPs coordinates error is X =1.5; Y =2.7, Z= 0.9 cm of control points and X = 3; Y =5, Z=7.2 cm errors of check points in snow free period (Table 10). The RMS of marker errors is 9.3 cm for snow free period. The difference raster indicates the negative difference values in vegetated areas where dwarf pines or forests are present (right part of the release area, Fig. 9-a). Interestingly, the middle-upper release area exhibits unusually high negative difference values, contradicting the snow cover observed in the winter UAS orthophoto, and summer present status where short grass was located, as we monitored the path after the last remnants of snow patches. This discrepancy may be better attributed to factors such as UAS flight settings, processing errors, or limitations of the UAS SfM method in steep, snow-covered, or forested (either trees or bushes) terrain. Additionally, tree shadows negatively impact the accuracy of snow height estimation. Nevertheless, the observed values fall within the SD error range. The average accumulation snow depth values range from approximately

0.6-4.8 m, with light blue areas indicating the presence of dwarf pines or trees within the accumulation area (Fig. 9-a). The GSD was 2.5 in snow cover and 3.1 in snow free period in Žlab Úpičky (Table 8).

Table 8: Overal survey parametres and image configuration in Žlab Úpičky avalanche path. Coordinate system: S-JTSK / Krovak East North (EPSG::5514). Source: Agisoft Photoscan.

DEM	Number of photoes	Ground resolution [cm/pix]	Flight altitude	Tie points	Point cloud	Coverage area [km²]	Reconstructed DEM	
					RMS reprojection error pix		Resolution [cm/pix]	Point density [points/m2]
Snow cover	678	2.5	66.1	1 465 306	0.69	0.18	9.86	103
Snow free	1 196	3.1	79.4	3 644 069	0.73	0.056	9.03	123

Table 9: GPSs collected in snow period and X, Y, Z coordinates of control points RMSE (upper table) and check points RMSE (lower table). The total error is the RMS of marker errors. Coordinate system: S-JTSK / Krovak East North (EPSG::5514). Source: Agisoft Photoscan.

RMSE of control points:

Count	X error [cm] (Easting)	Y error [cm] (Northing)	Z error [cm] (Altitude)	XY error [cm]	Total error [cm]
7	1.3	1.8	0.6	2.2	2.3

GCP number	X error [cm] (Easting)	Y error [cm] (Northing)	Z error [cm] (Altitude)	Total error [cm]	Image pixel
243	0.48	-0.92	-0.77	1.29	0.85
244	-0.92	0.42	0.11	1.02	1.52
260	-0.62	0.53	1.18	1.43	0.87
262	0.08	3.82	0.16	3.82	1.07
263	0.32	-1.34	0.40	1.43	0.99
265	2.12	-2.30	-0.33	3.14	0.79
269	-2.38	0.21	-0.64	2.47	0.92
Total	**1.3**	**1.8**	**0.6**	**2.3**	**0.92**

RMSE of check points:

Count	X error [cm] (Easting)	Y error [cm] (Northing)	Z error [cm] (Altitude)	XY error [cm]	Total error [cm]
2	3.2	3.1	12.0	4.4	12.8

GCP number	X error [cm] (Easting)	Y error [cm] (Northing)	Z error [cm] (Altitude)	Total error [cm]	Image pixel
261	0.86	-4.05	-12.75	s	0.60
270	4.48	-1.53	-11.15	12.11	2.91
Total	**3.2**	**3.1**	**12.0**	**12.8**	**1.4**

Table 10 : GCPSs collected in snow free period and X, Y, Z coordinates (X – Easting, Y – Northing, Z – Altitude) of control points RMSE (upper table) and check points RMSE (lower table). The total error is the RMS of marker errors). Coordinate system: S-JTSK / Krovak East North (EPSG::5514). Source: Agisoft Photoscan.

RMSE of control points:

Count	X error [cm] (Easting)	Y error [cm] (Northing)	Z error [cm] (Altitude)	XY error [cm]	Total error [cm]
7	1.5	2.7	0.9	3.1	3.2
GCP number	**X error [cm] (Easting)**	**Y error [cm] (Northing)**	**Z error [cm] (Altitude)**	**Total error [cm]**	**Image pixel**
21	0.94	2.07	1.04	2.50	1.05
23	-0.14	-0.19	0.00	0.24	0.47
27	2.00	-1.86	-0.93	2.89	0.31
28	-1.19	1.25	0.63	1.83	0.26
29	1.30	4.69	1.59	5.12	1.13
31	-2.38	-4.04	0.60	4.73	0.73
24	-1.61	-1.26	-0.73	2.18	0.23
Total	**1.5**	**2.7**	**0.9**	**3.2**	**0.6**

RMSE of check points:

Count	X error [cm] (Easting)	Y error [cm] (Northing)	Z error [cm] (Altitude)	XY error [cm]	Total error [cm]
2	3.0	5.0	7.2	5.8	9.3
GCP number	**X error [cm] (Easting)**	**Y error [cm] (Northing)**	**Z error [cm] (Altitude)**	**Total error [cm]**	**Image pixel**
20	-3.79	6.20	9.89	12.27	0.33
25	1.79	-3.45	2.34	4.54	0.29
Total	**3.0**	**5.0**	**7.2**	**9.3**	**0.3**

The actual marker erorr value is influenced by selection of combination and number of control and check points in Agisoft Photoscan.

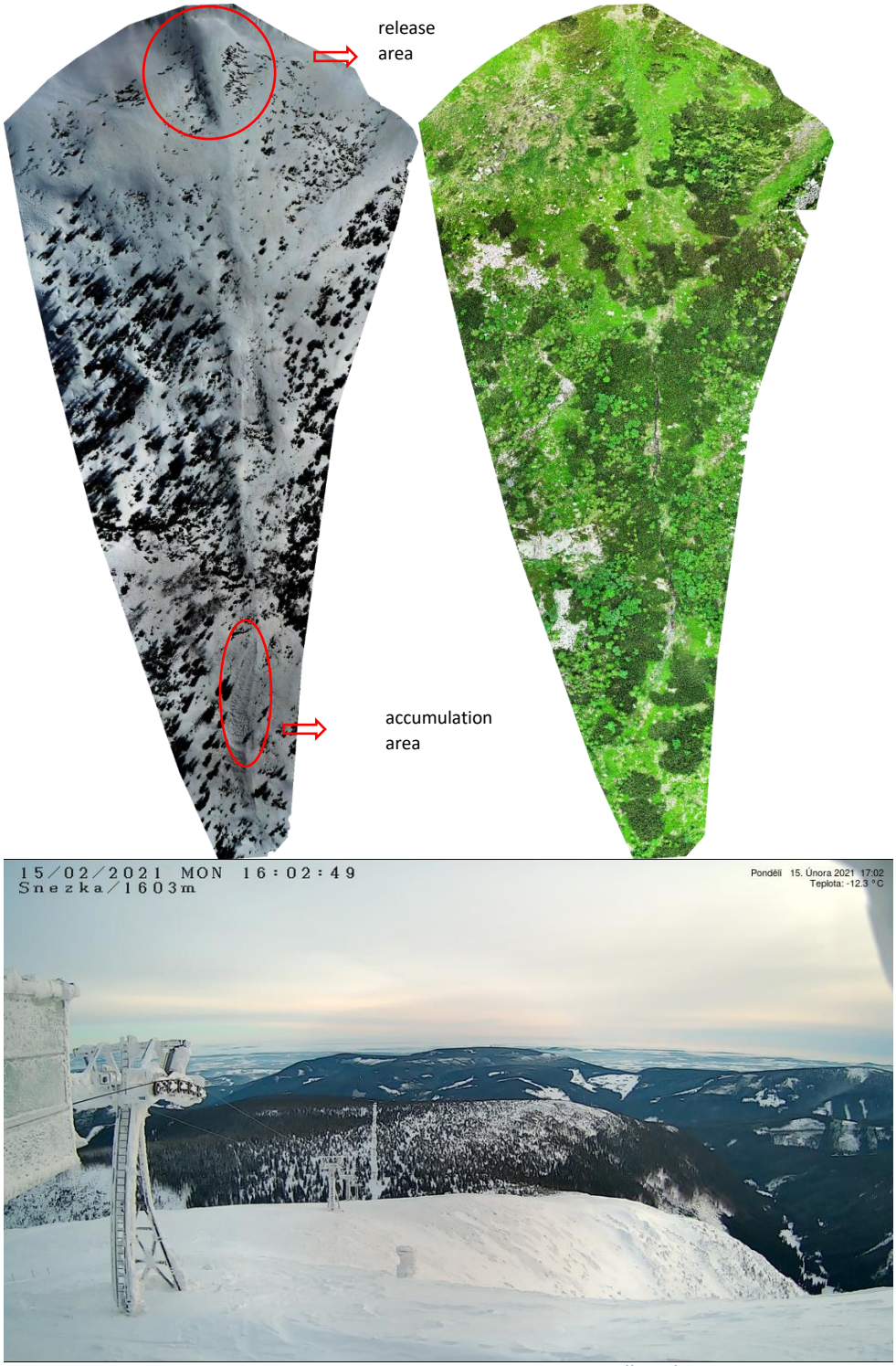

Fig. 9-a: Winter (upper left) and summer (upper right) orthophotos of Žlab Úpičky avalanche path, and weather situation in Krkonoše Mts. captured from the Sněžka camera (bottom image) on 15/02/2021 in the afternoon. Source: Sněžka camera.

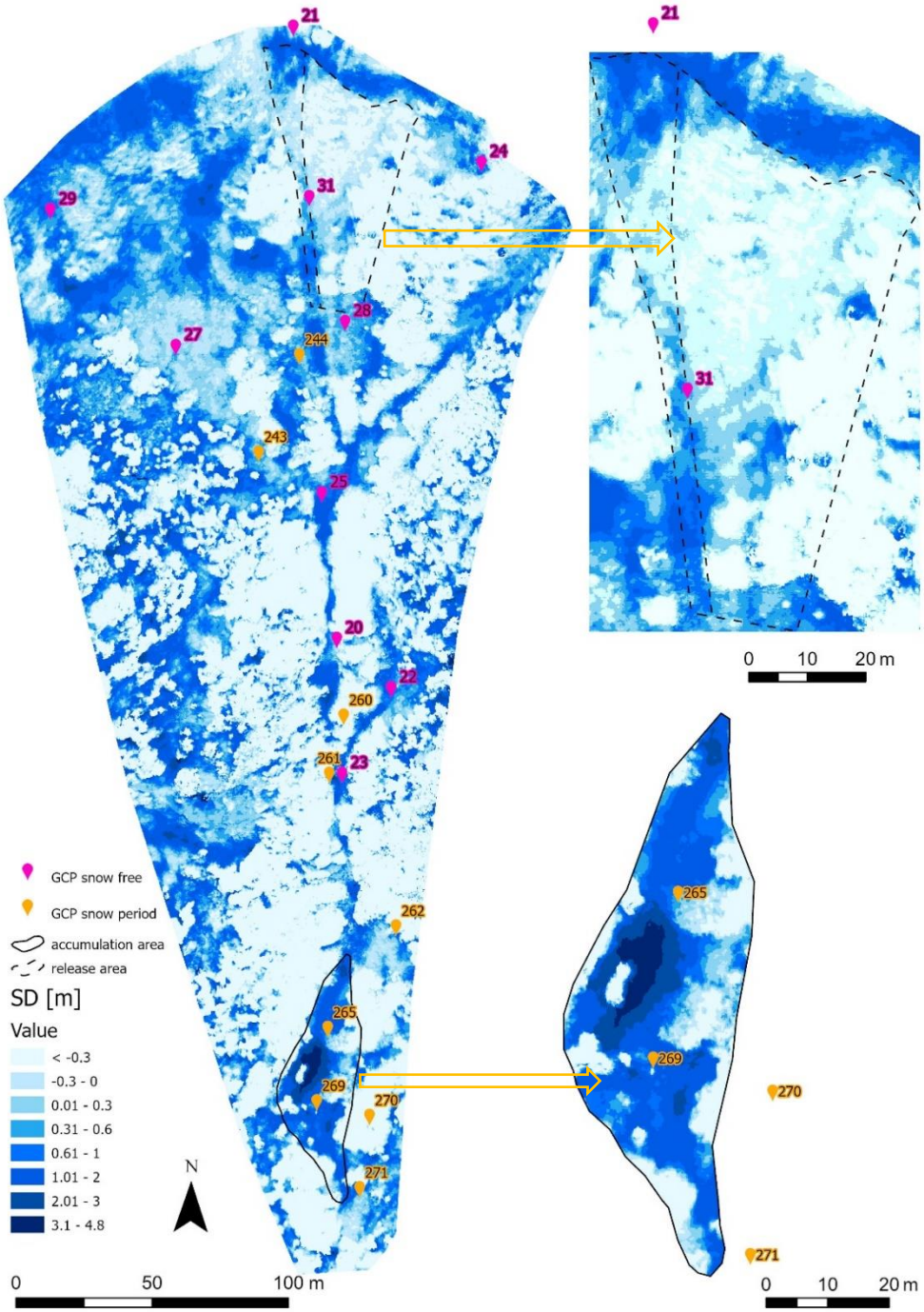

Fig. 9-b: Difference in snow depth between the Digital Surface Model (DSM) captured during winter and the Digital Elevation Model (DEM) from summer for the release and accumulation areas in the Žlab Úpičky. GCP numbers present measured points by Trimble R8s GNSS.

There are notable discrepancies between the UAS SD difference raster and manual snow probe values. For example, GCP coded 265 had a snow probe value of 187.8 cm compared to the UAS measurement of 48 cm, and GCP 269 had a snow probe value of 191 cm compared to the UAS measurement of – 27 cm). Similarly, GCP 263 had a snow probe value of 136 cm while the UAS measurement was 120 cm. GCP 270 and 271, which are located where dwarf pines are present (Fig. 8-h), have measured heights of 109.8 and 63.5 cm, respectively (Table 11). These measurements have the potential for significant errors due to the presence of vegetation. However, the elevation measurements obtained from UAS and GNSS for the winter GCPs show a maximum difference of 0.14 cm, indicating a high level of agreement between the two methods despite the challenging terrain conditions (Table 12, column "difference: difference GNSS and UAS"). There are three measurements (260, 262) in the mid-low position of the avalanche path (Table 12) that deviate from maximum difference of 0.14 cm. For the summer GCPs, the elevation differences between UAS and GNSS are within 10 cm, except for one measurement (15 cm) represented by code 22 in Table 13.

Table 11: Snow probe SD point measurements, SD mean and its deviation in the Žlab Úpičky avalanche path study area. Coordinate system: S-JTSK / Krovak East North (EPSG::5514).

ID GCP	SD1 [cm]	SD2 [cm]	SD3 [cm]	SD4 [cm]	mean	Standard deviation (sd)
243	**44**	**70**	**85**	**60**	**64.8**	**17.2**
244	**110**	**110**	**100**	**90**	**102.5**	**9.6**
245	90	101	97	70	89.5	13.8
246	100	95z	108	91	98.5	7.3
247	110	82	105	109	101.5	13.2
248	83	94	82	83	85.5	5.7
249	117	117	104	83	105.3	16.0
250	70	62	65	60	64.3	4.3
251	90	81	80	84	83.8	4.5
252	129	110	109	100	112.0	12.2
253	63	62	62	62	62.3	0.5
254	90	76	101	78	86.3	11.6
255	69	57	85	85	74.0	13.6
256	103	91	101	100	98.8	5.3
257	94	90	98	94	94.0	3.3
258	94	83	89	98	91.0	6.5
259	90	95	69	79	83.3	11.6
260	**43**	**50**	**75**	**53**	**55.3**	**13.8**
261	**102**	**114**	**112**	**85**	**103.3**	**13.3**
262	**75**	**95**	**66**	**93**	**82.3**	**14.1**
263	**130**	**145**	**130**	**139**	**136.0**	**7.3**

264	175	145	130	137	146.8	19.8
265	**173**	**186**	**187**	**205**	**187.8**	**13.1**
266	>300	>301	>302	>303		
267	125	117	145	136	130.8	12.3
268	201	212	215	214	210.5	6.5
269	**190**	**194**	**180**	**201**	**191.3**	**8.8**
270	**132**	**126**	**92**	**89**	**109.8**	**22.4**
271	**57**	**69**	**69**	**59**	**63.5**	**6.4**

Table 12: GNSS Trimble measurements of GCP points and UAS estimated snow depth measurements, and its difference value (GNSS – estimated UAS) in the Žlab Úpičky terrain survey in snow cover period. Coordinate system: S-JTSK / Krovak East North (EPSG::5514).

Trimble code	Northing	Easting	Elevation GNSS [m]	Code	estimated UAS winter [m]	difference GNSS and UAS [m]
243	-641761.1	-983086.9	1283.34	GCP	1283.22	0.11
244	-641746.1	-983051.1	1298.44	GCP	1298.36	0.08
245	-641744.3	-983038.7	1304.16	snow	1304.14	0.03
246	-641742.7	-983042.7	1301.66	snow	1301.70	-0.04
247	-641746.4	-983048.3	1299.86	snow	1299.72	0.14
248	-641746.5	-983053.8	1297.17	snow	1297.06	0.11
249	-641756.5	-983094.1	1278.62	snow	1278.59	0.03
250	-641742.1	-983092.1	1275.52	snow	1275.46	0.05
251	-641733.7	-983090.9	1275.23	snow	1275.19	0.04
252	-641727.3	-983093.3	1274.37	snow	1274.35	0.02
253	-641722.9	-983094.8	1274.43	snow	1274.52	-0.09
254	-641727.5	-983099.8	1271.52	snow	1271.50	0.02
255	-641730.6	-983103.2	1269.49	snow	1269.42	0.07
256	-641738.1	-983101.1	1269.71	snow	1269.66	0.06
257	-641734.9	-983105.7	1267.25	snow	1267.27	-0.02
258	-641745.4	-983105.6	1269.53	snow	1269.52	0.01
259	-641751.0	-983108.3	1270.66	snow	1270.76	-0.11
260	-641729.9	-983183.5	1219.78	GCP	1220.21	-0.43
262	-641710.6	-983260.9	1174.29	GCP	1174.65	-0.36
263	-641715.4	-983304.1	1152.93	GCP	1153.01	-0.08
264	-641733.4	-983299.8	1153.23	snow	1153.21	0.02
265	-641735.7	-983298.2	**1153.32**	**GCP**	1153.32	0.00
266	-641738.4	-983299.7	1152.86	snow	1152.89	-0.04
267	-641734.7	-983305.7	1151.71	snow	1151.76	-0.05

268	-641734.2	-983311.4	1150.18	snow	1150.22	-0.03
269	-641739.8	-983325.1	**1145.31**	**GCP**	1145.31	-0.01
270	-641720.4	-983330.4	**1143.46**	**GCP**	1143.53	-0.08
271	-641724.0	-983357.0	**1134.43**	**GCP**	1134.40	0.02

Table 13: GNSS Trimble measurements of GCP points and UAS estimated snow depth measurements and its difference value (GNSS – estimated UAS) in the Žlab Úpičky terrain survey in snow free period. Coordinate system: S-JTSK / Krovak East North (EPSG::5514).

ID GCP	Northing	Easting JT	Z	estimated UAS summer	dif_GNSS_UAS
20	-641732.4	-983155.3	1241.3	1241.4	-0.07
21	-641748.4	-982930.6	1377.4	1377.5	-0.05
22	-641712.4	-983173.4	1228.6	1228.4	0.14
23	-641730.4	-983204.8	1206.2	1206.2	0.02
24	-641679.3	-982980.5	1364.7	1364.6	0.00
25	-641737.9	-983101.8	1268.0	1268.0	-0.02
27	-641791.5	-983047.8	1311.9	1311.9	0.01
28	-641729.3	-983038.9	1303.5	1303.5	-0.02
29	-641837.6	-982997.8	1360.0	1359.9	0.09
31	-641742.5	-982993.1	1331.6	1331.6	-0.02

9.2 UAS monitoring of flat Graswang terrain (Northern Limestone Alps, Bayern region)

We received two sets of surface models and orthomosaics from UAS flights conducting during winter: snow cover and spring: snow free period (Fig. 9-d). For our analysis, we compared the elevation of GCP obtained using the Global Navigation System (GNSS) with the elevation data captured by the UAS. The comparison revealed that the elevation data from the GNSS and UAS deviated by up to 10 cm, except for GCP 02 (Fig. 9-d), which showed a deviation of 22 cm. This deviation was consistent for both snow cover and snow free period monitoring. Additionally, we compared the manually measured snow probe SD with the SD estimated by the UAS. The results showed that at the points where manual snow probing was conducted, the difference between the two methods ranged from 0 to 19 cm with satisfactory relative values of 0.97-1.26 in Table 14 (column relative value UAS/SDavg) except of the sample D2 with relative value of 1.75. We attribute the variations in the results to potential imprecision in the UAS snow depth screening due to fresh snow with has fallen. This finding is consistent with previous research by (Bühler et al., 2016) that highlights the challenges of accurately measuring snow depth with UAS in freshly fallen snow conditions.

Table 14: Manual snow depth samples and the difference between UAS estimation and manual snow depth measurements. Coordinate system: ETRS89 / UTM zone 32N (EPSG::25832).

Sam-ple	Mean Eleva-tion	DSM-DEM swe points [m]	SD1 [cm]	SD2 [cm]	SD3 [cm]	SD4 [cm]	SD5 [cm]	SDAvg [cm]	SDSd [cm]	SD man-ual mi-nus UAS	relative value UAS/SDavg
B2	863.7	0.47	41	48	53	53	47	**48.4**	4.98	-0.01	0.97
C1	863.4	0.42	40	41	42	42	44	**41.8**	1.48	0.00	1.01
C2	863.7	0.48	35	38	39	40	38	**38**	1.87	0.10	1.26
C3	863.7	0.41	34	34	36	37	37	**35.6**	1.52	0.06	1.16
D1	863.7	0.49	45	44	44	49	45	**45.4**	2.07	0.03	1.07
D2	863.9	0.43	20	25	28	22	28	**24.6**	3.58	0.19	1.75
D3	863.4	0.40	30	31	31	32	33	**31.4**	1.14	0.08	1.26
E1	863.8	0.54	48	40	41	43	41	**42.6**	3.21	0.11	1.26
E2	864.2	0.35	50	48	51	50	47	**49.2**	1.64	-0.14	0.72
E3	861.9	0.40	40	39	38	40	39	**39.2**	0.84	0.01	1.03

The GCPs coordinates in snow cover period have mean X = 1.0; Y = 0.9, Z= 0.65 cm errors of control points and X=1.1, Y= 1.5, Z = 1.6 cm of check points. Individual GCPs are displayed in Table 15. The XY error of check points is **1.9 cm**. The total error: RMS of marker errors is **2.5 cm** for snow covered period (Table 15).

Table 15: Graswang GPS coordinates (X – Easting, Y – Northing, Z – Altitude) in snow cover period of control points RMSE (upper table) and check points RMSE (lower table). Coordinate system: ETRS89 / UTM zone 32N (EPSG::25832).

Count	X error [cm] (Easting)	Y error [cm] (Northing)	Z error [cm] (Altitude)	XY error [cm]	Total error [cm]
7	**1.0**	**0.9**	**0.65**	**1.3**	**1.5**

GCP number	X error [cm] (Easting)	Y error [cm] (Northing)	Z error [cm] (Altitude)	Total error [cm]	Image pixel
04	-0.78	-1.00	-0.95	1.59	0.15
05	-0.43	-0.20	0.88	1.00	0.18
07	0.54	0.49	-0.54	0.91	0.20
08	0.46	1.69	0.86	1.95	0.25
09	-0.48	0.44	-0.31	0.72	0.20
13	-0.03	-0.71	0.20	0.74	0.25
14	2.33	0.52	0.05	2.39	0.14
Total	**1.0**	**0.9**	**0.6**	**1.5**	**0.2**

Count	X error [cm] (Easting)	Y error [cm] (Northing)	Z error [cm] (Altitude)	XY error [cm]	Total error [cm]
4	**1.1**	**1.5**	**1.6**	**1.9**	**2.5**

GCP number	X error [cm] (Easting)	Y error [cm] (Northing)	Z error [cm] (Altitude)	Total error [cm]	Image pixel
03	-1.60	-1.25	-0.19	2.04	0.19
06	1.37	-0.23	-1.56	2.09	0.22
12	0.19	-2.67	-1.11	2.89	0.22
15	0.56	0.88	2.54	2.75	0.69
Total	**1.1**	**1.5**	**1.6**	**2.5**	**0.4**

The GCPs coordinates errors of control points in snow free period are X =0.8; Y =0.4, Z= 0.3 cm and X = 0.2; Y =1.3, Z=3.0 cm errors of check points. The RMS of marker errors is 3.3 cm for snow free period (Table 16). The UAS x,y,z survey coordinates of GCPs are displayed in Table 16. The ground resolution of snow period model is 0.97 with 103 points/m^2 of reconstructed DEM and the ground resolution for snow free model is 1.21 with 427 points/m^2 of reconstructed DEM. The GSD was 1.0 in snow cover period and 1.2 in snow free period in Graswang (Table 17). The RMSE of check point marker errors of 2.5 for snow period model and 3.3 cm for snow free period is good, although there is still space for the improvement in mission planning and processing steps. The image overlaps are shown in Fig. 9-c.

Table 16: Graswang GPSs collected in snow free period and X, Y, Z coordinates (X – Easting, Y – Northing, Z – Altitude) of control points RMSE (upper table) and check points RMSE (lower table). The total error is the RMS of marker errors). Coordinate system: ETRS89 / UTM zone 32N (EPSG::25832). Source: Agisoft Photoscan.

Count	X error [cm] (Easting)	Y error [cm] (Northing)	Z error [cm] (Altitude)	XY error [cm]	Total error [cm]
7	**0.8**	**0.4**	**0.3**	**0.9**	**0.9**
GCP number	**X error [cm] (Easting)**	**Y error [cm] (Northing)**	**Z error [cm] (Altitude)**	**Total error [cm]**	**Image pixel**
gcp1	-0.86	0.41	0.03	0.95	0.31
gcp4	0.46	-0.29	0.48	0.73	0.47
gcp5	-0.69	0.62	-0.37	1.00	0.31
gcp6a	0.06	-0.60	0.38	0.71	0.41
gcp7	0.71	-0.30	-0.07	0.77	0.34
gcp8	-0.94	0.24	0.06	0.97	0.44
gcp9	1.25	-0.09	-0.51	1.35	0.36
Total	**0.8**	**0.4**	**0.3**	**0.9**	**0.4**

Count	X error [cm] (Easting)	Y error [cm] (Northing)	Z error [cm] (Altitude)	XY error [cm]	Total error [cm]
2	**0.2**	**1.3**	**3.0**	**1.3**	**3.3**
GCP number	**X error [cm] (Easting)**	**Y error [cm] (Northing)**	**Z error [cm] (Altitude)**	**Total error [cm]**	**Image pixel**
gcp3	-0.21	-1.77	3.42	3.86	0.23
gcp6	0.18	-0.34	-2.55	2.58	0.56
Total	**0.2**	**1.3**	**3.0**	**3.3**	**0.5**

Table 17: Information about survey data in Graswang. Coodinate system: ETRS89 / UTM zone 32N (EPSG::25832). Source: Agisoft Photoscan report.

DEM	number of photoes	mean flying altitude	ground resolution [cm/pix]	tie points	point cloud	coverage area [km²]	reconstructed DEM	
					RMS reprojection error (pix)		resolution cm/pix	point density [points/m²]
Snow cover	1320	39.7	0.97	2 126 258	1.24	0.10	1.25	103
Snow free	721	49.6	1.21	1 066 673	0.49	0.10	4.84	427

The UAS SD results variate mostly from 0.25 to 0.65 cm. Manual snow probe SD ranges between 24.8 -49.2 cm. The highest values are in the west of the surveyed area and along the asphalt road. The lowest SD values were where cross-country trails and paths are situated.

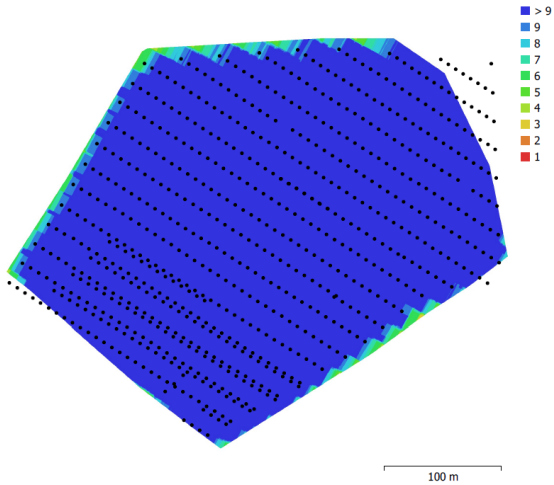

Fig. 9-c: Camera location and image overlaps in snow free Graswang study area. The higher the value the better.

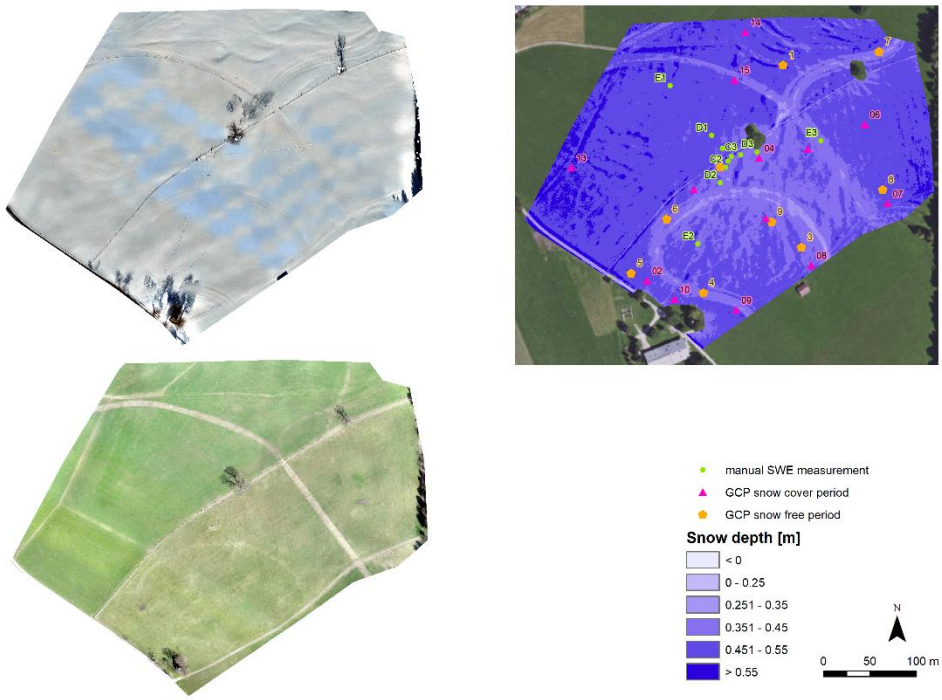

Fig. 9-d: Orthophoto of the snow surface (upper left), Orthophoto of the snow free DEM representing the ground lower left). The snow depth map was obtained by subtracting the snow cover DEM and snow free DEM with GCP points from the snow cover survey (pink triangle) and snow free survey (orange pentagon) used for georeferencing upper right). Coordinate system: ETRS89 / UTM zone 32N (EPSG::25832).

The shadows complicate the SD estimation for example around trees and church in Graswang study area (Fig. 9-e).

Fig. 9-e: Graswang monitoring station and its surroundings. Photo taken by M. Součková.

9.3 RAMMS simulation

The aim was to compare UAS SD results and RAMMS output. We applied the RAMMS software to back-calculate an avalanche event that occurred on February 15, 2021, in the avalanche path Žlab Úpičky, Obří důl, in Krkonoše. We examined three distinct scenarios:

1. Different DTM resolutions, 1m and 5 m. The results from the study showed that using a higher DTM resolution (1m) led to an **increase in both volume and maximum SD (SDmax) of the avalanche**, while **shortening the runout zone** compared to using a lower DTM resolution (5m).

2. Two scenarios of forest layer were included in the analysis to account for surface roughness: one without a forest layer and the other with forest values.

While the maximum height of the snow flow in the avalanche increased by about 28% in the models with an active forest layer, the presence of the forest had the opposite effect on the maximum avalanche velocity and the maximum pressures. The maximum velocity decreased by an average of 3 m/s (14%). The maximum avalanche pressures were lower by about 37 kPa (26%) in the models with active forest (Podaný, 2023).

Regarding the accumulation zone: The average height of the deposited snow increased slightly for the models with a forest layer compared to the models without forest. The opposite trend was observed for the maximum accumulated snow depth. Here, on the other hand, the maximum height decreased for the models with forest.
Including a forest layer, we can also observe a reduction in the spread of accumulated snow to the left (seen from the valley floor), which was not spread to the left in the real scenario.

3. Cohesion, a critical parameter in avalanche modelling, was set at 150 Pa, the results were published in (Podaný, 2023).

While the parameters like SDmax, maximum avalanche velocity, and maximum pressure forces did not show significant changes and showed a slight reduction with the addition of snow mass cohesion. The cohesion parameter had a more pronounced effect on the overall behaviour of the avalanche. Specifically, the length of the avalanche path was shortened, and the volume of accumulated snow was also significantly reduced.

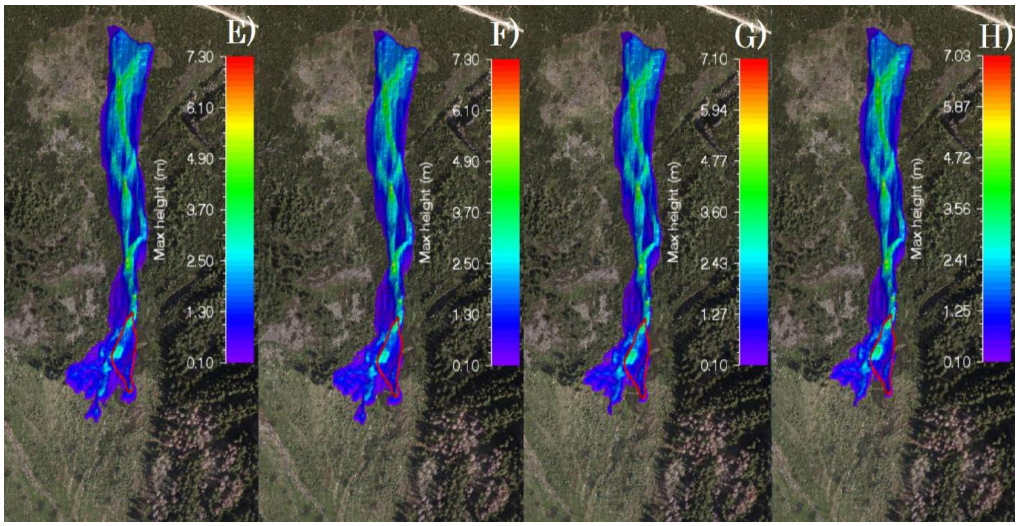

Fig. 9-f: Simulated maximum height (SDmax) with snow mass cohesion set at 150 Pa in images E-H. The red polygon indicates the visually delimited real accumulation zone, as identified from UAS orthophoto. E represents small 30-year simulations, F represents small 10-year simulations, G represents tiny 30-year simulations, H represents tiny 10-year simulations. The figure is reused from (Podaný, 2023). DEM 1m, including forest layer.

We compared RAMMS SDmax and SD measured by UAS in the upper part and accumulation zone of the Žlab Úpičky. For example, GCP number 265 reached SD of 1.5 m in RAMMS raster, 0.47 m was measured by UAS, and 1.88 m by manual snow probe (SP) measurement. According to orthophoto this GCP lies on dwarf pine, therefore SD errors related to vegetation cover might be present (Table 18).

Table 18: SD values at specific GCP points resulting from RAMMS modelling, UAS monitoring, snow probe (SP) measurements and elevation measured by Trimble GNSS.

GCP number	RAMMS SDmax value [m]	UAS SD value [m]	SD of SP [m]	GNSS elevation [m]
265	1.5	0.47	1.88	1153.32
269	0.62	0.27	1.91	1145.31
271	0.04	0.05	0.64	1134.43
244	1.66	0.6	1.02	1298.44

The values of RAMMS, UAS, and manual SP methods' SD results differ a lot. From these results, it is not possible to assess if the UAS are more accurate than the SP measuring. RAMMS data may be overestimated, and UAS data might be underestimated. The snow probe measuring contains some uncertainty related to dwarf pine vegetation, the icy layer in the snow profile, and the maximum snow depth and height of the snow probe equipment. Moreover, UAS SD data captures more details than RAMMS results due to input data DEM raster resolution of 0.09 cm UAS raster and 1 m raster LIDAR data input in RAMMS. The release area of UAS measured SD probably does not reach real values as they reach primarily

negative ones. The snow-free DEM may be doomed and elevated. The calculated RAMMS release area volume was 5006.1 m^3.

When we compare the SD results of the whole avalanche snow mass flow, the UAS SDmax is 4.8 m; oppositely, RAMMS best tiny 30 year period (T30y) SDmax simulation scenario of flowing snow reached 7.1 m (Fig. 9-h). The avalanche length of the T30y simulation, including 1 m resolution, forest layer and cohesion parameter (150kPa), was 432 m, which matches the estimated avalanche length of 432 m estimated by the Mt.Rescue Krkonoše.

According to the RAMMS output, the snow accumulated volume ranged between T10y 3718 and S30y = 3916 m3. The snow accumulated volume of the T30y simulation scenario was 3755 m^3. The average accumulated SD is 0.55 m. Maximum velocity speed was 17.9 $m.s^{-1}$. The maximum avalanche pressure equalled 96kPa (Tab. 7 in Podaný, 2023). If we extract the accumulation area of the RAMMS raster (T30y of SD snow simulation), we reach the SDmax of 3.8 m shown in Fig. 9-g. Agisoft Photoscan estimated accumulated SD dif volume is 1580.9 m^3.

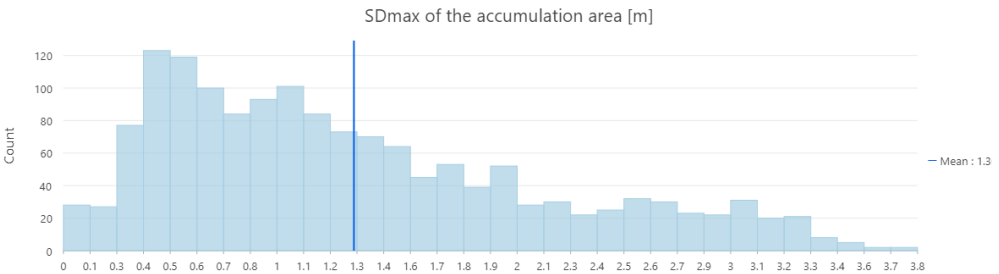

Fig. 9-g: Histogram of SDmax of the accumulation area of the RAMMS T30y simulation scenario.

The conclusion is that the position of the accumulation zone reaches satisfactory results, however the actual values variate. Perhaps we would need another method assessing SD data spatially which could be CRNS or height resolution lidar data. For these reasons we recommend use of a combination of multiple methods.

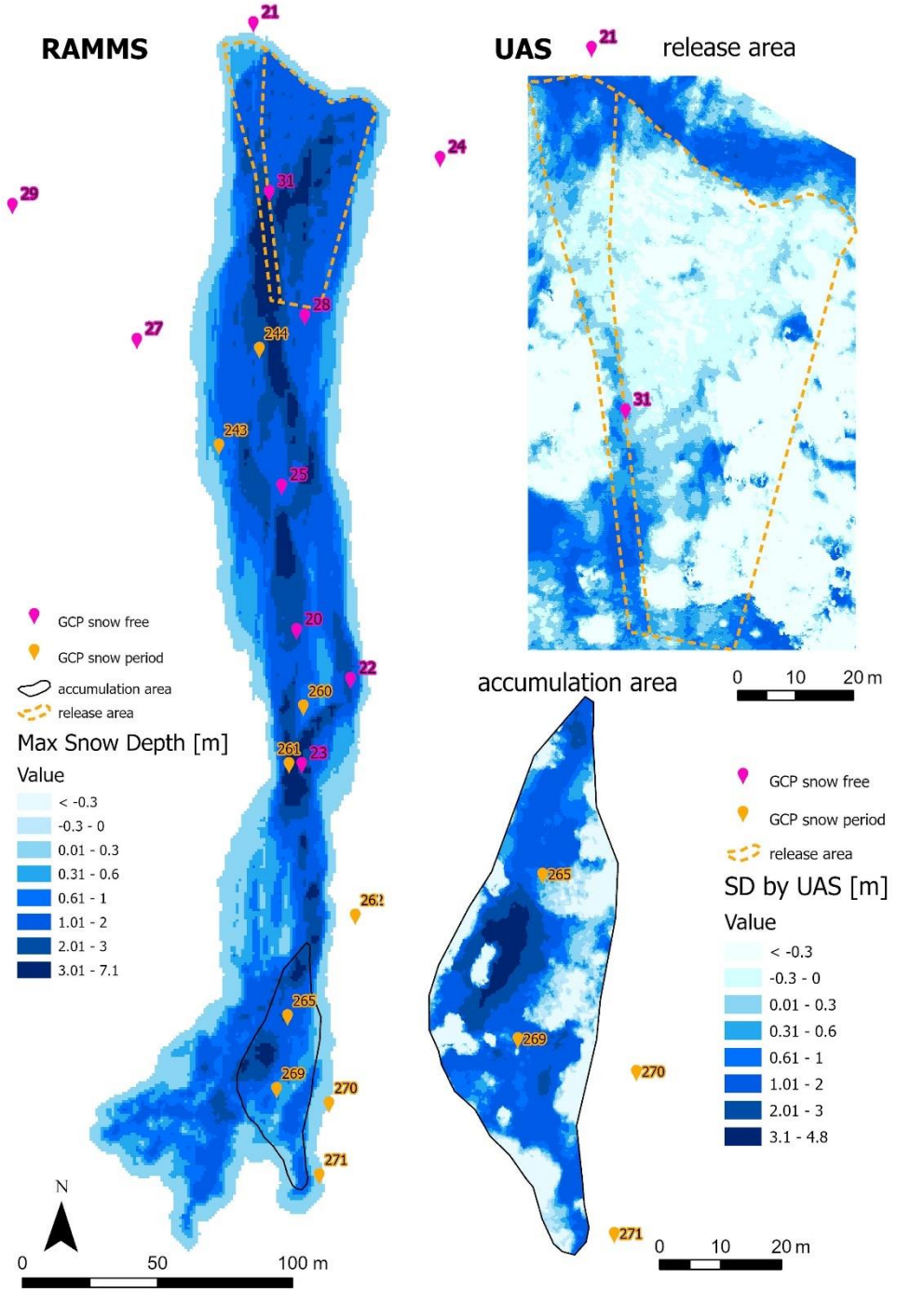

Fig. 9-h: RAMMS tiny 30 yr output of maximum snow depth with stop parametre = 7; 150 Pa and 1 m resolution with forrest layer compared to UAS snow depth output. Coordinate system: S-JTSK / Krovak East North (EPSG::5514).

9.4 Elevation dependent monitoring of snow water equivalent in the Northern Limestone Alps using neutron-based methods: CRNS

To obtain local to meso-scale spatial SWE data, the relationship between SWE and neutron counts was investigated. The goal was to assess the applicability of this relationship in different altitudes and locations. Initially, the same parameters (a0=-500, a1=0.6, Nmax=2300) were applied to all stations, and it yielded satisfactory results at Graswang (gwg), Esterbergalm (est), and Achele (ach) station (Fig. 9-i). The altitude ranges of stations are displayed in Table 5. However, this approach did not perform well at other stations, indicating that a one-size-fits-all parameter setting is not suitable for all locations. To address this issue, the pressure of all stations was levelled to 920 hPa, using the same parameter values. This step aimed to harmonize the measurements and improve the relationships between neutron counts and SWE across different stations. To refine the relationship further, more in-situ SWE data was used to manually fit the theoretical curve to other point measurements. This process was successful for some stations, as seen in the curves for Graswang, Esterbergalm, Sylveinsteinsee (syl) stations in Fig. 9-j. However, additional in-situ SWE measurements are still needed for stations Fendt: fen, Lerchkogel (lek), and Sylvensteinsee (Fig. 9-i) to improve the accuracy of the neutron count to SWE conversion for these locations. The incoming neutron counts translated into theoretical SWE, which is then compared to the manually obtained in-situ SWE measurements (Fig. 9-i). This comparison allows for an assessment of the accuracy of the relationships and the potential for using neutron count data to estimate SWE at different locations and altitudes.

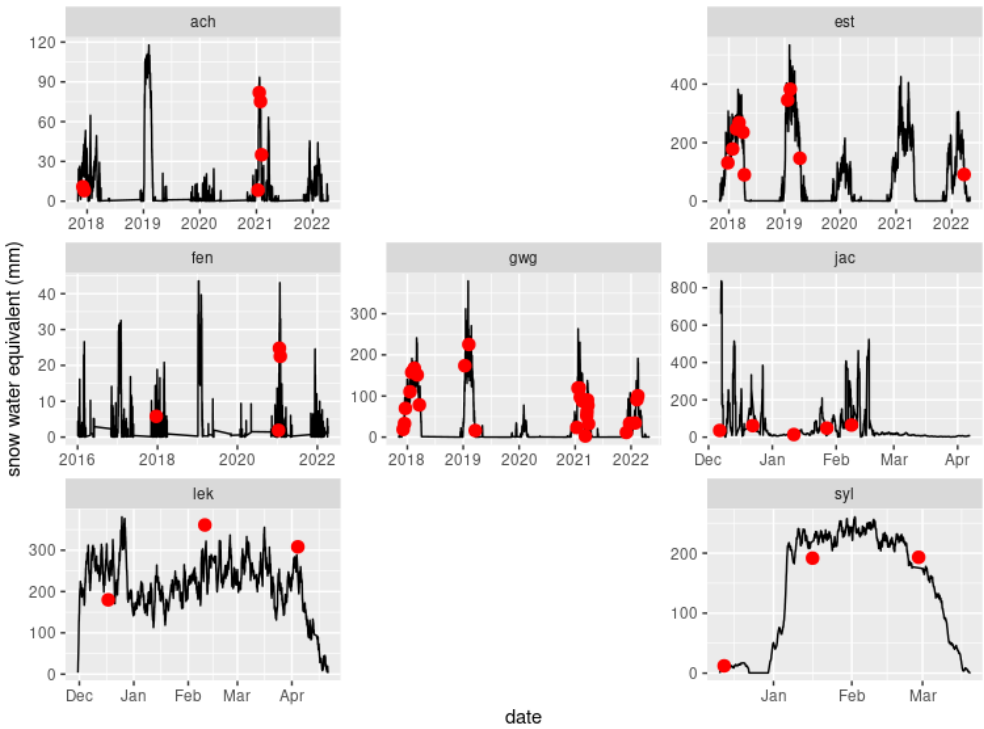

Fig. 9-i: Moderated neutron counts translated into snow water equivalent (black line) and in-site SWE measurements (red dots) for the season 2021-2022 at lek, jac, and syl locations .

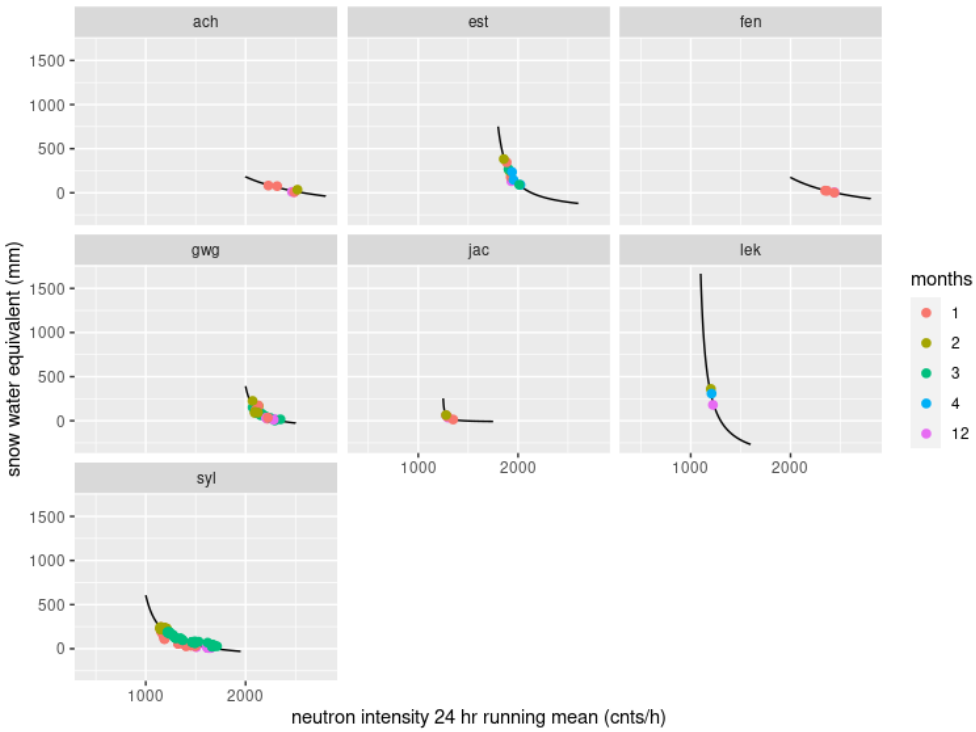

Fig. 9-j: Fitting the relationship between Snow Water Equivalent (SWE) and neutron counts .

Also, some outliers are apparent, the CRNS SWE and SD data indicate a linear relationship in most of the stations, except of the fen station. Thanks to this linear relationship, we can use a simple equation for calculating the SWE (Fig. 9-k), as mentioned above.

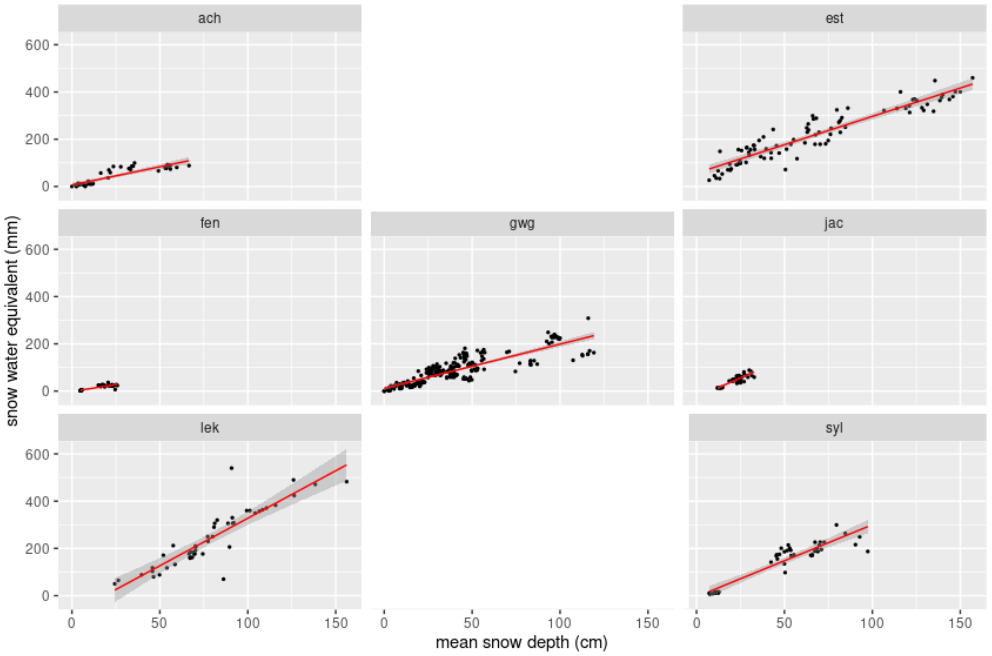

Fig. 9-k: Relationship between Snow Water Equivalent (SWE) and Snow Depth (SD). The trend line is displayed by the red line, and the grey confidence intervals indicate the uncertainty of the trend.

If we focus on SD and snow density, we observe diverse responses and a wide range of values (Fig. 9-l). As we know, snow density is dependent on type of snow (wet, powder, old snow, etc.), and this variability is reflected in the different responses and spread values observed in the data.

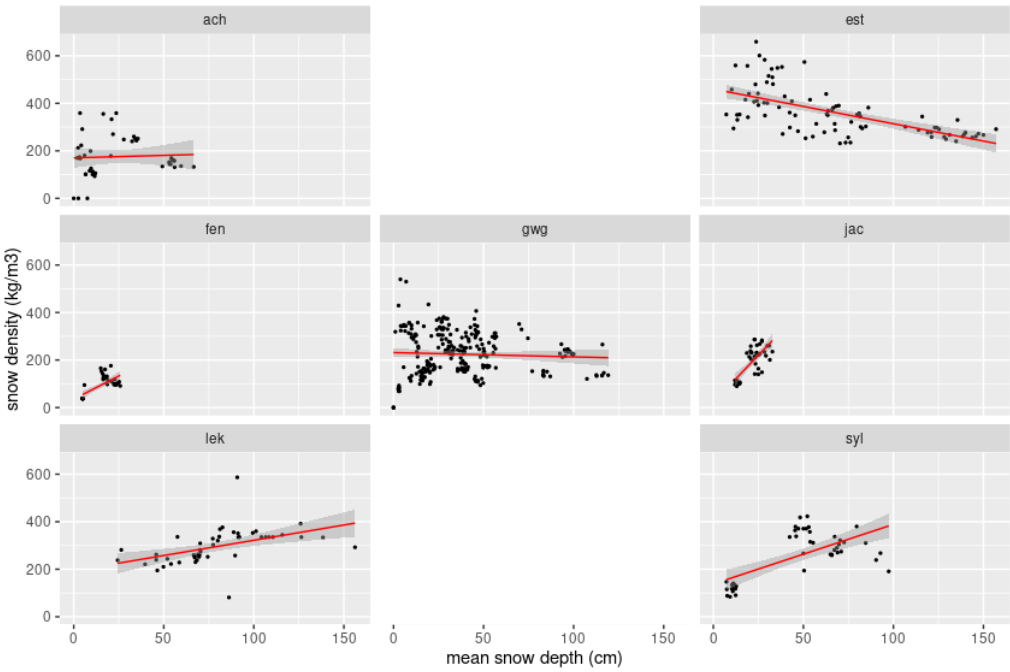

Fig. 9-I: Snow density (SnwDnst) and snow depth (SD) relationship.

IV. PART

PROMOTING SCIENCE VIA PUBLIC ENLIGHTEMENT AND TEACHING STUDENTS

10 PROMOTING SCIENCE

This chapter aims to bridge the gap between scientific research and public understanding by highlighting the critical role of outreach activities in both public and school settings. Additionally, it includes examples of 21st-century teaching methods and a case study of teaching methods and a case study of teaching at alternative Scio school are provided. By fostering engagement with science, we can improve communication between both scientists and the public. There are more scientific outreach activities: visiting students; public talks and lectures; engaging in social media; science fairs; newsletters; blogs; science policy, or advocacy (Woitowich et al., 2022). Low-cost programs exist for visiting students, such as "Present Your PhD Thesis to a 12-Year-Old" or "Shadow a Scientist," combining science communication training with outreach to area middle schools. "Shadow a Scientist" students meet with the scientist and are introduced to their research, ask them questions, do hands-on tasks in the lab, and are shown lab equipment (Clark et al., 2016). Science outreach has traditionally been perceived within academia as a low-status task (Johnson et al., 2014). The pursuit of science outreach and engagement activities is also often frowned upon by many scientific community members, whether because these activities are considered peripheral or because weighing in on a politically charged subject is deemed "too risky" (Canfield et al., 2020). Training for scientists wishing to contribute to these efforts is similarly lacking (Bevan et al., 2020).

There are several compelling **reasons** to promote science:

1. Primary reason is **advancing knowledge**: Science is the pursuit of knowledge through systematic investigation and experimentation. By promoting science, we can continue to discover new things about the world and improve our understanding of it.

2. **Improving technology**: Science is the foundation of technology, and advancements in science can lead to new and **improved technologies** that can benefit society in many ways. The example can be UAS carrying LIDAR device in Fig. 10-a.
3. **Find solutions to challenges**: Scientific research can help address **societal challenges** such as climate change, disease outbreaks, and food security. By promoting science, we can support the **development of solutions**.

4. **Economic growth**: Science and technology are essential for economic growth and development. By promoting science, we can create new industries, new technologies, products, services that can improve **the overall quality of life for people**.
5. **Education, critical thinking, and outreach**: Science promotes critical thinking and a scientific mindset, which are essential for understanding complex issues and making informed decisions. By promoting science, we can **support education** and help people become **more informed citizens: increase public awareness and interest.** Outreach programs, such as **workshops, seminars, and public talks lead by scientists**, can help promote science to a wider audience.
6. **Collaboration and networking**: Collaboration and connection between researchers, practitioners, and stakeholders can help foster innovation. Networking

opportunities, such as conferences and workshops, can help facilitate collaboration and knowledge exchange.

Conference attendance: presenting your research at conferences are a great way to network with other researchers and get feedback on your work, and it presents an opportunity to promote your research to a wider audience. Take time to really choose well-fitted conference and working group. If you are more into practical way of networking – choose **workshops/ summer, winter schools relevant to your topic**. Cooperation is usually performed in tiny groups; if you enjoy diverse team-work activities and quite often you go into field, work with new technologies or laboratory regarding your specialization (Fig. 10-a).

You can also co-author papers, give joint presentations, and share each other's research with your respective audiences. Furthermore, questionnaires what should be explained, what needs to be answered to public might help to better fit public enlightenment and target “hot topics, heat debates”.

Communicating research findings: Promoting research can help researchers communicate their findings to a broader audience, including policymakers, the media, and the general public. This can help ensure that research findings are understood and used to inform decision-making.

By collaborating we can get work done in a real time, move science forwards, we benefit from other people thinking, systematic working, competences. It is a time of shared, open data so make your data/ research transparent and accessible. Share your research within departments, cooperate and stay connected with other researchers/ policy makers and public.

Citizen science: Citizen science projects can help engage the public by providing opportunities for people to collect and report data.

7. **Advocacy and policy**: Advocating for policies and regulations that support science research and application can help promote the importance of the field and its potential benefits for society.

Fig. 10-a: UAS with LIDAR, screening in Obergurgl valley at Cosmic Ray Neutron Sensors meeting (gathered people with interest in CRNS: scientists, private companies). Photo taken by M. Součková.

10.1 Public awareness and Scio school projects

During and after publishing my first article, I took an active part: I included a pivotal figure in the paper and wrote short abstract for NHESS publication. We posted manuscript information on FB, Instagram and the department website[17]. Later on, I was contacted by the Ecolist magazine to write about the wet avalanches changes in Czechia[18] concerning our NHESS paper.

[17] https://www.fzp.czu.cz/cs/r-7185-aktuality/narust-teploty-vzduchu-patrne-zvysil-cetnost-mokrych-lavin-k.html

[18] https://ekolist.cz/cz/publicistika/priroda/jak-ovlivnuje-klimaticka-zmena-laviny-z-mokreho-snehu-v-pohori-krkonos

Within PhD Intern at KIT IFU, we educated public about snow monitoring using UAS and CRNS and the 20 minutes document about climate change in Bayer was produced and broadcasted at Bayer SAT1 TV. Due to broadcasting rights, it can be watched only in Germany.

Moreover, I aimed to teach school children how to behave in winter mountain environments. I was teaching a module called Horizont, where children learned basic principles of map navigation and snow avalanches and then within Scio February´s expedition (at Medvědí hut near Špindlerův Mlýn), children explored snow profile – it´s compactness, temperature within snow layers and observed snow crystals. They learned about local Krakonoš's myths, ice age remnants and Krkonoše National Park environment protection. Within the first aid workshop, they learned how to treat injuries and learn how to cope with emergencies in the mountains. In addition, guests from Krkonoše Mountain Rescue visited us and shared practical tips on what to avoid in the mountains and how to recognize the warning signs of weather changes in the terrain. Children used the holy trinity to find a buried object in the snow. SCIO elementary school students gained knowledge, abilities, discussed attitudes and mastered competencies. The challenge for scientists is to simply explain relatively complex things. The practice of working with children teaches me this skill.

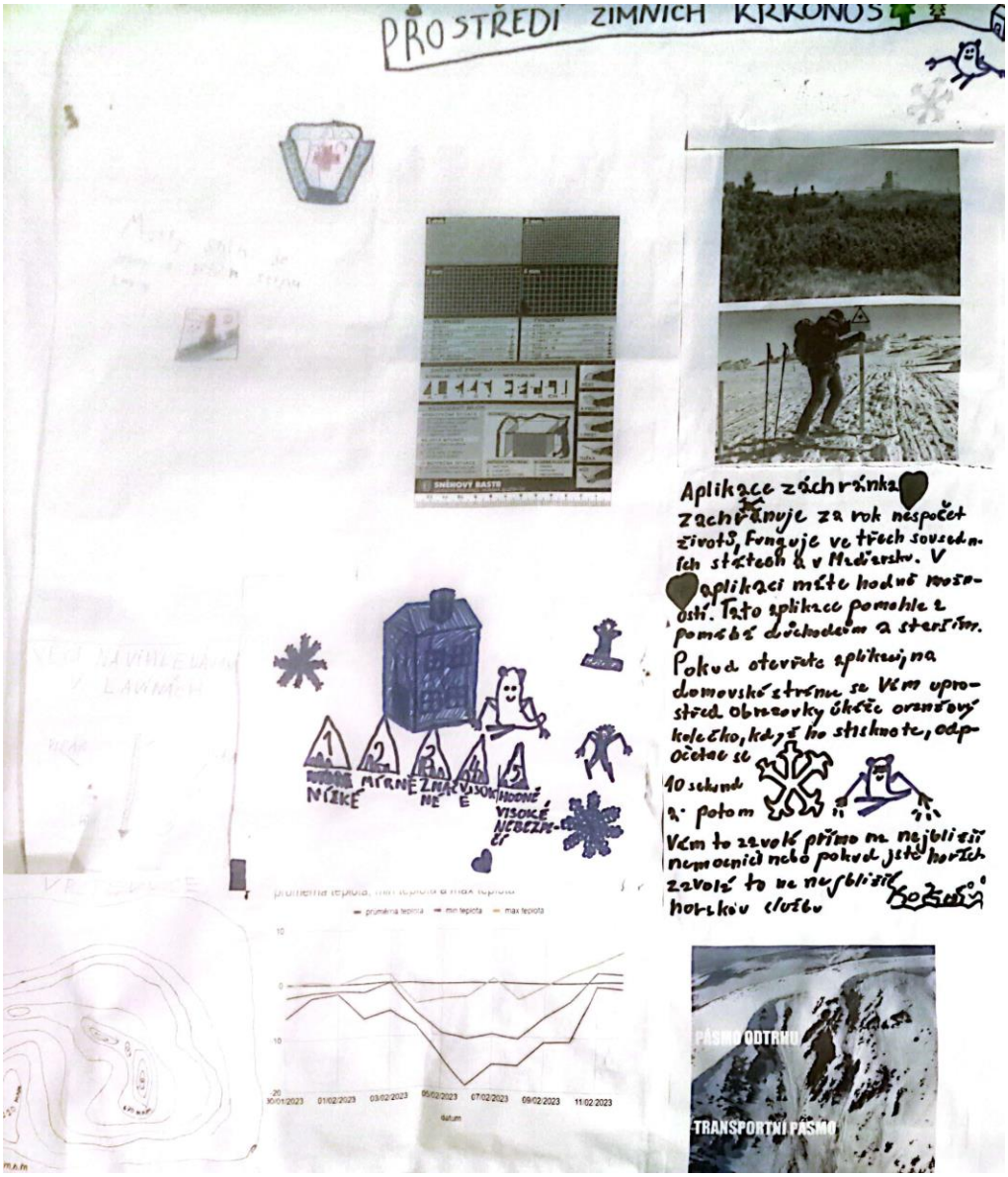

Fig. 10-b: Horizon called "Winter Krkonoše environment" taught at Expedition elementary Scio school. You might see an avalanche path, avalanche danger levels, wet avalanche problem, contours, and the Rescue application.

Within drones Horizont children learned about basic principles how to operate drone, European legislative of flying zones, drones use such as many industries, agriculture, and research purposes.

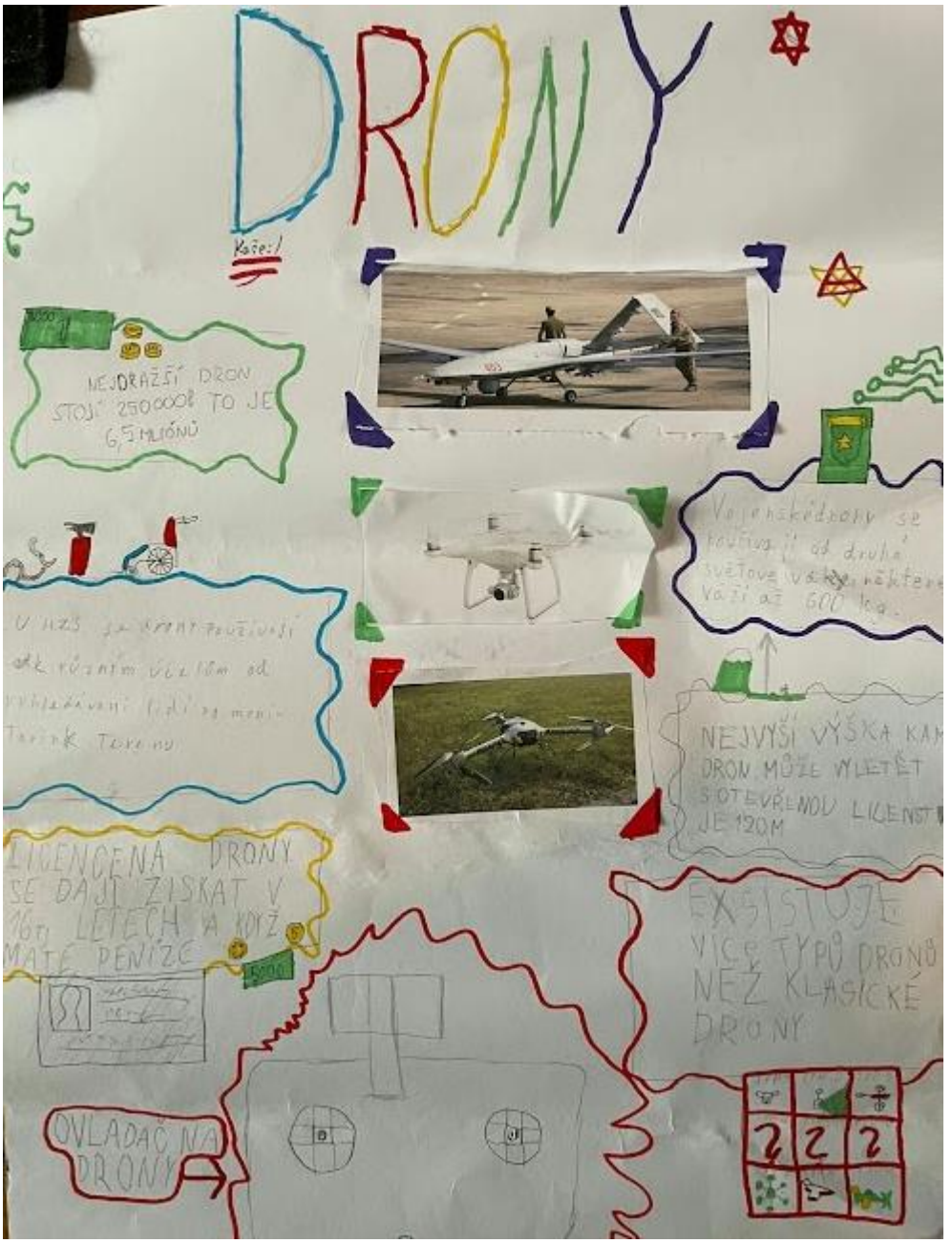

Fig. 10-c: Teaching module: Horizont "Drones" at Expedition elementary Scio school.

Overall, promoting scientific research is important because it can lead to new discoveries, advancements, and solutions that benefit society. Scientist should more actively engage society and drawing their attention.

10.2 21st century learning

Within the education the didactic pillars exist according to (Munerol et al., 2022):

1. strorytelling,
2. learning by doing[19], hands-on practice,
3. flipped classroom environment and
4. real world

"How to educate about Science by innovative learning methods"?

1. **Storytelling** can significantly reduce depersonalization, develop identities, promote empathy and diversity, aid with understanding of complex issues by linking them to the proximal world experienced by students, and ultimately generate new knowledge.
2. **Learn by doing** goes beyond the artificial setting of school education and allows for a more natural, immediate understanding of the subject matter.
3. **Flipped classroom** - stories and workshops led by the students. In this framework, storytelling introduces the minimum amount of knowledge required by students to conduct the workshops themselves (lack of preparation being a frequent problem with flipped classrooms, (Akçayır and Akçayır, 2018; Awidi and Paynter, 2019).
4. Focusing on the **real world** makes topics more tangible and so students are more interested in, as they can directly relate to their future in 21st century. This is in line with existing literature showing that climate-change education must be accessible and action-oriented (Lee et al., 2013).

The D-A-S-K framework for developing dispositions, attitudes, skills, and knowledge is a long-term instructional model that focuses on teaching "adaptive" dispositions for life-long learning in the 21st century. It embraces five zones of learning: 1) zone of instruction, 2) zone of practice, 3) zone of interaction, 4) zone of tinkering, and 5) zone of meta-cognition proposed by (Lee and Hung, 2012).

[19] https://web-archive.southampton.ac.uk/cogprints.org/637/1/LearnbyDoing_Schank.html

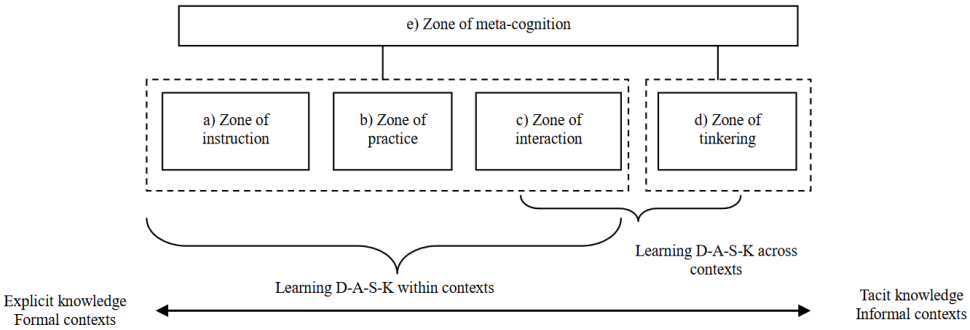

An Instructional Framework for D-A-S-K

Zones	Key Tenets
Zone of instruction	• Traditional IS model • Teacher is the sage • Focuses on acquiring conceptual knowledge without context • Learning is measured by reproducing conceptual knowledge (i.e. paper and pencil exam)
Zone of practice	• Traditional instructional system + in-field practice • Personal understanding of explicit knowledge through embodiment in authentic tasks and problems • Focuses on codified knowledge + practical experience = personal, tacit knowledge • Assessment of learning = paper and pencil exam + practicum
Zone of interaction	• Learning by embodying in practices, social interactions, and collective knowledge of communities of practitioners • Experiential knowledge is constructed through interacting with members and embracing thinking processes of practitioners • Experiential knowledge = Tacit knowledge + explicit knowledge + collective social knowledge
Zone of tinkering	• Learning by "playing" in informal community • Formal or informal community dependant on learner's role involvement • Informal communities provide affordances to "pick up" 21st century dispositions, like risk-taking, experimentation, and adaptability
Zone of meta-cognition	• A "systems-level" zone that links and manages learning in the different zones through metacognitive brokering • Teacher brokers dialogue with learners to compare and contrast learning experiences between formal and informal contexts • Teacher brokers probe learners to articulate their cognition and reflect their strengths and weaknesses • Teacher brokers need not be content experts but act as facilitators to enable across context learning experiences

Fig. 10-d: An instructional framework for D-A-S-K and zones of metacognition presented in (Lee and Hung, 2012).

10.3 Promoting avalanche awareness: A Call for Science Education and Public Engagement about promoting science to schools and public

Science plays a pivotal role in understanding and mitigating natural hazards, including avalanches. However, the vast majority of the public lacks an in-depth understanding of avalanche science, which can hinder their ability to make informed decisions and stay safe in avalanche terrain. Additionally, its essential to recognize that avalanchesare natural phenomenom necessary for the unique fauna and flora in Krkonoše Mts. To address this knowledge gap, promoting science education and public engagement, particularly in schools and communities that visit avalanche-prone areas, is imperative.

Promoting science education in schools provides a solid foundation for students to grasp the complexities of natural phenomena like avalanches. By incorporating science curricula that delve into avalanche formation, dynamics, and risk assessment, we can equip future generations with the knowledge and skills to navigate avalanche terrain responsibly. Therefore, school projects were conducted to raise awareness about avalanche safety using drones and education in the Krkonoše Mts. These initiatives not only enhance safety awareness but also foster an appreciation for the ecological role of avalanches in supporting biodiversity in the region.

Beyond schools, engaging the broader public is equally crucial in promoting avalanche awareness and risk management. This can be achieved through a variety of initiatives, such as public lectures, workshops, and interactive exhibits, that showcase the science behind avalanches and emphasize the importance of preparedness.

Teaching in todays world presents challenges, especially with the need to capture the attention of primary school children using more attractive methods. As Confucius declared over 2400 years ago :

- “Tell me and I will forget”.
- “Show me and I may remember”.
- Involve me and I will understand”.

One effective approach to transfering knowledge into practical skills is through experiential learning or learning by doing. Therefore, our educational efforts included both theoretical lectures using interactive aids and practical lessons where the students could experience measuring snow profiles and simulating avalanche rescues, all while incorporating drone technology. In terms of advancing knowledge and skills, I advocate for a comprehensive approach that considers the entire spectrum of perspectives and utilizes well-connected and sustainable systems. I resonate with the sentiment expressed in the quotation:

- What I hear, I forget
- What I hear and see, I remember a little
- What I hear and see and ask questions about or discuss with someone else. I begin to understand.

- What I hear, see, discuss, and do, I acquire knowledge and skills
- What I teach to another, I master.

By incorporating hands-on experiences, encouraging questioning and discussion, and promoting teaching others, we can affectively impart avalanche awareness and preparedness skill to the broader public.

The Swiss White Risk web-based platform is an excellent example of a Learning by Doing platform focused on avalanches. This platform enhances education by providing users with knowledge skills, and competences in various aspects related to avalanches, including:

A good example of Learning by doing platform focusing on avalanches is the Swiss White Risk web-based[20] platform. It improves education and users gain knowledge, skills, and competences about:

1. Avalanches: Users can learn about different types of avalanches, avalanche problems, avalanche bulletin reports, and avalanche danger levels.
2. Snow: The platform provides information on new snow, SD, snow profiles, and weekly reports to help users understand snow conditions.
3. Ski-tours: It offers a planning tool with features like slope inclinometer analyzer, and graphical reduction method for risk reduction aiding in ski-tour preperation and safety.

Other practical apps for avalanche hazard management include the SnowSafe Avalanche app[21], as well as tour planning apps like Ortovox[22] and Bergfex[23].

Furthermore, the scientific community often utilizes Twitter accounts to promote their work, as it has became a primary medium of academic communication (European Commission. Directorate General for Research and Innovation., (2020). In addition to ensuring clarity of their communications with scientists, policymakers, and the public,scientists can develop online strategies to counter campaigns of misinformation and disinformation, particularly regarding topics like climate change. This proactive approach, as suggested by (Lyengar and Massey, (2019) can help combat misinformation and ensure accurate dissemination of scientific findings.

[20] https://whiterisk.ch/en/welcome
[21] http://snowsafe.at/
[22] https://play.google.com/store/apps/details?id=com.ortovox.lvs&pcampaignid=web_share
[23] https://www.bergfex.com/c/apps/

V. PART

DISCUSSION & CONCLUSION

DISCUSSION

Even though there is a lot of evidence of anthropogenic impacts on climate (e.g., Hock et al., 2019; Strapazzon et al., 2021), the effect of climate change on snow avalanches is poorly understood. Additionally, snow avalanche forecasting remains challenging (e.g., in Czechia, the avalanche forecasting model is missing, and human-made avalanche danger level alerts are still more precise than forecasting models). Therefore, in this work, machine learning (ML) was employed to determine the main meteorological and snow variables of wet- and slab-avalanche releases using variable importance rating and significance methods in a low-altitude mountain range. This might help incorporate identified driving variables into avalanche warning decisions. Trend analysis was also performed to broaden awareness of how warming will influence the type and number of avalanches. To identify avalanche release zones, estimate avalanche hazard, and mitigate possible risks, high-resolution spatial-temporal SD data is crucial (Eberhard et al., 2020; Singh et al., 2022). For this reason, we chose a study site and employed UAS to measure SD in the Žlab Úpičky avalanche release area. Mapping avalanche mass balance/ snow storage is essential, similar to understanding water balance for water reservoirs. SD serves as a key input parameter for numerical avalanche dynamic simulation tools, such as the RAMMS model we used to explore the Žlab Úpičky avalanche mass balance. Moreover, multi-temporal images of snow evolution over time are beneficial for monitoring SD and snow cover at the study location. For instance, time-lapse cameras capture the process, including movements of shadows during the day. These images can serve for verification of automatic station data if errors appear in data loggers. Time-laps camera was available at the Lerchkogel CRNS station in Germany. Another aspect is that snow depth is used for estimating snow SWE. For hydrology, snow and mountain ecology, and avalanche research, having information on SD and its spatial distribution in high-mountain catchments is essential. Currently, SDs are primarily conducted at specific points, such as automatic weather stations or by snow field observers, and then extrapolated using mathematical formulas to estimate larger scale SD.

However, in the Czech Republic, the station network, while relatively dense, is not sufficient, particularly in mountainous areas. Spatial interpolation of point measurements is an option, but its accuracy is limited. Moreover, Czechia lacks snow-gridded data that is common in Western European countries. Studies consistently report high spatial variability of SD and other snowpack parameters in mountainous regions, which cannot be fully captured by point measurements. Although high-resolution platforms develop rapidly, satellite data has still low resolution for Czechia extend and are quite expensive. As a result, there exists a gap in between in-situ measurements and satellite data. However, promising alternatives that can bridge this resolution gap are methods based on UAS and CRNS. To address this gap in resolution, we conducted SD variability measurements using UAS and gravimetry in the Bayer region of Germany (Ammer and Isar river catchments) and Czechia, respectively. UAS-based photogrammetry has emerged as an attractive and cost-effective alternative to create 3D surface data, offering flexibility and high-resolution capabilities compared to laser scanning methods (Bühler et al. 2016).

11 Which variables drives wet and slab avalanches according to machine learning?

11.1 Wet-avalanche days determined by weather variables assessed by DT and RF methods

Using the RF method, we have identified that the most significant factors contributing to wet avalanche activity in the Krkonoše Mts. are primarily the following: 3-day minimum and maximum air temperatures, a 3-day moving-average of SD, as well as the mean wind direction and wind speed over a 3-day period. As anticipated, both wet and slab avalanches exhibit dependence on SD. Moreover, a rising trend in wet avalanches is presumably influenced more by air-temperature-related variables (specifically maximum and minimum air temperature) than by liquid or solid precipitation (Rain_Tw_value, P_value). The underlying physical process might be associated with a gradual weakening of the snowpack as it becomes isothermal. While precipitation and sunlight duration do impact wet avalanches, our RF results suggest that their contribution is almost twice as low as that or air temperature in the Krkonoše mountains (Fig. 9 e). The main variables likely triggering wet avalanches include air temperature, SD, wind speed, and wind direction as determined by both RF and DT models. Sunlight duration and rainfall (Rain_Tw_value) emerge as important variables in the RF (Fig. 9 e), but they are not included in the DT model (Fig. 9 d). Wind direction plays a crucial role in wet avalanches, as wind often redistributes snow. The dry, warm wind known as "föhn" can lead to intense melting or avalanches. In the Czech part of the Krkonoše mountains, this phenomenon typically occurs when the wind originates from the north, specifically from Poland.

11.2 Slab-avalanche days determined by weather variables assessed by DT and RF methods

Slab avalanches are influenced by SD, variables related to rainfall, new snow variables, and wind speed, as indicated by the RF method. Slab avalanches potentially triggered by rainfall (depending on the air temperature threshold) are likely influenced by snow depth, new snow accumulation, and wind speed (Fig. 6-f). While air temperature does play a role to some extent , daily mean air temperature was approximately 10 % less important than daily mean SD. According to our results, it appears that rainfall has a greater impact on slab avalanches compared to snow. Physically it could be related to overloading due to precipitation of partially weakened and wet snowpack.

Furthermore, both wet and slab avalanches are influenced by wind speed. This influence may be attributed to the position of the LBOU meteorological station. In the vicinity of the station, there are open, level plains that enhance the prevailing westerly winds. Subsequently, the wind descends into the deep cirques located behind these plains, such as Obří důl near Luční bouda station and Labský důl near Labská bouda station (Zenodo: Součková, Markéta et al., 2022).This descending wind creates significant air turbulence, which in turn affects the snow conditions within avalanche paths. Wind commonly redistributes new snow, so new snow accumulation may be a less influential variable for

slab avalanches. This appears to be the case in our data for the Krkonoše Mts. In our analysis, daily mean SD (SD_value) emerged as the most variable in the RF model for predicting slab avalanches, and it served as the primary split variable for DTs. Both the DT and RF methods are consistent in identifying the most important variables, with MDA values exceeding 25 (Fig. 6-i, Fig. 6-j), except for rainfall-related variables (Rain_Ta_value, Rainfall_Ta_value3, Rainfall_sum3).

11.3 Model performance: random forest as a relevant machine learning method for avalanche activity

Our models demonstrate intriguing forecasting potential. The RF method proves to be a suitable approach for identifying both avalanche days or non-avalanche days within wet- and slab-avalanche activity, as indicated by the metrics used in our datasets and the model performance assessments which exibit a very low error rate and high prediction accuracy for the wet- and slab-avalanche datasets. We assessed the skill of the the RF model against the original dataset and obtained satisfactory results for model metrics (Fig. 6-f) within the Krkonoše Mts. The selection of the RF selection as relevant method aligns well with the previous study by Sielenou et al. (2021).

11.4 Wet and slab avalanche trends in Czechia

It is becoming increasingly common for very large avalanches, initially released in dry snow, to entrain warm snow in the avalanche path below (Eckert et al., 2013; Naaim et al., 2016; Sielenou et al., 2021). This observation aligns with a medium level of confidence in the rise of avalanche activity involving wet snow and a reduction in the size and runout distance of snow avalanches over recent decades, particularly in Europe (Hock et al., 2019). Our findings support this trend, revealing a significant increase in wet-avalanche occurrences over the last 30 years (seven times more avalanches than in the preceding 30-year period) (Fig. 6-a). According to Naaim et al. (2016), wet avalanches occur more frequently, even during the winter months of December through February. However, we have not observed a growing number of wet avalanches in December. Instead, in January and primarily in February, there have been more occurrences over the last three decades than in the rest of the study period (Fig. 6-b). Medium slab-avalanche sizes (0.4–0.5) have exhibited a slight decrease, while small-sized avalanches have increased during the period from 1991 to2021. Interestingly, a limited number of very large avalanches are present (Fig. 6-b), potentially due to gradual overloading from precipitation and wind or gradual weakening and warming of the snowpack.

11.5 Limitations in avalanche, weather data and machine learning methods

11.5.1 Related to the avalanche records

Uncertainty regarding the quality of the avalanche survey may arise due to unfavorable weather conditions on the occurrence date. Specifically, during stormy weather, avalanches

may not have been recorded on the day of release, or the avalanche type may have been misclassified. To address this, the data undergo quality assurance and assessment by avalanche observers. Furthermore, detailed information about separate avalanche records and meteorological and weather parameters for each winter from 2006/07 to 2018/19 can be found in Spusta et al. (2020). Moreover, written description of monthly and winter-period weather conditions are available in avalanche cadastres for the period from winter 1962 to 2006 (Vrba and Spusta, 1975, 1991; Spusta and Kociánová, 1998; Spusta et al., 2003, 2006). Regarding the validity of the observations over time, advanced techniques such as drones and camera photos were not available at the inception of avalanche records. However, the avalanche-prone area was regularly monitored in person, and avalanche occurrences were cross-checked with weather data by the avalanche support staff of the Krkonoše MRS. Regarding the length of avalanche data, our dataset is considered unique for low-altitude mountain ranges, spanning 59 winter seasons. Furthermore, data are accessible and have a compact sources. While it is true that studies by Giacona et al., (2021, 2018) and Peitzsch et al.,(2021) enable inferences about longer-term changes in avalanche activity using dendrochronology, which relies on tree-ring reconstruction dating back to the 19th century or even 18th century (Mainieri et al., 2020), it is important to note that their data sources extend beyond professional records. They incorporate information from written and oral sources such as newspapers, old postcards, local non-scientific literature, which may introduce potential errors. Furthermore, these studies must address non-stationarities arising g from forest recolonization, afforestation, and socio-environmental changes.

It is worth noting that wet and slab avalanche datasets overlap to some extent. Slab avalanches are defined bason on the criterion of (a) the manner of starting in the zone-of-origin, known as the release zone, while wet avalanches are defined by (b) the presence of liquid water in the snow within the zone of origin, following the Quervain, (1973) avalanche classification. There are 53 avalanche days with the identical weather conditions that are common to both wet and slab avalanche datasets. This overlap results in similar model outcomes to some degree and accounts for the analogous variable importance observed in the RF plots.

11.5.2 Related to the weather variable

The LBOU weather station used in Krkonoše Mts. is located approximately 0.2–15 km away from the closest (27) and furthest (01) avalanche paths in the west and east (as shown in Krkonoše Fig. 5 a). On one hand, this station is the sole station used for our analysis; on the other hand, having only one professional weather station for an area of this extent and data series length is typical in mountainous environments. The selection of a relevant meteorological station was primarily determined by data availability, and the stations location was the only viable option. Other meteorological stations in the vicinity have shorter time series, such as Luční bouda (LUCB, 1413 m a.s.l., with data availability since 2009), Vítkovice (VITK, 1410 m a.s.l.), a station replaced by the LBOU station), or they are positioned farther away, like Harrachov (HARR, 675 m a.s.l.). Had we alternative stations, the ranges of identified variables may have varied, potentially altering the interpretation. However, it is essential to note that such variations do not necessarily invalidate the models (Gauthier et al., 2017). The results obtained may be somewhat site-specific. When interpreting the data, it is important to consider the predominant aspects of the avalanche release areas. The actual weather conditions at the LBOU station, located on a windward open plain, may

exhibit slight differences from weather conditions at avalanche paths, which are often situated in leeward positions. Additionally, its worth noting that there is a data gap in the records of the LBOU station, spanning from 1 October 1999 to the end of September 2001. During this period, the station was not operational, as its measuring sensors were replaced.

11.5.3 Related to the modelling processes used: decision trees and random forest models

DTs are valuable tools for descriptive purposes, serving as decision support systems or reflecting a specific process. However, one of the practical challenges associated with DT models is overfitting. Overfitting occurs when the learning algorithm keeps generating hypotheses that reduce the error in the training dataset, but in doing so, increases the error in the test dataset. Furthermore, DTs are less suitable for handling continuous numerical variables. Even a minor change in the data can lead to significant difference in the tree structure, which, in turn, results in instability.

An RF model using synthetic data could serve as a valuable starting point for developing a practical system to complement decision support in estimating snow avalanche hazard, as suggested by Sielenou et al. (2021). However, it is important to note that the most important variables may vary depending on the length of the data series being explored Therefore, it is advisable to re-run models using data from the most recent season every year to ensure the optimal performance of the RF method. This approach aligns with the recommendation made by Gauthier et al. (2017). Inferring the physical processes that drive avalanche activity can be challenging because these statistical methods rely on correlations, which may not necessarily represent causal links, as emphasized by Sielenou et al. (2021). Since the primary focus of this analysis was to explore relationships rather than construct predictive models, further improving the model's performance falls beyond the scope of this study. Nevertheless, a potential next step for achieving a more precise prediction model could involve using gradient boosting or neural networks. Additionally, enhancing RF performance might be achieved by removing variables with low importance.

Another limitation to consider is that the RF/DT analysis assumes stationary, meaning that the effect of the drivers does not change over time (the models were fitted to the entire period, and non-stationarity was not taken into account). The number of ADs in the dataset is relatively low, and the inclusion of additional data would be beneficial.

The estimated importance of variables often changes across different models (Gauthier et al., 2017), and this variability can also be influenced by the statistical methods and ML approaches used (such as RF, logistic regression, and classification tree), as well as the length of the examined period. Therefore, we recommend that the model performance be assessed using metrics like confusion matrices. These metrics allow us to differentiate between false positive and false negatives in predictions, which were not considered in some previous studies (Baggi and Schweizer, 2009; Dreier et al., 2016; Eckerstorfer and Christiansen, 2011). Evaluating these metrics provides valuable insights into the potential reliability of the forecasts.

12 Advances in higher-resolution snow monitoring methods

Snowpack monitoring holds significance at the regional level due to its various implications for environmental research, regional climate studies, water resource management, and disaster risk reduction, particularly in the context of avalanche risk management (Awasthi and Varade, 2021). Snow monitoring is crucial for studying the evolution of Earth's energy budget[24] and plays a vital role in global-scale climate modelling. Various methods, encompassing both active and passive approaches, can be utilized for snow monitoring (Awasthi and Varade, 2021). In this chapter, we delve into discussion and assessment of snow monitoring methods presented in the thesis: snow depth spatio-temporal variability through manual measurements, employing airborne techniques such as UAS and utilizing gravimetry: neutron-based methods, and their results in mainly two study areas in steep Žlab Úpičky avalanche path in Krkonoše Mts. and predominantly flat Graswang study area in Bayern region.

This thesis investigated the feasibility of using a low-cost rotary UAS to monitor snow-covered terrain. The P4P. V2.0 performed well in flat terrain, aligning with the findings of Redpath et al., (2018), who reported that UAS provide a suitable and repeatable means of reliably determining SD in low-relief alpine catchment areas. The results suggest that rotary drones can be also a viable solution for monitoring snow in hard-to-access and risky areas that demand multiple skills (including drone operating, terrain assessment, weather understanding and snow profile knowledge - akin to ski-touring competences). This finding is consistent with the studies of Gábrlík et al. (2019) and Bühler et al., (2017). However, their effectiveness in high-alpine terrain is limited due to challenging steep topography, significant elevation differences, adverse weather conditions (thin air, cold temperatures, high wind speeds) as noted by Redpath et al.(2018), insufficient light, and limited contrast in imagery. For decades, photogrammetry in mountainous, snow-covered terrain was deemed infeasible owing to harsh topographic and meteorological conditions, coupled with the challenges of limited contrast in imagery. Therefore, SfM algorithms face difficulties in identifying meaningful matching points, especially on smoother snow surfaces.

Another potential tool for snow monitoring is CRNS, which offer the advantage of providing continuous measurements of snowpack characteristics. However, CRNS devices tend to be more expensive compared to manual and more affordable UAS monitoring devices. Additionally, their usability of transforming neutron count to SWE requires different parameter calibration and their usability: the unique function which would be able to translate cosmic neutrons into SWE in snow environment at various elevation is still under development. They can monitor mesoscale = catchment scale study areas.

[24] https://www.nasa.gov/centers-and-facilities/langley/what-is-earths-energy-budget-five-questions-with-a-guy-who-knows/

12.1 Limitations in mission Planning and setting up flying parameters

To ensure successful UAS flight missions in mountainous regions, we highlight several key considerations:

1. **Weather:**

- Potential impact of strong winds, common but variable in mountainous regions.
- Schedule flights during periods with minimal or light wind (maximum speed: 10m.s^{-1}), stable lightning, consistent cloud cover, and an operating air temperature of 0-40°C for P4P V.20. For newer drones, it differs, and they are more resistant to colder temperatures. Note that sunny weather in areas with trees or building shadows can complicate model assessment, and such ideal weather conditions are less common during Krkonoše winter season.

2. **Equipment:**

- Choosing a robust UAS platform and sensors capable of withstanding harsh environmental conditions, including strong winds, low temperatures, and steep or avalanche-prone terrain.
- Ensure UAS equipment is easily transportable in a backpack, especially for ski tours or snowshoes outings.
- Practice proper battery management by keeping batteries in a warm environment close to the body to prevent rapid drainage to ensure longer flight times.

3. **UAS App Recommendation:**

- In flat terrain, from our experience we recommend Pix4D Capture for automatic flying, offering an image overlap function and being free of charge. Terrain reconstruction using JPEG images is sufficient.
- Good X, Y, Z accuracy was achieved (Table 16) with an image overlap set up of 70-82%, as belongs to recommended values in Lee et al. (2021), and a preplanned function to stop when capturing images in the nadir direction (90° downward-looking camera/sensor).
- However, in steep terrain, Litchi was preferred, especially in the Žlab Úpičky site, allowing for flight height adjustment following the topography and accommodating five batteries, eventhrough the app does not provide to set up image overlap (waypoints are places manually). LiPo battery capacity lasted approximately 20-22 min under subzero temperatures.

4. **Image Capture:**

- Consider stopping with P4P V2.0 when capturing when it is possible regarding batteries and size of the area to reduce RMSE error. The findings of (Tekeli and Dönmez, 2018) claim that when a UAS stops and maintains its position in the air (achieving fixed position image acquisition using multi-rotor platforms), it results in

a lower RMSE error 1.79 cm in compared to 2.43 cm without stopping. The disadvantage is that the flight takes longer when it stops when capturing.

- Taking oblique images if you have more batteries. We agree with findings of James et al., (2020), Lee et al., (2021) and Štroner et al., (2021) that it would be essential to take oblique with a higher percentage of image overlap to lower the accuracy error.

12.2 Limitations in monitoring: terrain work and data acquisition

12.2.1 Snow depth avalanche probe

We recommend taking 3 to 5 SD measurements with a snow probe at each measured point, allowing for the exclusion of an extreme measurement if needed. Although we initially used the average value of manual SD points, upon reflection, the median value might be more indicative measure. A limitation of our manual measurements was the inability to measure snow accumulations exceeding 280 cm in Žlab Úpičky due to the probe's height. Additionally, determining the actual ground level, rocks, and layers of ice proved challenging, leading to some inaccuracies. The quality of ground measurements could be improved by using and ensuring higher snow probe.

In general, manual snow probing or GNSS measuring fixed points are suitable for verification purposes, especially in flat, easily accessable terrain. However, efforts should be made to minimize disturbance to the snow surface caused by footsteps, whether from snowshoes or ski-touring during manual measuring. Regarding steep terrain, manual measuring is time-consuming in risky avalanche-prone areas and lacks satisfactory spatial accuracy. Therefore, we recommend using UAS, which can provide a timely and relatively cost-effective solution with higher spatial resolution.

Regarding CRNS measuring, we recommend making 3 lines with a 120° angle to cover the spatial variability of SD and SWE diversity near CRNS stations. The use of SWE tubes (long lasting, resistant material) from the Rudolf Hancvencl factory is recommended for this purpose.

12.2.2 GCPs placement and counts

Due to challenging terrain and avalanche risk (another avalanche paths in Obří důl intersect with the Žlab Úpičky avalanche path from the left side (Fig. 4-a), GCP placement had less-than-ideal in the Žlab Úpičky study site. We played 10 GCPs during winter fieldwork, unfortunately, it was not possible to distribute GCPs evenly across the entire study and altitude bands as suggested by Martínez-Carricondo et al., (2018) due to limitations related to the presence of steep and icy terrain with obstacles, including rocks in snow covered period daylight, and suitable weather conditions (Fig. 9-a). To redistribute GCPs evenly we would need to place at least two GCPs (left and right side) in the upper part of the avalanche release area. During the summer season, access to the transport zone of the path was obstructed by dense dwarf pine vegetation, rocky areas with waterfalls, and a lack of available manpower to complete terrain work during one daylight. To address this challenge, it would require for example coordinating two groups, one starting from the top and the other from the bottom to place GCPs, or the establishment of stable co-registering points.

Installing stable, artificial co-registering points in Krkonoše requires permission from KRNAP, long-term planning, and materials resistant to landslides and avalanches. Stable points in such conditions are limited, especially during the snow-cover period. Many research-relevant locations in Krkonoše are challenging to monitor using point-based methods and UAS indirect georeferencing, primarily due to the avalanche risk and inaccessibility caused by dense vegetation hindering GCP placement. In the Žlab Úpičky terrain, GCP targets were used, as there are not many distinct terrain features not completely covered by snow. In Graswang station, stable landmarks such as a church, fence, and CRNS monitoring station were available for regular monitoring.

In both study areas, results accuracy could be improved by using stable co-registering points or utilizing the navigation function in Trimble device to consistently maintain GCP locations throughout both summer and winter. Another approach could involve subtracting the GCP elevations from Trimble elevation report.

12.2.3 Image acquisition formats and influence of flight surveying time and accuracy influenced by sizes of shadows

In steep Žlab Úpičky study site, there is room for improvement in the accuracy of UAS results. We used JPEG imagery obtained by converting video footage into JPEG photos due to SD card response issues. Unfortunately, some of the photos were blurry, likely caused by the camera not being fixed during capturing or not being autofocus-enabled). To solve this, we converted the video to JPEG images, which were not blurry like the original photos. The use of an automatic flight setup across the entire avalanche path would be essential for improvement; however, we faced challenges, including the loss of GPS signal l in the avalanche release area during the snow-covered period.

The primary objective of this thesis was to obtain DEMs and generate orthophotos, leading us to utilize JPEG photos. Capturing UAS imagery in JPEG format is recommended for complex 3D models (Alfio et al., 2020), as it facilitates an accurate representation of the terrain. However, in case of low contrast or poor lighting, RAW photos might be more suitable. It is essential to note that RAW images come with the drawback of longer processing time and higher storage requirements. Careful planning is necessary to determine storage locations and devise efficient data downloading strategies to avoid time-consuming USB extraction processes (Nguyen and Brown, 2018). Newer methods of data capturing uploading the images directly into cloud, but we did not have this option when we were taking images in 2021. While RAW-generated textures may exhibit slightly higher noise levels, they potentially more accurate colour representation compared to JPEG. Overall, the selection of 1. appropriate image formats, 2. compression levels, and 3. processing methods is crucial for achieving accurate and detailed orthophotos, especially in complex 3D modelling scenarios.

The interval between images captured in different swaths can be several minutes, and even within this short span, shadows may change noticeably during the dawn and dusk periods. Photogrammetry results accuracy generally decrease with increases of shadow sizes (Lee et al., 2021) and SD appears greater in areas with shadows (Bühler et al., 2016). Fig. 12-a shows

image shadows from buldings and trees (left) and trees and fence (right) during a day in Graswang.

Fig. 12-a: Shadows from buildings and trees (left) and trees and fence (right) in Graswang.

12.3 Limitations in data processing

12.3.1 Challenges in UAS results and DEMs resolution

We found that UAS photogrammetry can generate high-resolution DSMs, aligning with recent studies such as Bühler et al., (2016); De Michele et al., (2013); Harder et al., (2016); Nolan et al., (2015); and Vander Jagt et al., (2015). We achieved a resolution up to one $dm.px^{-1}$ for both snow-covered and snow free surfaces in our two study areas. It is essential to emphasize that favourable illumination conditions and weathered snow surface, such as those created by ski tracks, are crucial for deploying GCPs to match tie-points in images. The number of tie points we were able to identify increased with lower flight altitudes and the higher the overlap ratio, leading to more accurate DSM. This led to more accurate DSMs. In Graswang, the DSM had an average accuracy of 2.5-9 cm and a resolution of 0.4-0.7 pixels. In Žlab Úpičky, the DSM exhibited an average accuracy of 12.8-7.6 cm and a resolution of 1.4-0.4 pixels during the snow-covered and snow-free period, respectively. Some DEMs may offer centimeter-level accuracy in x, y, z direction, but they can also have systematic errors limiting their broader application. These errors, known as vertical 'doming' of the surface, result from a combination of **near-parallel imaging directions and inaccurate correction of radial lens distortion** (James et al., 2017). One method to reduce errors is to align the datasets and match fixed, visible surface points between snow-free and snow-covered point clouds (Vander Jagt et al., 2015).

12.3.2 Challenges in underlaying vegetation

Both study sites, The Žlab Úpičky and Graswang were screened after snowmelt. The Žlab Úpičky avalanche path was screened in late July when the grass was short and after snow patches melted in the avalanche path. In the upper part of the avalanche area, there are meadows and rocks. In the transport area there are dwarf pines, and in the accumulation zone there is a combination of forest, dwarf pines and grassy areas (Fig. 8-h). The vegetation at the base of the snow cover strongly influences the results. According to Bühler et al.,

(2016), small bushes, mainly alpine rose, juniper and erica, can rise to 0.50 m above ground in the summer. In winter, they are pressed down to the ground by the snowpack and may form a snow-free layer at the bottom of the snowpack, which can have a depth of a few centimetres to decimeters (Feistl et al., 2015). This leads to a systematic underestimation of SD mapped with photogrammetry (snow-free DSM is too high) as well as a systematic overestimation of SD measured manually with the avalanche probe as the probe penetrates the snow-free bottom layer and sometimes even the first layers of the ground. The "real" SD is probably a value between the manual probe and the photogrammetric measurements. This could be a potential source of error in Žlab Úpičky study site. In forested, steep terrain laser scanning could result in smaller accuracy of SD errors. The Graswang study site grass was short when screened and we masked tree features out of the DEMs. The error might be detected because of shades of trees or objects and thin fence (Fig. 12-a).

12.4 Which method should be used in the future?

High-resolution snow monitoring methods are revolutionizing our understanding of snowpack dynamics. These methods provide valuable insights for various applications, and their development is crucial for addressing climate change and water scarcity challenges. The future of snow monitoring lies in integrating multiple data sources, enabling a more comprehensive view of snow cover conditions and improved decision-making.

Photogrammetric processing UAS and LIDAR are sensing technologies that can be used to generate 3D models and point clouds. Photogrammetry is generally less expensive but requires good image quality and GCPS for indirect georeferencing. On the other hand, LIDAR is more accurate, can operate in low-light conditions and in areas covered by vegetation, as shown in Guimarães et al., (2020). However, LiDAR is more expensive than photogrammetry and can be slower in data collection. The choice of technology depends on specific needs and budget constraints (Table 19). An affordable method for generating 3D models is photogrammetric processing using UASs. If high-accuracy 3D models are required, especially in low light conditions or through vegetation, then LIDAR is the preferable choice or LiDAR device mounted on a drone vehicle. Another consideration is that the presence of alpine vegetation, such as bushes and dwarf pines, can lead to an overestimation of snow-free DSM elevations, resulting in an underestimation of SD. This factor might contribute to the observed conditions in the Žlab Úpičky avalanche path. According to Bühler et al., (2016), the underestimation of SD values can be as much as 0.50 meters.

Table 19: Comparison of the UAS photogrammetric processing and LIDAR factors.

Factor	Photogrammetric processing UAS	LIDAR
Accuracy	Good	Excellent
Level of detail	High	Very high
Cost	Less expensive	More expensive
Speed	Faster to collect data	Slower to collect data
Ability to penetrate vegetation	Limited	Good
Conditions in which it can be used	Good light conditions, limited vegetation	Any light conditions, any vegetation

Within snow environment, UAS are currently being tested for various applications, including the search and rescue of missing victims on snow and in woods, as demonstrated by Silvagni et al., (2017). UAS equipped with radars are mounted to achieve more precise monitoring of SD, as highlighted in the work of Bremer et al. (2019). Additionally, drone-based ultrawideband (UWB) radar sensors are employed to measure snow density and stratigraphy (snow layering). This technology aims to enhance personnel safety and extend coverage areas in avalanche starting zones, as discussed by Jenssen et al. (2020).

Future recommendations: If high budget is available, we recommend PPK method (PPK antenna from Topo Drone compatible with P4P v2.0 and process it in TOPOSETTER[25]) or RTK

[25] https://topodrone.com/company/news/743/

antenna on the drone. It would be beneficial to create an interactive map of avalanche hazard levels 1 to 5 according to avalanche risk reduction strategies [26]in Krkonoše Mts.

12.5 Limitations in sparce SWE manual sampling for CRNS stations located in Bayern region

The analysis of Bayern data shows that the relationship between neutron counts and SWE varies across different sites. Currently, this relationship needs adaptation for each study site and requires further in situ observations on additional dates and SWE levels to develop a universal approach that works for different locations and elevations. The hyperbolic solution proposed by Köhli et al. (2021) for the relationship between near- surface epithermal neutron intensity and water content in the soil and atmosphere moisture seems not to be applicable to above-snow snow monitoring. Our findings indicate that the relationship between SWE and neutron counts is nonlinear, aligning with the results presented by Schattan et al. (2017). This relationhip depends on various factors, including soil moisture, terrain features, and snow free areas. UAS and camera-based SD measurements could help broaden the database, validate results, and robustness of the fitting. Incorporating 3D neutron modelling could further improve the understanding of local process. We hypothesize that both methods UAS and CRNS, can contribute to improving modelling, for example, through data assimilation. Potential future solutions may involve the use of 1) physically based calibration functions and 2) spatial weighting for in-situ SWE averaging to account for variable CRNS footprint sensitivity.

[26] https://www.alpy4000.cz/lavinove-strategie

13 Conclusion

Our investigation focused on analysing a long-term dataset of avalanches along with weather variables associated with avalanche activity. We observed significant changes in avalanche patterns:

1a) Avalanche type: we observed a notable increase in the occurrence of wet avalanches (defined as C2 in Quervain, (1973), alongside a gradual decrease in slab avalanches from 1962 to 2021. Slab avalanches are particularly hazardous for off-piste skiers and tourists (Schweizer and Föhn, 1996).

1b) Timing: Additionally, we noted a shift towards earlier occurrences of wet avalanches, now predominantly observed in February and March, compared to the previously typical months as April and May. This shift has been documented in the mid-elevations of the Krkonoše Mts in northeast Czechia, likely attributable to climate change.

Over the past three decades, the frequency of wet avalanches has surged approximately sevenfold. This increase may be linked to the 1.8°C rise in air temperature during the winter season since 1979. These findings underscore the influence of climate change on avalanche dynamics, highlighting the necessity for ongoing monitoring and adaption measures to ensure the safety of individuals in avalanche-prone areas.

1c) We applied the RF method to determine the importance of meteorological and snow variables of wet and slab avalanches for a daily timescale within a low-altitude mountain range in Czechia from 1979-2020. According to RF method, the most important weather variables influencing the wet avalanche activity are 3-day maximum and minimum temperature, SD, wind direction and speed, and precipitation. Conversely, slab avalanche activity is primarly influenced by SD, rainfall variables based on threshold temperature, new snow, and wind speed. Air temperature has a notable impact on wet avalanches. However, for the period spanning 1979 to 2020, rain- and snow-related variables were found to be more important variable than air temperature in influencing slab avalanches. Notably, the important variables identified by the RF method are those susceptible to the effects of climate change. Although additional factors like sunlight are important, they are comparatively less important than the aforementioned variables. The methodology has the power to identify driving weather variables of wet and slab avalanches.
Utilizing ML techniques such as RF allows for the rapid processing of large datasets and the identification of important variables explaining different types of avalanches with high accuracy. However, it's important to note that while these models are powerful tools, they have not yet surpassed expert assessment in terms of reliability and precision. Further validation and refinement are necessary to fully assess their effectiveness in avalanche prediction and mitigation.

2a) Predicting avalanche hazards requires accurate estimation of snow volume in avalanche release areas. Conducting field-based monitoring is hazardous, therefore we aim to measure snow volume remotely to reduce risks. We seek to refine avalanche volume estimation using low-cost methods such as UAS P4P V2.0 (a close-range remote sensing method) and spatial SD or SWE estimation by CRNS, which offer affordable alternatives to laser scanning. We

tested the UAS method on flat terrain in Graswang, yielding precise X, Y, Z results. However, data collection and processing improvements are still needed. We hypothesize that if relevant on flat areas, the UAS method can be applied to more complex terrain, including avalanche-prone areas. Despite challenges faced in UAS screening and image processing in avalanche terrain, GPS results showed errors within 12 cm. Nevertheless, unreliable results were obtained in the avalanche release area, possibly due to issues (maybe dooming) with the snow-free DEM. Despite these challenges, we believe that combining UAS and CRNS methods can aid in estimating snow volume accurately.

2b) I contributed to collecting more data at Ammer and Isar river catchments, especially at the Graswang and Lerchkogel stations, during my internship in the winter season of 2022. However, manual sampling of SWE in mid-elevations (600-1600 m a.s.l.) remains sparse, necessitating continued data collection in the upcoming winter seasons.

2c) The CRNS method on aboveground snow is still under investigation to determine if a universal function can be applied to all altitudes, translating neutron counts into SWE while considering the physio-geographic environments of the stations. Alternatively, it may be necessary to adapt CRNS stations for each site. Ongoing research by the Cosmic Sense research unit aims to further investigate the CRNS method.

3) We typically learn and compare current situation with historical events. With the RAMMS model, we understand that if the full-depth slab avalanche layer releases, it can reach a maximum avalanche length. We can assess the probability of a full-depth slab avalanche release through human expertise. However, we can rely on avalanche records to document the furthest run-out distance if such an event occurs. According to avalanche records the maximum length of Žlab Úpičky release has been 1100 m.

Our findings offer vital information for avalanche forecasting and can be public authorities such as the Krkonoše NP administration, Czech mountain rescue services, and the Forest Management Institute. Land use management practitioners should adjust their behaviour and planned management activities to both mitigate avalanche hazards and conserve unique ecosystems, which may require controlled avalanche releases in Krkonoše NP. We recommend a combination of expert knowledge on avalanche activity, snow profile measurements (including stability tests and monitoring snowpack meteorological conditions to understand avalanche initiation and propagation), and identification of meteorological and snow variables on daily or hourly basis, where available, to assess avalanche hazard. Close-range sensing techniques, such as contactless UAS or LIDAR methods, are advised for hazardous terrain, while a combination of manual, UAS, and CRNS methods is suitable for flat, easily accessible terrain. Additionally, public discussions and school projects can be valuable tools for raising awareness about avalanche environments and safety measures. By disseminating information through these channels, we can enhance public understanding and preparedness for avalanche hazards.

14 References

Adams, M.S., Bühler, Y., Fromm, R., 2018. Multitemporal Accuracy and Precision Assessment of Unmanned Aerial System Photogrammetry for Slope-Scale Snow Depth Maps in Alpine Terrain. Pure Appl. Geophys. 175, 3303–3324. https://doi.org/10.1007/s00024-017-1748-y

Akçayır, G., Akçayır, M., 2018. The flipped classroom: A review of its advantages and challenges. Comput. Educ. 126, 334–345. https://doi.org/10.1016/j.compedu.2018.07.021

Alfio, V.S., Costantino, D., Pepe, M., 2020. Influence of Image TIFF Format and JPEG Compression Level in the Accuracy of the 3D Model and Quality of the Orthophoto in UAV Photogrammetry. J. Imaging 6, 30. https://doi.org/10.3390/jimaging6050030

Andreasen, M., Jensen, K.H., Desilets, D., Zreda, M., Bogena, H.R., Looms, M.C., 2017. Cosmic-ray neutron transport at a forest field site: The sensitivity to various environmental conditions with focus on biomass and canopy interception. Hydrol. Earth Syst. Sci. 21, 1875–1894. https://doi.org/10.5194/hess-21-1875-2017

Avanzi, F., Bianchi, A., Cina, A., De Michele, C., Maschio, P., Pagliari, D., Passoni, D., Pinto, L., Piras, M., Rossi, L., 2018. Centimetric Accuracy in Snow Depth Using Unmanned Aerial System Photogrammetry and a MultiStation. Remote Sens. 10, 765. https://doi.org/10.3390/rs10050765

Avanzi, F., Bianchi, A., Cina, A., De Michele, C., Maschio, P., Pagliari, D., Passoni, D., Pinto, L., Piras, M., Rossi, L., 2017. Measuring the snowpack depth with Unmanned Aerial System photogrammetry: comparison with manual probing and a 3D laser scanning over a sample plot (preprint). Seasonal Snow. https://doi.org/10.5194/tc-2017-57

Avanzi, F., De Michele, C., Ghezzi, A., Jommi, C., Pepe, M., 2014. A processing–modeling routine to use SNOTEL hourly data in snowpack dynamic models. Adv. Water Resour. 73, 16–29. https://doi.org/10.1016/j.advwatres.2014.06.011

Awasthi, S., Varade, D., 2021. Recent advances in the remote sensing of alpine snow: a review. GIScience Remote Sens. 58, 852–888. https://doi.org/10.1080/15481603.2021.1946938

Awidi, I.T., Paynter, M., 2019. The impact of a flipped classroom approach on student learning experience. Comput. Educ. 128, 269–283. https://doi.org/10.1016/j.compedu.2018.09.013

Baggi, S., Schweizer, J., 2009. Characteristics of wet-snow avalanche activity: 20 years of observations from a high alpine valley (Dischma, Switzerland). Nat. Hazards 50, 97–108. https://doi.org/10.1007/s11069-008-9322-7

Barnett, T.P., Adam, J.C., Lettenmaier, D.P., 2005. Potential impacts of a warming climate on water availability in snow-dominated regions. Nature 438, 303–309. https://doi.org/10.1038/nature04141

Bartelt, P. et al., 2022. RAMMS: Avalanche User Manual v1.8.0, p. 106.

Bartelt, P., Valero, C.V., Feistl, T., Christen, M., Bühler, Y., Buser, O., 2015. Modelling cohesion in snow avalanche flow. J. Glaciol. 61, 837–850. https://doi.org/10.3189/2015JoG14J126

Beniston, M., Farinotti, D., Stoffel, M., Andreassen, L.M., Coppola, E., Eckert, N., Fantini, A., Giacona, F., Hauck, C., Huss, M., Huwald, H., Lehning, M., López-Moreno, J.-I., Magnusson, J., Marty, C., Morán-Tejéda, E., Morin, S., Naaim, M., Provenzale, A., Rabatel, A., Six, D., Stötter, J., Strasser, U., Terzago, S., Vincent, C., 2018. The European mountain cryosphere: a review of its current state, trends, and future challenges. The Cryosphere 12, 759–794. https://doi.org/10.5194/tc-12-759-2018

Biecek, P., Burzykowski, T., 2021. Explanatory Model Analysis: Explore, Explain and Examine Predictive Models, 1st ed. Chapman and Hall/CRC. https://doi.org/10.1201/9780429027192

Blahůt, J., Klimeš, J., Balek, J., Hájek, P., Červená, L., Lysák, J., 2017. Snow avalanche hazard of the Krkonoše National Park, Czech Republic. J. Maps 13, 86–90. https://doi.org/10.1080/17445647.2016.1262794

Boesch, R., Bühler, Y., Marty, M., Ginzler, C., 2016. COMPARISON OF DIGITAL SURFACE MODELS FOR SNOW DEPTH MAPPING WITH UAV AND AERIAL CAMERAS. Int. Arch. Photogramm. Remote Sens. Spat. Inf. Sci. XLI-B8, 453–458. https://doi.org/10.5194/isprs-archives-XLI-B8-453-2016

Bogena, H.R., Herrmann, F., Jakobi, J., Brogi, C., Ilias, A., Huisman, J.A., Panagopoulos, A., Pisinaras, V., 2020. Monitoring of Snowpack Dynamics With Cosmic-Ray Neutron Probes: A Comparison of Four Conversion Methods. Front. Water 2, 1–17. https://doi.org/10.3389/frwa.2020.00019

Bremer, M., Wichmann, V., Rutzinger, M., Zieher, T., Pfeiffer, J., 2019. SIMULATING UNMANNED-AERIAL-VEHICLE BASED LASER SCANNING DATA FOR EFFICIENT MISSION PLANNING IN COMPLEX TERRAIN. Int. Arch. Photogramm. Remote Sens. Spat. Inf. Sci. XLII-2/W13, 943–950. https://doi.org/10.5194/isprs-archives-XLII-2-W13-943-2019

Bühler, Y., Adams, M.S., Stoffel, A., Boesch, R., 2017. Photogrammetric reconstruction of homogenous snow surfaces in alpine terrain applying near-infrared UAS imagery. Int. J. Remote Sens. 38, 3135–3158. https://doi.org/10.1080/01431161.2016.1275060

Bühler, Y., Adams, M.S., Bosch, R., Stoffel, A., 2016. Mapping snow depth in alpine terrain with unmanned aerial systems (UASs): Potential and limitations. Cryosphere 10, 1075–1088. https://doi.org/10.5194/tc-10-1075-2016

Bühler, Y., Marty, M., Egli, L., Veitinger, J., Jonas, T., Thee, P., Ginzler, C., 2015. Snow depth mapping in high-alpine catchments using digital photogrammetry. The Cryosphere 9, 229–243. https://doi.org/10.5194/tc-9-229-2015

Chawla, N.V., Bowyer, K.W., Hall, L.O., Kegelmeyer, W.P., 2002. SMOTE: Synthetic Minority Over-sampling Technique. J. Artif. Intell. Res. 16, 321–357. https://doi.org/10.1613/jair.953

Cho, J.M., Lee, B.K., 2023. GCP and PPK Utilization Plan to Deal with RTK Signal Interruption in RTK-UAV Photogrammetry. Drones 7, 265. https://doi.org/10.3390/drones7040265

Christen, M., Kowalski, J., Bartelt, P., 2010. RAMMS: Numerical simulation of dense snow avalanches in three-dimensional terrain. Cold Reg. Sci. Technol. 63, 1–14. https://doi.org/10.1016/j.coldregions.2010.04.005

Cignoni, P., Montani, C., Scopigno, R., 1998. A comparison of mesh simplification algorithms. Comput. Graph. 22, 37–54. https://doi.org/10.1016/S0097-8493(97)00082-4

Cimoli, E., Marcer, M., Vandecrux, B., Bøggild, C.E., Williams, G., Simonsen, S.B., 2017. Application of Low-Cost UASs and Digital Photogrammetry for High-Resolution Snow Depth Mapping in the Arctic. Remote Sens. 9, 1144. https://doi.org/10.3390/rs9111144

De Michele, C., Avanzi, F., Ghezzi, A., Jommi, C., 2013. Investigating the dynamics of bulk snow density in dry and wet conditions using a one-dimensional model. The Cryosphere 7, 433–444. https://doi.org/10.5194/tc-7-433-2013

Deems, J.S., Painter, T.H., Finnegan, D.C., 2013. Lidar measurement of snow depth: a review. J. Glaciol. 59, 467–479. https://doi.org/10.3189/2013JoG12J154

Delunel, R., Bourlès, D.L., van der Beek, P.A., Schlunegger, F., Leya, I., Masarik, J., Paquet, E., 2014. Snow shielding factors for cosmogenic nuclide dating inferred from long-term neutron detector monitoring. Quat. Geochronol. 24, 16–26. https://doi.org/10.1016/j.quageo.2014.07.003

Desilets, D., 2017. Calibrating a non-invasive cosmic ray soil moisture probe for snow water equivalent. Hydroinnova Tech. Doc. 17–01. https://doi.org/10.5281/zenodo.439105.Hydroinnova

Desilets, D., Zreda, M., Ferré, T.P.A., 2010. Nature's neutron probe: Land surface hydrology at an elusive scale with cosmic rays. Water Resour. Res. 46. https://doi.org/10.1029/2009WR008726

Dietz, A.J., Kuenzer, C., Gessner, U., Dech, S., 2012. Remote sensing of snow – a review of available methods. Int. J. Remote Sens. 33, 4094–4134. https://doi.org/10.1080/01431161.2011.640964

Dreier, L., Harvey, S., Van Herwijnen, A., Mitterer, C., 2016. Relating meteorological parameters to glide-snow avalanche activity. Cold Reg. Sci. Technol. 128, 57–68. https://doi.org/10.1016/j.coldregions.2016.05.003

Eberhard, L.A., Sirguey, P., Miller, A., Marty, M., Schindler, K., Stoffel, A., Bühler, Y., 2020. Intercomparison of photogrammetric platforms for spatially continuous snow depth mapping (preprint). Snow/Remote Sensing. https://doi.org/10.5194/tc-2020-93

Eckerstorfer, M., Christiansen, H.H., 2011. Relating meteorological variables to the natural slab avalanche regime in High Arctic Svalbard. Cold Reg. Sci. Technol. 69, 184–193. https://doi.org/10.1016/j.coldregions.2011.08.008

Eckert, N., Keylock, C.J., Castebrunet, H., Lavigne, A., Naaim, M., 2013. Temporal trends in avalanche activity in the French Alps and subregions: from occurrences and runout altitudes to unsteady return periods. J. Glaciol. 59, 93–114. https://doi.org/10.3189/2013JoG12J091

Engel, Z., Nývlt, D., Křížek, M., Treml, V., Jankovská, V., Lisá, L., 2010. Sedimentary evidence of landscape and climate history since the end of MIS 3 in the Krkonoše Mountains, Czech Republic. Quat. Sci. Rev. 29, 913–927. https://doi.org/10.1016/j.quascirev.2009.12.008

European Commission. Directorate General for Research and Innovation., 2020. Science communication: achievements in Horizon 2020 and recommendations on the way forward. Publications Office, LU.

Farinotti, D., Magnusson, J., Huss, M., Bauder, A., 2010. Snow accumulation distribution inferred from time-lapse photography and simple modelling. Hydrol. Process. n/a-n/a. https://doi.org/10.1002/hyp.7629

Feistl, T., Bebi, P., Christen, M., Margreth, S., Diefenbach, L., Bartelt, P., 2015. Forest damage and snow avalanche flow regime (preprint). Other Hazards (e.g., Glacial and Snow Hazards, Karst, Wildfires Hazards, and Medical Geo-Hazards). https://doi.org/10.5194/nhessd-3-535-2015

Fersch, B., Francke, T., Heistermann, M., Schrön, M., Döpper, V., Jakobi, J., Baroni, G., Blume, T., Bogena, H., Budach, C., Gränzig, T., Förster, M., Güntner, A., Franssen, H.J.H., Kasner, M., Köhli, M., Kleinschmit, B., Kunstmann, H., Patil, A., Rasche, D., Scheiffele, L., Schmidt, U., Szulc-Seyfried, S., Weimar, J., Zacharias, S., Zreda, M., Heber, B., Kiese, R., Mares, V., Mollenhauer, H., Völksch, I., Oswald, S., 2020. A dense

network of cosmic-ray neutron sensors for soil moisture observation in a highly instrumented pre-Alpine headwater catchment in Germany. Earth Syst. Sci. Data 12, 2289–2309. https://doi.org/10.5194/essd-12-2289-2020

Fierz, C., Armstrong, R. L., Durand, Y., Etchevers, P., Greene, E., McClung, D. M., Nishimura, K., Satyawali, P. K., and Sokratov, S. A., 2009. The international classification for seasonal snow on the ground, in: IHP-VII Technical Documents in Hydrology Nr. 83, IACS Contribution Nr.1.

Gábrlík, P., Janata, P., Zalud, L., Harcarik, J., 2019. Towards Automatic UAS-Based Snow-Field Monitoring for Microclimate Research. Sensors 19, 1945. https://doi.org/10.3390/s19081945

Gaiani, M., Remondino, F., Apollonio, F., Ballabeni, A., 2016. An Advanced Pre-Processing Pipeline to Improve Automated Photogrammetric Reconstructions of Architectural Scenes. Remote Sens. 8, 178. https://doi.org/10.3390/rs8030178

Gauthier, F., Germain, D., Hétu, B., 2017. Logistic models as a forecasting tool for snow avalanches in a cold maritime climate: northern Gaspésie, Québec, Canada. Nat. Hazards 89, 201–232. https://doi.org/10.1007/s11069-017-2959-3

Giacona, F., Eckert, N., Corona, C., Mainieri, R., Morin, S., Stoffel, M., Martin, B., Naaim, M., 2021. Upslope migration of snow avalanches in a warming climate. Proc. Natl. Acad. Sci. U. S. A. 118, 1–10. https://doi.org/10.1073/pnas.2107306118

Giacona, F., Eckert, N., Mainieri, R., Martin, B., Corona, C., Lopez-Saez, J., Monnet, J.-M., Naaim, M., Stoffel, M., 2018. Avalanche activity and socio-environmental changes leave strong footprints in forested landscapes: a case study in the Vosges medium-high mountain range. Ann. Glaciol. 59, 111–133. https://doi.org/10.1017/aog.2018.26

Gindraux, S., Boesch, R., Farinotti, D., 2017. Accuracy Assessment of Digital Surface Models from Unmanned Aerial Vehicles' Imagery on Glaciers. Remote Sens. 9, 186. https://doi.org/10.3390/rs9020186

Goetz, J., Brenning, A., 2019. Quantifying Uncertainties in Snow Depth Mapping From Structure From Motion Photogrammetry in an Alpine Area. Water Resour. Res. 55, 7772–7783. https://doi.org/10.1029/2019WR025251

Gregorutti, B., Michel, B., Saint-Pierre, P., 2017. Correlation and variable importance in random forests. Stat. Comput. 27, 659–678. https://doi.org/10.1007/s11222-016-9646-1

Guidicelli, M., Gugerli, R., Gabella, M., Marty, C., Salzmann, N., 2021. Continuous Spatio-Temporal High-Resolution Estimates of SWE Across the Swiss Alps – A Statistical Two-Step Approach for High-Mountain Topography. Front. Earth Sci. 9, 1–22. https://doi.org/10.3389/feart.2021.664648

Guimarães, N., Pádua, L., Marques, P., Silva, N., Peres, E., Sousa, J.J., 2020. Forestry Remote Sensing from Unmanned Aerial Vehicles: A Review Focusing on the Data, Processing and Potentialities. Remote Sens. 12, 1046. https://doi.org/10.3390/rs12061046

Hanzer, F., Carmagnola, C.M., Ebner, P.P., Koch, F., Monti, F., Bavay, M., Bernhardt, M., Lafaysse, M., Lehning, M., Strasser, U., François, H., Morin, S., 2020. Simulation of snow management in Alpine ski resorts using three different snow models. Cold Reg. Sci. Technol. 172, 102995. https://doi.org/10.1016/j.coldregions.2020.102995

Harder, P., Schirmer, M., Pomeroy, J., Helgason, W., 2016. Accuracy of snow depth estimation in mountain and prairie environments by an unmanned aerial vehicle. The Cryosphere 10, 2559–2571. https://doi.org/10.5194/tc-10-2559-2016

Hejcman, M., Dvorak, I.J., Kocianova, M., Pavlu, V., Nezerkova, P., Vitek, O., Rauch, O., Jenik, J., 2006. Snow Depth and Vegetation Pattern in a Late-melting Snowbed Analyzed by GPS and GIS in the Giant Mountains, Czech Republic. Arct. Antarct. Alp. Res. 38, 90–98. https://doi.org/10.1657/1523-0430(2006)038[0090:SDAVPI]2.0.CO;2

Hock, R., Rasul, G., Adler, C., Cáceres, B., Gruber, S., Hirabayashi, Y., Jackson, M., Kääb, A., Kang, S., Kutuzov, S., Milner, A., Molau, U., Morin, S., Orlove, B., Steltzer, H.I., 2019. Chapter 2: High Mountain Areas. IPCC Special Report on the Ocean and Cryosphere in a Changing Climate. IPCC Spec. Rep. Ocean Cryosphere Chang. Clim. 131–202.

Horton, S., Towell, M., Haegeli, P., 2020. Examining the operational use of avalanche problems with decision trees and model-generated weather and snowpack variables. Nat. Hazards Earth Syst. Sci. 20, 3551–3576. https://doi.org/10.5194/nhess-20-3551-2020

Howat, I.M., De La Peña, S., Desilets, D., Womack, G., 2018. Autonomous ice sheet surface mass balance measurements from cosmic rays. Cryosphere 12, 2099–2108. https://doi.org/10.5194/tc-12-2099-2018

Iyengar, S., Massey, D.S., 2019. Scientific communication in a post-truth society. Proc. Natl. Acad. Sci. 116, 7656–7661. https://doi.org/10.1073/pnas.1805868115

Jaakkola, A., Hyyppa, J., Puttonen, E., 2014. Measurement of Snow Depth Using a Low-Cost Mobile Laser Scanner. IEEE Geosci. Remote Sens. Lett. 11, 587–591. https://doi.org/10.1109/LGRS.2013.2271861

James, G., Witten, D., Hastie, T., Tibshirani, R., 2021. An Introduction to Statistical Learning: with Applications in R, Springer Texts in Statistics. Springer US, New York, NY. https://doi.org/10.1007/978-1-0716-1418-1
James, M.R., Antoniazza, G., Robson, S., Lane, S.N., 2020. Mitigating systematic error in topographic models for geomorphic change detection: accuracy, precision and considerations beyond off-nadir imagery. Earth Surf. Process. Landf. 45, 2251–2271. https://doi.org/10.1002/esp.4878
James, M.R., Robson, S., Smith, M.W., 2017. 3-D uncertainty-based topographic change detection with structure-from-motion photogrammetry: precision maps for ground control and directly georeferenced surveys: 3-D uncertainty-based change detection for SfM surveys. Earth Surf. Process. Landf. 42, 1769–1788. https://doi.org/10.1002/esp.4125
Jenssen, R.O.R., Eckerstorfer, M., Jacobsen, S., 2020. Drone-Mounted Ultrawideband Radar for Retrieval of Snowpack Properties. IEEE Trans. Instrum. Meas. 69, 221–230. https://doi.org/10.1109/TIM.2019.2893043
Jin, S., Qian, X., Kutoglu, H., 2016. Snow Depth Variations Estimated from GPS-Reflectometry: A Case Study in Alaska from L2P SNR Data. Remote Sens. 8, 63. https://doi.org/10.3390/rs8010063
Johnson, J.B., Marks, D., 2004. The detection and correction of snow water equivalent pressure sensor errors. Hydrol. Process. 18, 3513–3525. https://doi.org/10.1002/hyp.5795
Juras, R., Blöcher, J.R., Jenicek, M., Hotovy, O., Markonis, Y., 2021. What affects the hydrological response of rain-on-snow events in low-altitude mountain ranges in Central Europe? J. Hydrol. 603, 127002. https://doi.org/10.1016/j.jhydrol.2021.127002
Köhli, M., Weimar, J., Schrön, M., Baatz, R., Schmidt, U., 2021. Soil Moisture and Air Humidity Dependence of the Above-Ground Cosmic-Ray Neutron Intensity. Front. Water 2. https://doi.org/10.3389/frwa.2020.544847
Korzeniowska, K., Bühler, Y., Marty, M., Korup, O., 2017. Regional snow-avalanche detection using object-based image analysis of near-infrared aerial imagery. Nat. Hazards Earth Syst. Sci. 17, 1823–1836. https://doi.org/10.5194/nhess-17-1823-2017
Kupfer, J.A., Emerson, C.W., 2005. Remote Sensing, in: Encyclopedia of Social Measurement. Elsevier, pp. 377–383. https://doi.org/10.1016/B0-12-369398-5/00340-6
Lato, M.J., Frauenfelder, R., Bühler, Y., 2012. Automated detection of snow avalanche deposits: segmentation and classification of optical remote sensing imagery. Nat. Hazards Earth Syst. Sci. 12, 2893–2906. https://doi.org/10.5194/nhess-12-2893-2012
Lee, S., Park, J., Choi, E., Kim, D., 2021. Factors Influencing the Accuracy of Shallow Snow Depth Measured Using UAV-Based Photogrammetry. Remote Sens. 13, 828. https://doi.org/10.3390/rs13040828
Lee, S.-S., Hung, D., 2012. Is There an Instructional Framework for 21st Century Learning? Creat. Educ. 03, 461–470. https://doi.org/10.4236/ce.2012.34071
Lendzioch, T., Langhammer, J., Jenicek, M., 2019. Estimating Snow Depth and Leaf Area Index Based on UAV Digital Photogrammetry. Sensors 19, 1027. https://doi.org/10.3390/s19051027
Lendzioch, T., Langhammer, J., Jenicek, M., 2016. TRACKING FOREST AND OPEN AREA EFFECTS ON SNOW ACCUMULATION BY UNMANNED AERIAL VEHICLE PHOTOGRAMMETRY. Int. Arch. Photogramm. Remote Sens. Spat. Inf. Sci. XLI-B1, 917–923. https://doi.org/10.5194/isprs-archives-XLI-B1-917-2016
Liaw, A. and Wiener, M.,2002. Classification and Regression by randomForest, R News, 2, 18–22, https://CRAN.R-project.org/doc/Rnews/ (last access: 2 September 2022).
López-Moreno, J.I., Revuelto, J., Alonso-González, E., Sanmiguel-Vallelado, A., Fassnacht, S.R., Deems, J., Morán-Tejeda, E., 2017. Using very long-range terrestrial laser scanner to analyze the temporal consistency of the snowpack distribution in a high mountain environment. J. Mt. Sci. 14, 823–842. https://doi.org/10.1007/s11629-016-4086-0
Lunardon, N., Menardi, G., Torelli, N., 2014. ROSE: a Package for Binary Imbalanced Learning. R J. 6, 79. https://doi.org/10.32614/RJ-2014-008
Machguth, H., Eisen, O., Paul, F., Hoelzle, M., 2006. Strong spatial variability of snow accumulation observed with helicopter-borne GPR on two adjacent Alpine glaciers. Geophys. Res. Lett. 33, L13503. https://doi.org/10.1029/2006GL026576
MaGICLandscapes: Krkonoše National Park and surroundings, Czech Republic, 2020. https://www.interreg-central.eu/Content.Node/MaGICLandscapes.html (last access: 14 July 2022).
Maier, K., Nascetti, A., Van Pelt, W., Rosqvist, G., 2022. Direct photogrammetry with multispectral imagery for UAV-based snow depth estimation. ISPRS J. Photogramm. Remote Sens. 186, 1–18. https://doi.org/10.1016/j.isprsjprs.2022.01.020
Mainieri, R., Favillier, A., Lopez-Saez, J., Eckert, N., Zgheib, T., Morel, P., Saulnier, M., Peiry, J.-L., Stoffel, M., Corona, C., 2020. Impacts of land-cover changes on snow avalanche activity in the French Alps. Anthropocene 30, 100244. https://doi.org/10.1016/j.ancene.2020.100244

Marti, R., Gascoin, S., Berthier, E., De Pinel, M., Houet, T., Laffly, D., 2016. Mapping snow depth in open alpine terrain from stereo satellite imagery. The Cryosphere 10, 1361–1380. https://doi.org/10.5194/tc-10-1361-2016

Martínez-Carricondo, P., Agüera-Vega, F., Carvajal-Ramírez, F., Mesas-Carrascosa, F.-J., García-Ferrer, A., Pérez-Porras, F.-J., 2018. Assessment of UAV-photogrammetric mapping accuracy based on variation of ground control points. Int. J. Appl. Earth Obs. Geoinformation 72, 1–10. https://doi.org/10.1016/j.jag.2018.05.015

Marty, C., Tilg, A.-M., Jonas, T., 2017. Recent Evidence of Large-Scale Receding Snow Water Equivalents in the European Alps. J. Hydrometeorol. 18, 1021–1031. https://doi.org/10.1175/JHM-D-16-0188.1

Miller, Z.S., Peitzsch, E.H., Sproles, E.A., Birkeland, K.W., Palomaki, R.T., 2022. Assessing the seasonal evolution of snow depth spatial variability and scaling in complex mountain terrain. The Cryosphere 16, 4907–4930. https://doi.org/10.5194/tc-16-4907-2022

Miziński, B., Niedzielski, T., 2017. Fully-automated estimation of snow depth in near real time with the use of unmanned aerial vehicles without utilizing ground control points. Cold Reg. Sci. Technol. 138, 63–72. https://doi.org/10.1016/j.coldregions.2017.03.006

Morin, S., Lejeune, Y., Lesaffre, B., Panel, J.-M., Poncet, D., David, P., Sudul, M., 2012. An 18-yr long (1993–2011) snow and meteorological dataset from a mid-altitude mountain site (Col de Porte, France, 1325 m alt.) for driving and evaluating snowpack models. Earth Syst. Sci. Data 4, 13–21. https://doi.org/10.5194/essd-4-13-2012

Mountain Rescue Service, 2021. Avalanche danger in Krkonoše National Park, https://www.horskasluzba.cz/cz/pocasi-na-horach/lavinova-predpoved/krkonose, last access: 1 November 2023.

Munerol, F., Avanzi, F., Panizza, E., Altamura, M., Gabellani, S., Polo, L., Mantini, M., Alessandri, B., Ferraris, L., 2022. Water and Us: tales and hands-on laboratories to educate on sustainable and nonconflictual water resources management (preprint). Geoscience education/Public communication of science. https://doi.org/10.5194/egusphere-2022-1250

Naaim, M., Eckert, N., Giraud, G., Faug, T., Chambon, G., Naaim-Bouvet, F., Richard, D., 2016. Impact du réchauffement climatique sur l'activité avalancheuse et multiplication des avalanches humides dans les Alpes françaises. Houille Blanche 102, 12–20. https://doi.org/10.1051/lhb/2016055

Nguyen, R.M.H., Brown, M.S., 2018. RAW Image Reconstruction Using a Self-contained sRGB–JPEG Image with Small Memory Overhead. Int. J. Comput. Vis. 126, 637–650. https://doi.org/10.1007/s11263-017-1056-0

Nolan, M., Larsen, C., Sturm, M., 2015. Mapping snow depth from manned aircraft on landscape scales at centimeter resolution using structure-from-motion photogrammetry. The Cryosphere 9, 1445–1463. https://doi.org/10.5194/tc-9-1445-2015

Oniga, V.-E., Breaban, A.-I., Statescu, F., 2018. Determining the Optimum Number of Ground Control Points for Obtaining High Precision Results Based on UAS Images, in: The 2nd International Electronic Conference on Remote Sensing. Presented at the International Electronic Conference on Remote Sensing, MDPI, p. 352. https://doi.org/10.3390/ecrs-2-05165

Parajka, J., Haas, P., Kirnbauer, R., Jansa, J., Blöschl, G., 2012. Potential of time-lapse photography of snow for hydrological purposes at the small catchment scale: POTENTIAL OF TIME-LAPSE PHOTOGRAPHY OF SNOW FOR HYDROLOGICAL PURPOSES. Hydrol. Process. 26, 3327–3337. https://doi.org/10.1002/hyp.8389

Peitzsch, E.H., Pederson, G.T., Birkeland, K.W., Hendrikx, J., Fagre, D.B., 2021. Climate drivers of large magnitude snow avalanche years in the U.S. northern Rocky Mountains. Sci. Rep. 11, 10032. https://doi.org/10.1038/s41598-021-89547-z

Podaný, A., 2023. Využití lavinového modelu ramms v podmínkách krkonoš. Česká zemědělská univerzita v Praze.

Prokop, A., 2008. Assessing the applicability of terrestrial laser scanning for spatial snow depth measurements. Cold Reg. Sci. Technol. 54, 155–163. https://doi.org/10.1016/j.coldregions.2008.07.002

Prokop, A., Schirmer, M., Rub, M., Lehning, M., Stocker, M., 2008. A comparison of measurement methods: terrestrial laser scanning, tachymetry and snow probing for the determination of the spatial snow-depth distribution on slopes. Ann. Glaciol. 49, 210–216. https://doi.org/10.3189/172756408787814726

Quervain, M., 1973. AVALANCHE CLASSIFICATION. Hydrol. Sci. Bull. 18, 391–402. https://doi.org/10.1080/02626667309494054

Racek, O., Blahůt, J., 2016. Snow avalanche in the Modrý důl valley in the Krkonoše Mts from February 2015 back-calculated by numerical model RAMMS. Opera Concordica.

Redpath, T.A.N., Sirguey, P., Cullen, N.J., 2018. Repeat mapping of snow depth across an alpine catchment with RPAS photogrammetry. The Cryosphere 12, 3477–3497. https://doi.org/10.5194/tc-12-3477-2018

Richnavský, J., Bobáľ, P., Šír, B. & Ďuricha M. 2010: Avalanche and debris fl ow modelling in the chosen location of the Moravskoslezské Beskydy Mountains. In: T. Hoch & M. Šumberová (eds.), Sborník abstraktů XXII. sjezdu České geografi cké společnosti. Ostravská Univerzita, Ostrava. 82 str.

Salm, B., 1993. Flow, flow transition and runout distances of flowing avalanches. Ann. Glaciol. 18, 221–226. https://doi.org/10.3189/S0260305500011551

Schattan, P., Baroni, G., Oswald, S.E., Schöber, J., Fey, C., Kormann, C., Huttenlau, M., Achleitner, S., 2017. Continuous monitoring of snowpack dynamics in alpine terrain by aboveground neutron sensing. Water Resour. Res. 53, 3615–3634. https://doi.org/10.1002/2016WR020234

Schattan, P., Köhli, M., Schrön, M., Baroni, G., Oswald, S.E., 2019. Sensing Area-Average Snow Water Equivalent with Cosmic-Ray Neutrons: The Influence of Fractional Snow Cover. Water Resour. Res. 55, 10796–10812. https://doi.org/10.1029/2019WR025647

Schön, P., Prokop, A., Vionnet, V., Guyomarc'h, G., Naaim-Bouvet, F., Heiser, M., 2015. Improving a terrain-based parameter for the assessment of snow depths with TLS data in the Col du Lac Blanc area. Cold Reg. Sci. Technol. 114, 15–26. https://doi.org/10.1016/j.coldregions.2015.02.005

Schrön, M., Köhli, M., Scheiffele, L., Iwema, J., Bogena, H.R., Lv, L., Martini, E., Baroni, G., Rosolem, R., Weimar, J., Mai, J., Cuntz, M., Rebmann, C., Oswald, S.E., Dietrich, P., Schmidt, U., Zacharias, S., 2017. Improving calibration and validation of cosmic-ray neutron sensors in the light of spatial sensitivity. Hydrol. Earth Syst. Sci. 21, 5009–5030. https://doi.org/10.5194/hess-21-5009-2017

Seifert, E., Seifert, S., Vogt, H., Drew, D., Van Aardt, J., Kunneke, A., Seifert, T., 2019. Influence of Drone Altitude, Image Overlap, and Optical Sensor Resolution on Multi-View Reconstruction of Forest Images. Remote Sens. 11, 1252. https://doi.org/10.3390/rs11101252

Sielenou, P., Viallon-Galinier, L., Hagenmuller, P., Naveau, P., Morin, S., Dumont, M., Verfaillie, D., Eckert, N., 2021. Combining random forests and class-balancing to discriminate between three classes of avalanche activity in the French Alps. Cold Reg. Sci. Technol. 187, 103276. https://doi.org/10.1016/j.coldregions.2021.103276

Sigouin, Mark J. P., Si, B.C., 2016. Calibration of a non-invasive cosmic-ray probe for wide area snow water equivalent measurement. The Cryosphere 10, 1181–1190. https://doi.org/10.5194/tc-10-1181-2016

Silvagni, M., Tonoli, A., Zenerino, E., Chiaberge, M., 2017. Multipurpose UAV for search and rescue operations in mountain avalanche events. Geomat. Nat. Hazards Risk 8, 18–33. https://doi.org/10.1080/19475705.2016.1238852

Singh, K.K., Singh, D.K., Thakur, N.K., Dewali, S.K., Negi, H.S., Snehmani, Mishra, V.D., 2022. Detection and mapping of snow avalanche debris from Western Himalaya, India using remote sensing satellite images. Geocarto Int. 37, 2561–2579. https://doi.org/10.1080/10106049.2020.1762762

Smith, M.W., Carrivick, J.L., Quincey, D.J., 2016. Structure from motion photogrammetry in physical geography. Prog. Phys. Geogr. Earth Environ. 40, 247–275. https://doi.org/10.1177/0309133315615805

Součková, M., Juras, R., Dytrt, K., Moravec, V., Blöcher, J.R., Hanel, M., 2022. What weather variables are important for wet and slab avalanches under a changing climate in a low-altitude mountain range in Czechia? Nat. Hazards Earth Syst. Sci. 22, 3501–3525. https://doi.org/10.5194/nhess-22-3501-2022

Součková, M., Juras, R., Dytrt, K., Moravec, V., Blöcher, J. R., and Hanel, M.: What weather variables are important for wet and slab avalanches under a changing climate in low altitude mountain range in Czechia?, Zenodo [data set] and [code], https://doi.org/10.5281/zenodo.7041129, 2022.

Spandre, P., François, H., Thibert, E., Morin, S., George-Marcelpoil, E., 2017. Determination of snowmaking efficiency on a ski slope from observations and modelling of snowmaking events and seasonal snow accumulation. The Cryosphere 11, 891–909. https://doi.org/10.5194/tc-11-891-2017

Spusta, V., Spusta, V., Kociáová, M., 2020. Lavinový katastr a zimní situace v české části Krkonoš. Avalanche cadastre and winter conditions in the czech part of the Krkonoše Mts. in the winter seasons. Opera Corcon. 56, 21–110.

Spusta, V., Spusta, V. J., and Kociánová, M., 2006: Lavinový katastr české části Krkonoš v zimním období 2003/04 až 2005/06. Avalanche cadaster of the Czech part of the Giant Mountains in winter season 2003/04–2005/06, Opera Corcontica, 43, 81–93.

Spusta, V., Spusta, V. J., and Kociánová, M., 2003: Lavinový katastr a zimní situace na hřebenu české části Krkonoš v období 1998/99–2002/03. Avalanche Cadastre and Winter Condition in Summit Area of the Giant Mts. (Czech part) during 1998/1999–2002/2003, Opera Corcontica, 40, 5–86.

Spusta, V. and Kociánová, M., 1998: Avalanche cadastre in the Czech part of the Krkonoše Mts. (Giant Mts.) during winter seasons 1961/62–1997/98, Opera Corcontica, 35, 3–205.

Steiner, L., Meindl, M., Fierz, C., Geiger, A., 2018. An assessment of sub-snow GPS for quantification of snow water equivalent. The Cryosphere 12, 3161–3175. https://doi.org/10.5194/tc-12-3161-2018

Štroner, M., Urban, R., Seidl, J., Reindl, T., Brouček, J., 2021. Photogrammetry Using UAV-Mounted GNSS RTK: Georeferencing Strategies without GCPs. Remote Sens. 13, 1336. https://doi.org/10.3390/rs13071336

Stull, R., 2011. Wet-Bulb Temperature from Relative Humidity and Air Temperature. J. Appl. Meteorol. Climatol. 50, 2267–2269. https://doi.org/10.1175/JAMC-D-11-0143.1
Štursa, J., Jeník, J., and Váňa, J., 2010: The alpine forest-limit in the Giant Mts (Central Europe) and Abisko Mts (subarctic Sweden), Opera Corcontica, 47, 129–164.
Tekeli, A.E., Dönmez, S., 2018. Image acquisition effects on Unmanned Air Vehicle snow depth retrievals. Proc. Int. Assoc. Hydrol. Sci. 380, 81–85. https://doi.org/10.5194/piahs-380-81-2018
Tesař, P., 2007. Úvod do GNSS.
Tomaštík, J., Mokroš, M., Surový, P., Grznárová, A., Merganič, J., 2019. UAV RTK/PPK Method—An Optimal Solution for Mapping Inaccessible Forested Areas? Remote Sens. 11, 721. https://doi.org/10.3390/rs11060721
Tominaga, Y., Okaze, T., Mochida, A., 2011. CFD modeling of snowdrift around a building: An overview of models and evaluation of a new approach. Build. Environ. 46, 899–910. https://doi.org/10.1016/j.buildenv.2010.10.020
Van Sickle, J., 2015. GPS for Land Surveyors, Fourth Edition, 4th ed. ed. Chapman and Hall/CRC, Boca Raton.
Vander Jagt, B., Lucieer, A., Wallace, L., Turner, D., Durand, M., 2015. Snow Depth Retrieval with UAS Using Photogrammetric Techniques. Geosciences 5, 264–285. https://doi.org/10.3390/geosciences5030264
Viviroli, D., Dürr, H.H., Messerli, B., Meybeck, M., Weingartner, R., 2007. Mountains of the world, water towers for humanity: Typology, mapping, and global significance. Water Resour. Res. 43, 1–13. https://doi.org/10.1029/2006WR005653
Vrba, M. and Spusta, V.,1991: The avalanche cadastre of the Krkonoše Mountains, Opera Concordica, 28, 47–58.
Vrba, M., Spusta, V., 1975. Avalanche Survey and Map of Krkonoše Mountains. Opera Corcon. 12, 65–90.
Warren, S.G., 1982. Optical properties of snow. Rev. Geophys. 20, 67–89. https://doi.org/10.1029/RG020i001p00067
Westoby, M.J., Brasington, J., Glasser, N.F., Hambrey, M.J., Reynolds, J.M., 2012. 'Structure-from-Motion' photogrammetry: A low-cost, effective tool for geoscience applications. Geomorphology 179, 300–314. https://doi.org/10.1016/j.geomorph.2012.08.021
Wolf, P.R., Dewitt, B.A., Wilkinson, B.E., 2014. Elements of photogrammetry with applications in GIS, 4. ed. [fully updated]. ed. McGraw-Hill Education, New York.
Zahradníček, P., Brázdil, R., Štěpánek, P., and Řezníčková, L., 2019: Differences in wind speeds according to measured and homogenized series in the Czech Republic, 1961–2015, Int. J. Climatol., 39, 235–250.
Zweck, C., Zreda, M., Desilets, D., 2013. Snow shielding factors for cosmogenic nuclide dating inferred from Monte Carlo neutron transport simulations. Earth Planet. Sci. Lett. 379, 64–71. https://doi.org/10.1016/j.epsl.2013.07.023